INITIAL SWELLING MECHANISM OF EXPANSIVE CLAYS –

A MOLECULAR DYNAMICS STUDY

A Thesis
Submitted to the Graduate Faculty
Of the
North Dakota State University
Of Agriculture and Applied Science

By

Lakshmikanth Srinivasamurthy

In Partial Fulfillment
for the Degree of
MASTER OF SCIENCE

Major Department:
Civil Engineering

October 2012

Fargo, North Dakota

North Dakota State University
Graduate School

INITIAL SWELLING MECHANISM OF EXPANSIVE CLAYS – A MOLECULAR DYNAMICS STUDY

By
Lakshmikanth Srinivasamurthy

The Supervisory Committee certifies that this ***disquisition*** complies with North Dakota State University's regulations and meets the accepted standards for the degree of

MASTER OF SCIENCE

SUPERVISORY COMMITTEE:

Dr. Dinesh Katti
Chair

Dr. Kalpana Katti (Co-Chair)

Dr. Sivapalan Gajan

Dr. Bernhardt Saini-Eidukat

Approved:

9/27/2013	Dr. Dinesh Katti
Date	Department Chair

ABSTRACT

Expansive soils are widely found in many parts of the world. Highly active smectite clay mineral Montmorillonite is the major constituent in these clays and can expand or contract up to 15 times of their original volume. Constrained swelling exert large amount of stress causing damage to structures, pavements etc. These clays are also used as barrier materials, Nano-materials in polymer clay Nano composites and drug delivery systems. Several factors influence the swelling potential such as water content, density, voids, electrolyte content and cation exchange capacity. However, molecular scale mechanisms that control swelling behavior in these clays need to be understood. Objectives of this research are to provide an insight into mechanisms that result in swelling of these clays. Molecular modeling is used to build and study solvation of Na-Montmorillonite system. Trajectories of water molecules are captured and the evolutions of interaction energies with swelling are calculated.

ACKNOWLEDGEMENTS

I would like to thank NDSU Civil Engineering department for the opportunity and support. I would like to acknowledge Dr. Dinesh Katti for his advice and input in learning MD simulations. I also thank Dr. Kalpana Katti for the advice and suggestions.

I thank the members of my advisory committee for the assistance. Thanks to Jan Lofberg and Milka Singha for the assistance and support. Thanks to all group members for their valuable suggestions in group meetings.

Thanks to my wife Ambika for the encouragement, understanding and patience.

I would like to convey my thanks to Dr. K.R. Prabhu, Mrs. Jyothi Prabhu, Dr. J.M. Chandra Kishen, Dr. Sudhakar M. Rao, Prof. H. P. Sudarshan, Mrs. Tripura Sheshadri, Mr. Sheshadri, Dr. K.V. Guruprakash, Mr. K.R. Praveen and Mr. Naveen Kumar for supporting and encouraging me to pursue this degree.

I thank my parents Mrs. Nagarathna and Mr. Srinivasamurthy for inspiring and supporting me throughout all my studies at university.

This research was funded by National science Foundation. The MD simulations were performed at NDSU Center for Computationally Assisted Science and Technology and all the supporting staff of CCAST are acknowledged.

TABLE OF CONTENTS

LIST OF TABLES

LIST OF FIGURES

LIST OF APPENDIX FIGURES

CHAPTER 1. INTRODUCTION

Occurrence of Expansive soils or swelling clay minerals is observed all over the world. Expansive soils swell in the presence of water and damage the structure. Figure1 shows the underlying regions of swelling clay minerals in the United States of America.

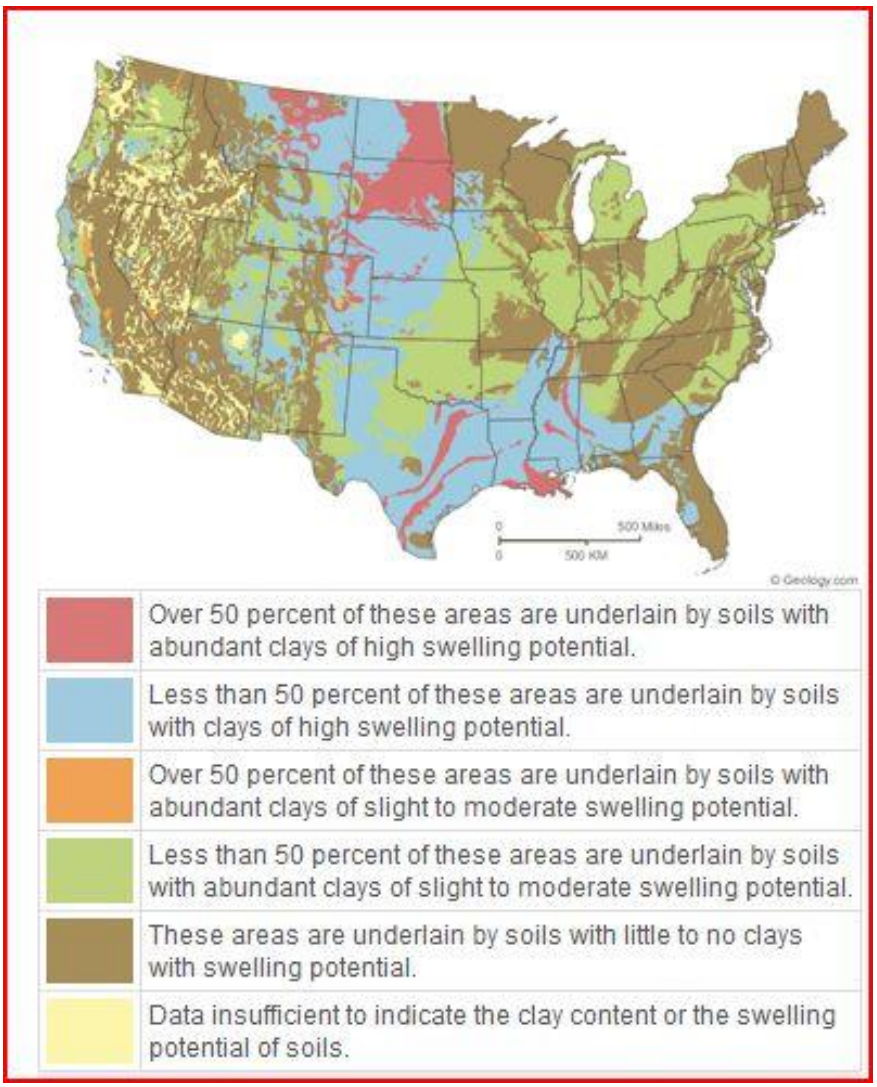

Figure 1. Expansive soils sites in United States
(http://ngmdb.usgs.gov/Prodesc/proddesc_10014.htm)

Occurrence of kaolinite can be seen in southeastern part, vermiculite in northern states, smectite, and mica in Great Plains and south western states respectively. Clay minerals and its

chemical composition greatly affect soil properties. The term clay represents both soil and mineral type. Generally, for most of the engineering applications the dimension of the clay minerals ranges from 10^3 to 10^6 A° and thickness about 10 A°. Because of the surface-mass ratio and colloidal properties, clay minerals have highly reactive surfaces, cationic exchange capacities and swelling potential when exposed to moisture content(Van Olphen, 1979).

Shape, size, surface chemistry of minerals and interaction with solvents can be determined by using mineralogy. These mineralogical properties play a huge role in evaluating geotechnical properties like plasticity, swelling, compression and fluid conductivity; these properties can be further applied to resolve environmental issues like hazardous waste disposal and radioactive waste disposal (Mitchel, 1993).

Clay minerals are used extensively in petroleum and pharmaceutical industries, in cosmetic industries as an additive for polymeric materials. It is very important to understand interaction of clay minerals with other materials and solvents. This literature review describes the necessity of clay swelling models. The diffuse double layer theory developed by Stern-Guoy explained interaction of clay sheets with bound water. However, diffuse double layer theory has limitations in explaining interlayer hydration and swelling of clay minerals accurately (Jo et al., 2001).

DLVO theory explains colloidal behavior of clay-water suspension, but it is limited to explain the colloidal behavior of the clay water system above 20A° separation distance. However, these theories cannot accurately predict the crystalline swelling nature of smectite clay minerals. The evolution of microstructure and particle breakdown was reported by Katti and Shanmugasundaram (2001). Hydraulic properties, FT-IR spectroscopic study and XRD analysis of clay-water interactions was done by (Amarasinghe et al., 2008).

In recent years, continuum mechanics approaches like Finite element methods and granular mechanics were used to predict the macroscopic properties of granular materials like soils. Most of these methods fail to predict the nature of cohesive soils due to several factors like particle size variation, irregular geometry, geological formation, chemical composition and environmental history (Anderson and Lu, 2001).Hence it requires a fundamental understanding of the nature of the cohesive soils at micron and sub-micron level in order to predict their macroscopic properties.

However, approaches like Discrete Element techniques are used to explain the behavior of clay minerals. These methods are limited to explain the swelling behavior of kaolinite. Particle sub-division of clay minerals also showed performing DEM simulations, but it requires a fundamental understanding of atomic and molecular properties of expansive soils in order to explain the swelling mechanism, microstructure evolution and interaction energies involved in clay-water interactions.

Molecular Dynamics (MD) simulations and Monte Carlo (MC) simulations are widely used computational techniques to predict the atomic properties of materials; In 2005 Steven R. Schmidt et al., evaluated the mechanical response of dry and hydrated sodium-Montmorillonite performing steered molecular dynamics simulations (Katti et al., 2007). SMD simulations are also used to calculate the stress-strain response of clay minerals with amino acids (Katti et.al 2005b).

The present work quantitatively estimates the molecular interactions involved in a clay-water system, initiation of the swelling mechanism of Na-MMT and the mobility of water molecules in the interlayer.

Though MD simulations cannot be used to predict microstructure evolution and particle break down, other properties like interaction energy, variation of d-spacing with time and speed at which water molecules entering interlayer etc. can be estimated by performing MD simulations. The obtained molecular properties can be incorporated further in simulation techniques like discrete element modeling (DEM). In future multi-scale modeling approach can be developed by using MD simulation results and mechanisms like microstructure evolution, particle breakdown at swelling and swelling pressure can be explained.

1.1. Summary

This literature review is an attempt to explain the works involved in multidisciplinary areas like engineering, soil sciences, geo sciences, physics and chemistry. It also includes the theoretical and computational studies associated with Molecular dynamics and Monte Carlo simulations.

CHAPTER 2. CLAY MINERALOGY

Expansive soils consist of clay minerals which are commonly found in soils. Clay minerals are the results of natural weathering and deterioration of igneous rocks. Clay minerals are layered structures and come under the category of phyllosilicates. The basic unit cell of silica tetrahedral sheet consists of one silicon atom at the center; this silicon atom is surrounded by four oxygen atoms to make one silicon tetrahedron cell (Birkeland, 1999). These silicon tetrahedrons are interconnected to make a sheet like structure. The oxygen atoms in silicon tetrahedrons are shared to form a hexagonal net as shown in Figure2. The bases of tetrahedrons share the same plane and the tips of all silica tetrahedrons pointing in the same direction. The silica tetrahedral sheet has chemical composition of $(Si_4O_{10})^{4-}$. The negative charge of silica sheets are balanced by bonding (Mitchell, 1993)by a positively charged sheet or by replacing oxygen ions by hydroxyls (Mitchell, 1993).

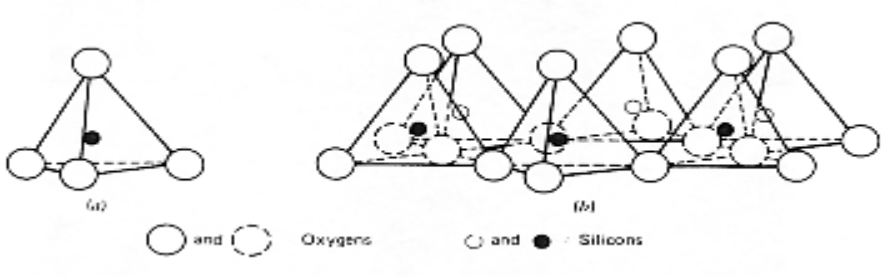

Figure 2. Silica tetrahedron cell and silicon tetrahedral sheet forming a hexagonal net (Grim, 1968, as cited by Mitchell, 1993)

The octahedral sheet of clay minerals consists aluminum, magnesium and iron atoms (Mitchell, 1993). These atoms are located at the center of basic octahedron and oxygen or hydroxyl atoms are coordinated at octahedral corners(Birkeland, 1999; Mitchell, 1993). Figure 3 shows interconnected octahedrons to form an octahedral sheet (Mitchell, 1993).

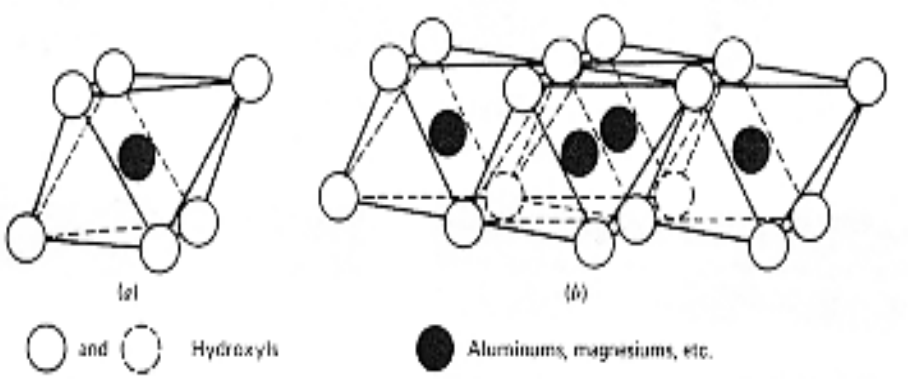

Figure 3. The octahedral unit cell and the octahedral sheet (Grim, 1968, as cited by Mitchell, 1993)

When a trivalent octahedral cation fills two thirds of cationic spaces available inside the octahedral sheet, the structure is called as a dioctahedral sheet. The composition for aluminum centered octahedron or gibbsite mineral is $Al_2 (OH)_6$. When a divalent cation positioned at the center fills all the available cationic spaces inside an octahedron, the structure is called as a trioctahedral sheet. If magnesium is coordinated at the center instead of an aluminum atom, it is called brucite (Birkeland, 1999; Mitchell, 1993).Figure.4 and Figure.5 shows Dioctahedral and trioctahedral sheets respectively.

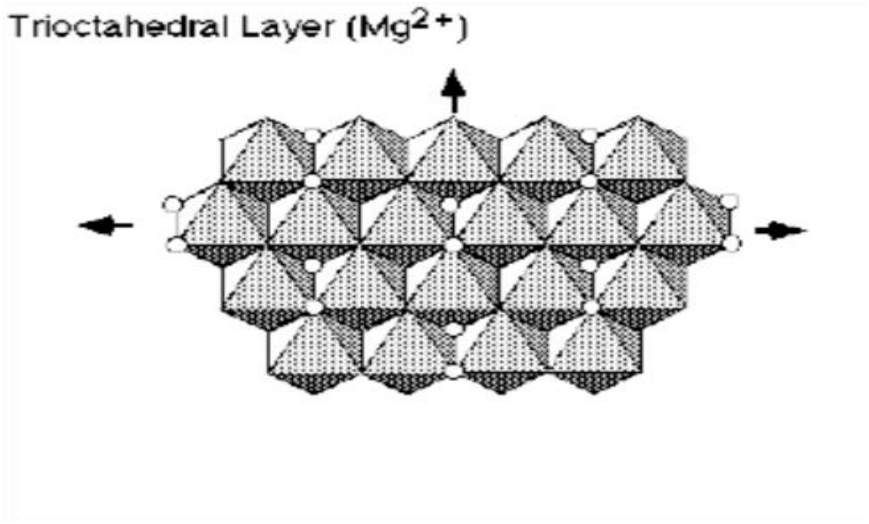

Figure 4. Trioctahedral layer (Grim, 1968, as cited by Mitchell, 1993)

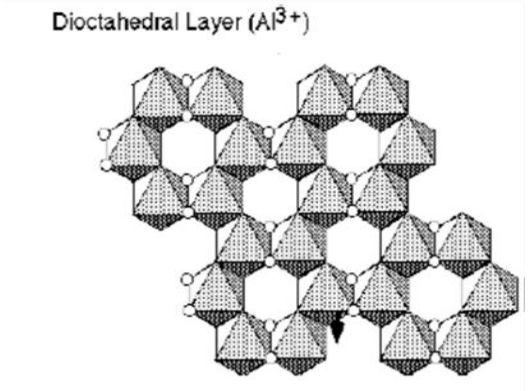

Figure 5. Dioctahedral layer (Grim, 1968, as cited by Mitchell, 1993)

Clay minerals are layered structures they stack one above the other to form tetrahedral-octahedral sheets. The Tetrahedral sheet consists of Si^{4+} atoms and octahedral sheets consist of Al^{3+}, Mg^{2+} and Fe^{3+}atoms.A combination of one tetrahedral and one octahedral is referred as 1:1 clay (T-O clay). Similarly, a sandwich of tetrahedral-octahedral-tetrahedral sheets is called 2:1 clay (T-O-T clay). The Tetrahedral and octahedral sheets share same oxygen atoms located at the basal plane. A combination of the tetrahedral and an octahedral sheet makes one clay layer.

Clay sheets are negatively charged particles; this is due to the isomorphic substitution of metal atoms in octahedral or tetrahedral sheets. When Si^{4+} atoms in the tetrahedral sheet are replaced with Al^{3+}, Mg^{2+} and Fe^{3+} atoms and Fe^{3+} for Al^{3+} in the octahedral sheet. The overall process is called isomorphic substitution. The empty space between any two successive clay layers is called interlayer or interlayer spacing; this interlayer is filled with cations or counter ions like sodium, magnesium, potassium and calcium. These cations are positively charged ions and balance the overall net negative charge created by clay sheets. Cations generate non-bonded interactions with clay sheets and hold these clay sheets together. These non-bonded interactions decrease in the presence of water which leads to swelling of clay minerals. The layer charge decreases as the surface hydrophobicity increases. Pyrophyllite and talc are uncharged mineral types of

Montmorillonite and vermiculite, which have hydrophobic siloxane surfaces. The siloxane surfaces are coordinated at the base of tetrahedral sheets, these sheets consist of oxygen atoms exposing on the surface of the clay layer (Sposito et al., 1999).

The 1:1 and 2:1 clay minerals are stacked in c-direction to form clay layers. The bonded interaction between layers is explained with several mechanisms. Surface oxygen atoms are bonded with hydroxyls of an adjacent layer; this creates hydrogen bonds between layers. Hydrogen bonds also form between two successive clay layers in the presence of water molecules in the interlayer. The counter ions can form a bond with surface oxygen atoms. The bonding between cations and TOT sheets are relatively loose when they are far from each other. The minerals can contract and expand during in the presence of water molecules.

2.1. Cation Exchange Capacity

The counter ions present inside the interlayer can be replaced with other cations under suitable conditions; this property is often referred as cation exchange capacity (CEC). CEC depends upon pH, electrolyte content and size of the clay mineral. The chemical activity and interaction with ions of clay minerals can be described by CEC. Water molecules are often adsorbed with cations to cause swelling. The total number of cations adsorbed by clay surface is not same for all ionic species (Velde, 1992). When more than one type of cations are mixed with soils, clay minerals normally adsorb the cations with a higher charge, this due to the lower atomic radius of high charge cations (Dixon, 1989). The selection of cations depends on the attraction between clay surface and residual ions in the solution. When ions are displaced by other ionic species, ions are desorbed. The desorbed ionic species is displaced by other ionic species , the ion is exchanged (Velde, 1992).

The broken bonds of smectite minerals may also contribute to CEC. The broken bonds of smectite minerals have OH's which is a pH dependent charge (Dixon, 1989). These broken bonds create charge difference at the edge of the clay structure; the charge is balanced by adsorbed cations. The particle breakdown of clay minerals decreases clay mineral size and increase the number of broken bonds, this also increases CEC. Generally in smectite and vermiculite clay minerals 20% of CEC is contributed by broken bonds. Smectite clay minerals have the ability to hold fertilizer ions strongly; this property of smectite minerals avoids leaching of cations from the surface of clay sheets and helps in retaining fertility of soil.

2.2. Type of Clay Minerals

Clay minerals are largely classified in to smectite, kaolinite, illite, halloysite, chlorite vermiculite, attapulgite-palygoskite-sepiolite, and allophone. Smectite, kaolinite and illite are commonly found clay minerals in soils.

2.2.1. Kaolinite

Kaolinite minerals are 1:1 minerals; these minerals do not show swelling behavior in water. There are no cations in the interlayer(Mitchell, 1993; Van Olphen, 1979). Electrostatic and Van der Waals interactions dominate bonding between layers is dominated by electrostatic attraction with some VdW interactions between clay sheets. Hydroxyls of a clay sheet make a bond with oxygen atoms of the other clay sheet. The dimensions of kaolinite clay minerals normally vary from 0.1 to 0.4 μm and thickness 0.05 and 2 μm (Mitchell, 1993).

2.2.2. Pyrophyllite

These 2:1 clay minerals are electrically neutral and do not swell in water. The chemical composition of pyrophyllite is as follows $Al_4Si_8O_{20}$ $(OH)_4$ (Newman, 1987). Pyrophyllite minerals have Dioctahedral sheets. These minerals occur where weathering of soils is observed.

2.2.3. Illite

Illite are 2:1 minerals and do not swell in water. Isomorphic substitutions only restricted to tetrahedral sheets, potassium ions are present in the interlayer as counter ions and these counter ions are not available for cation exchange. The clay sheets are intact with each other due to the non-bonded interactions generated with interlayer cations. Potassium ions are coordinated with oxygen atoms of hexagonal cavity. The CEC of Illite is 10 to 40 meq/100g. Normally, minerals with CEC values more than 10 to 15 meq/100g exhibit some swelling. The non-bonded interaction between potassium ions and clay sheets is so strong, the d-spacing remain 10A° in the presence of polar liquids. These minerals are small flaky plate like structures. The dimensions of Illite minerals vary from 0.1μm to several micrometers and the thickness of these minerals is 30A°. The specific surface area of Illite minerals is about 65 to 100 m^2/g (Mitchell, 1993).

2.2.4. Vermiculite

Vermiculite minerals are 2:1 clay minerals; these clay sheets have Dioctahedral and Trioctahedral sheets. The isomorphic substitution can be observed mainly in tetrahedral sheets. The successive sheets held together tightly by interaction with cations, the swelling behavior of these minerals is limited (Birkeland, 1999).

The negative charges of vermiculite clay minerals normally range in between 1 to 1.4. These minerals exhibit high CEC in the range 100 to 150 meq/100g. The d-spacing of these minerals

normally varies from 10.5 to 12.2A° and the specific surface area of these minerals is about 40 to 80 m^2/g (Mitchell, 1993).

2.2.5. Chlorite

Chlorite is a 2:1:1 clay mineral. Chlorite minerals consist of an extra octahedral sheet alternating in 2:1. The isomorphic substitutions of Al^{+3} and Si^{+4} are found in the tetrahedral sheet resulting in negative charge. The octahedral sheets have Mg, Fe, Fe and Al atoms. The layer expansion is not observed due to strong interactions between the sheets (Birkeland, 1999). CEC of chlorite minerals is in the range 10 to 40 meq/100g and basal spacing is about 14A°.

2.2.6. Sodium-Montmorillonite

Smectite clay minerals with the rich source of sodium ions as counter ions are called sodium Montmorillonite (Na-MMT); these are 2:1 clay minerals. These clay minerals undergo huge volumetric changes when they interact with water; this behavior is often referred as swelling. The Na-MMT clay minerals are found with varying swelling potential. Within the zone of weathering these clay minerals can exert a large amount of stresses to surrounding areas and damage substructure and superstructure. Sodium-Montmorillonite (Na-MMT) is an active clay mineral which shows very high swelling characteristics. The swelling behavior is classified in to crystalline swelling and osmotic swelling. Crystalline swelling is a short-range swelling; it explains the initial hydration mechanism of smectite minerals. Crystalline swelling describes the swelling behavior of smectite minerals within in the range of 9.6A° to 20 A° of the layered spacing. Water molecules enter in to the interlayer and initiate the process of swelling. The water molecules inside the interlayer stack one above the other in layers.

Smectite clay minerals exhibit osmotic swelling. This is due to a large ionic concentration of counter ions in the interlayer than the surrounding moisture content, which increases interaction between water and counter ions, as a result more water molecules flow in to interlayer to balance the ionic equilibrium. Osmotic swelling can increase the layer spacing from 20 A° to 130 A°.

Generally smectite clay minerals have negative charge in the range of 0.5 to 1.20. The octahedral sheets are sandwiched between two tetrahedral sheets and generate T-O-T structure. Oxygen atoms located at the tip of tetrahedral sheets are pointing in the same direction. The hexagonal cavities are formed at the basal planes of silica tetrahedrons and anions of octahedral sheet is located above and below of hexagonal cavities (Mitchell, 1993). The structure of Montmorillonite is shown in figure 6

Sodium-Montmorillonite is continuous in horizontal (a-b) axes and stacks one above other in vertical (c) axis. The bond between layers can be separated by adsorption of water and other polar solvents. Distance from the bottom of a top clay sheet to the bottom of the bottom clay sheet is called d (001)-spacing. The unit cell dimensions normally are in the range a≈5.15A° to b≈8.9A°, Figure 7 shows the unit cell dimension of clay sheets (van Olphen, 1977).

The ditrigonal and hexagonal symmetry occurs due to the clockwise and counter clockwise rotation of silica tetrahedrons along the vertical axis. These ditrigonal cavity of smectite minerals consist oxygen atoms. Figure.8 and Figure.9 shows hexagonal and ditrigonal cavities of smectite minerals.

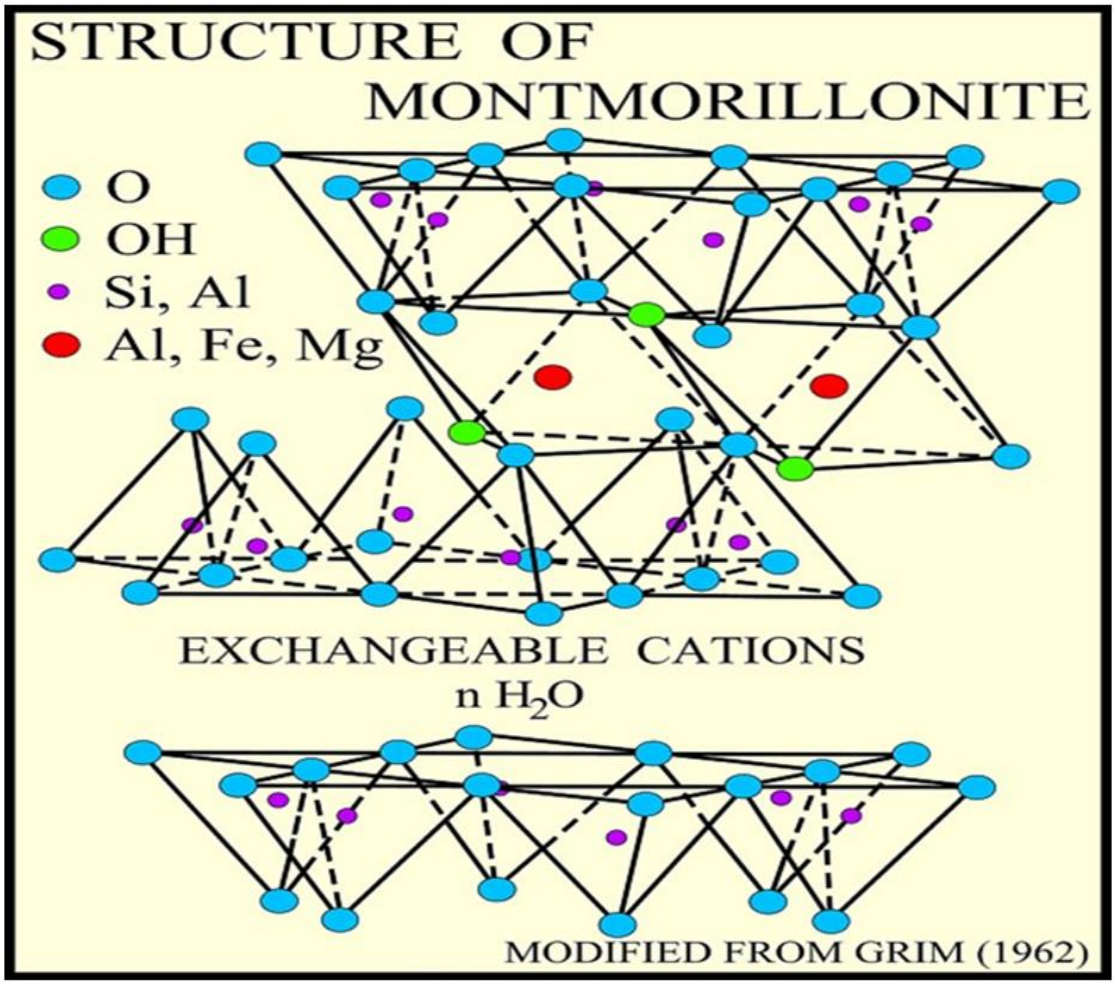

Figure 6. Structure of Montmorillonite (Grim, 1962, cited by Mitchell 1993)

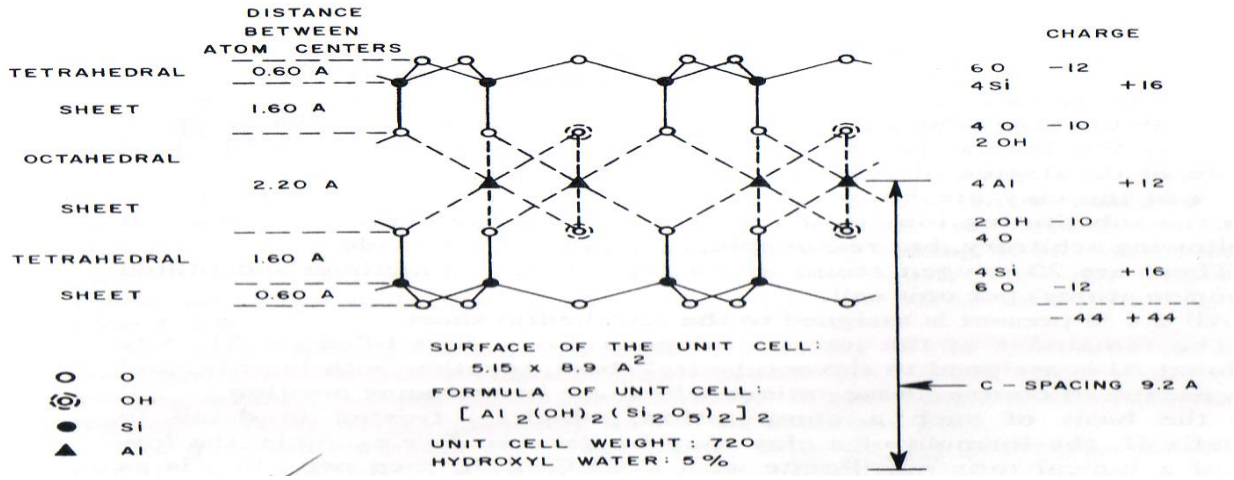

Figure 7. Unit cell dimensions of a 2:1 clay mineral (van Olphen, 1977)

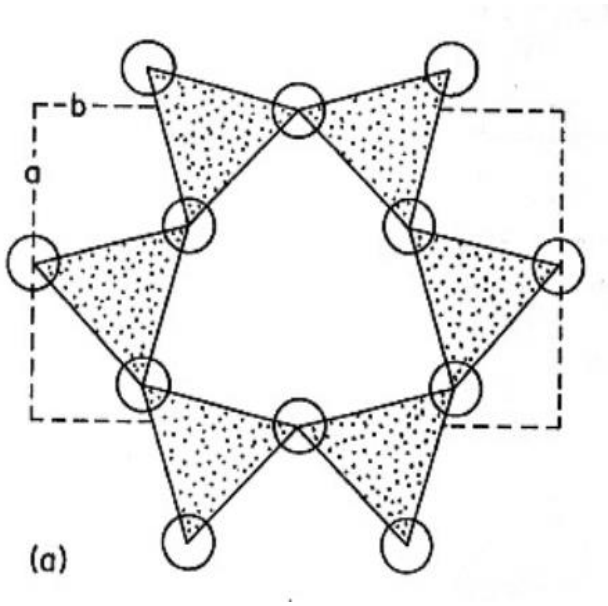

Figure 8. Ditrigonal cavity (van Olphen, 1977)

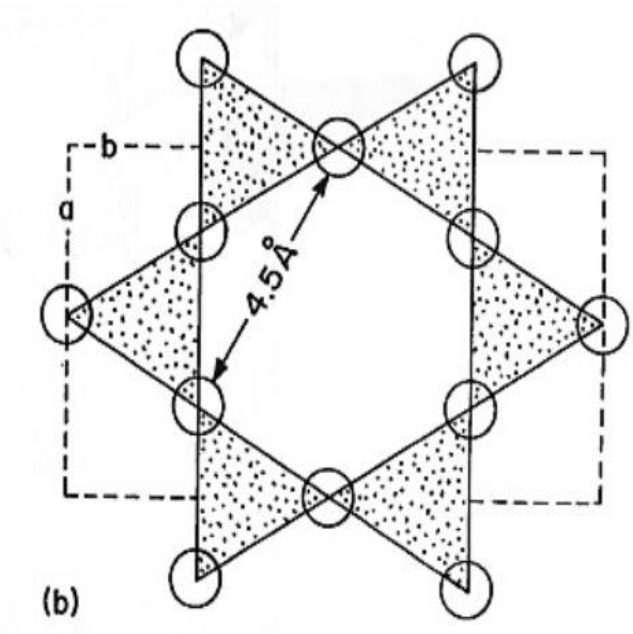

Figure 9. Hexagonal cavity formed by smectite minerals (van Olphen, 1977)

2.3. Water Molecules

Physical behavior and structure of a water molecule near the surface of a clay sheet is different than normal water. This behavior is limited for the smaller distances from the surface. Different clay minerals interact with water molecules differently to change its structure from ordinary water to non-ordinary water (Grim, 1968). These water molecules form a thin film over the clay surface, the thickness of the film can reach the maximum in smectite clay minerals.

Several theories are developed to explain the behavior of hydrated water molecules near the clay surface. Water molecules are dipolar, the positive charges of water molecules orient towards the negative charge surface of the clay layer. Water molecules near the surface arrange themselves in layers, this self-arrangement break as the distance between water molecules and clay surface increase. Some theories have predicted that the structure of water molecules near the surface of the clay layer is similar to ice; this is because of the hexagonal surface of clay sheet and hydrogen bonding between water molecules (Grim, 1968).

At atmospheric temperature and pressure, the water molecules of ice form strong hydrogen bonds with each other and build a strong hydrogen bond network. The same behavior of the regular arrangement of water molecules is predicted in the interlayer. Silicate sheet and cations also interact with water molecules (Brindley and Brown, 1980).

Hydrogen bond links also observed between water molecules and surface oxygen atoms of clay sheet, the strength of this hydrogen bond depends upon tetrahedral charge of clay minerals. Generally weak hydrogen bonds form between clay surface and water molecules in the proximity of clay surface. Interlayer water molecules are more acidic than normal water molecules (Dixon, 1989).

Interlayer cations hold clay sheets; these cations are located near the clay surface. Water molecules also held by these cations, interaction between cations and water molecules also affect the structure of water molecules near a clay surface. The charge, electronegativity, hydration-energy and the size of counter ions also influence the properties of water molecules near the surface. During the time of hydration counter ions are attracted towards the surface oxygen atoms of dry clay sheets (Grim, 1968).

At a lower layer charge and high chemical potential of water, cations trigger the hydration process by attracting water molecules and forms first mono layer of water inside the interlayer (Bleam, 1993). Water molecules form one, two, three and four layers. Basal spacing increases as the number of water molecules or the water layers increase in the interlayer (Brindley, 1980).

Water content in the interlayer can be removed from three different areas. Water content around clay sheets, in the pores and on the surface can be removed at lower temperature. Interlayer water molecules also found in vermiculite and smectite minerals (Grim, 1968; Dixon, 1989). Smectite minerals lose Interlayer water molecules at temperature 100 °C. Drying at higher temperature dehydrates the interlayer. Dehydrating clay minerals at temperature 450 °C would dehydrate the interlayer completely, this collapses the interlayer. Rehydration of interlayer is slightly difficult after complete dehydration or collapse of the interlayer. This is probably due attraction between cations and octahedral charge of the sheet (Grim, 1968, Brindley, 1980). If there is some moisture content left in the interlayer rehydration can take place under atmospheric humid conditions (Newman, 1987).

2.4. Occurrence of Clay Minerals

Clay minerals occur in rain fall regions, high intensity of the rainfall increases weathering process of clay mineral formation (Jenny, 1994). Normally, weathering takes place below the surface of a water table or at the surface of the water table. The percentage free moisture content also affects cation concentration of clay-water system. Porosity, cleavage, permeability and water retaining capacity of parental minerals influence the cationic concentration. Pore solutions have chemical composition, biological activity influence the chemical composition and the organic matter (Gillot, 1987)present in the soil (Gillot, 1987; Jackson, 1953).

CHAPTER 3. INTER MOLECULAR FORCES

3.1. Van der Waals Interaction

Van der Waals studied the long range attractive force between neutral atoms or molecules in 1873 while performing experiments on non-ideal gases and liquids (Overbeek, 1952).VdW forces are weak forces exists between neutral atoms, where Coulomb's electro static attraction is between charged species (Anandarajah, 1997b). The net charge of an atom at any specific location and at any given moment is a result of revolving electrons around the nucleus at a high frequency. The frequency of a rapidly revolving electron around the nucleus generates dipole moment fluctuation at a frequency 10^{15} to 10^{16} per second. Mutual polarization of dipole moment between any two atoms attract each other (Overbeek, 1952). The dipole moment continuously fluctuate every moment, a net attractive force develops between the induced and inducing dipoles (De Boer, 1936).

The VdW forces influences physical properties of gases-liquids, adhesion, surface tension, flocculation and agglomeration of fine particles in aqueous solutions. (Israelachvili, 1985).

The VdW interaction between any two atoms in a fluid is always attractive. The Net force become repulsive if the composition of solution is different (Hamaker, 1937).Generally, VdW attractive forces decay at very short distances, for the colloidal particles the attractive force acts over long distances. The VdW attraction between any two atoms can be added over time. The sum of the attractive force between large numbers of atoms is equal to the sum of the attractive force between individual atoms with every atom of the other molecule. The net force is larger and it decreases with an increase in the distance (Overbeek, 1952).

Induction, dispersion and orientation forces are the three important forces which influences Van der Waals force. The dispersion force normally dominates at a separation distance of $1/r^6$ (Israelachvili, 1985).

The VdW attractive force between atoms was treated with London's $1/r^7$ relationship, an attractive force between two atoms decreases beyond the separation distance $1/r^7$ where r is the separation distance (London, 1937). This relationship is valid for gases, in condensed system attractive energy decreases faster than London's distance (Chen, 1996).

London equations for the Van der Waals force were modified by Lifshitz (1956). Lifshitz developed equations for molecules in the vacuum at a separation distance were integrated over the volume of bodies. These equations did not consider the retardation effect proposed by Hamaker (1937). However, Lifshitz equations are applied to calculate the VdW forces of complex geometries (Chen, 1996).

Lifshitz equations and Hamaker's approach was combined together to explain the retardation effect by applying corrections to London's equations (Chen, 1996).

London's equations for dispersion energy with a separation distance r and London constant B, in the vacuum is

$$\boldsymbol{U(r) = -\frac{B}{r^6}} \qquad \textbf{(1)}$$

For two semi-infinite rigid parallel plates with separation distance h and molecular densities ρ_1, $\rho 2$, van der Waals attractive energy was computed by modifying London's equation (Anandarajah, 1995).

$$\boldsymbol{U(h) = -\frac{B\pi\rho_1\rho_2}{12h^2} = -\frac{A}{12\pi h^2}} \qquad \textbf{(2)}$$

Van der Waals attraction and repulsive forces are normally explained by Lennerd-Jones potential, Morse potential and Buckingham potential. Lennerd-jones potential is one of the widely used mathematical models to describe a VdW energy system.

3.2. Double Layer Repulsion in Clay-Water System

Clay minerals are colloidal particles with low water solubility and diameters ranging about 0.1 to 10μm. These particles do not dissolve in water to form a solution. Colloidal particles create a large interfacial phase between solid and liquid phases. Clay minerals are negatively charged and dissolved ions of salts are attracted towards clay sheets in a colloidal suspension (LU, 1991; Sposito, 1989).

Due to the thermal energy carried by colloidal particles, they are under continuous and chaotic motion in a solution, this is called Brownian movement (Sposito, 1989).

The net charge of a clay-water solution can be positive, negative or zero. The zero charge of the system could be observed in well dispersed phase, where particles collide with each other and move away from each other due to Brownian motion. This type of interaction is influenced by thermal motion of water molecules around the colloidal particles. A small amount of addition of salt to a zero charge system changes the ionic concentration of solution and colloids flocculate to settle down. Thermal motions of particles are counteracted by attractive force created dissolved salt in the system so that particles stick with each other and flocculate (LU, 1991).

A deflocculated stable system can be achieved by stirring and removing salt. This behavior shows an existence of a repulsive force between particles (LU, 1991).

The concentration of salt in a solution influences the intensity of electric repulsive forces between particles. The Repulsive force is dominant in a solution of very small concentration and attractive force is dominant in a high concentrated salt solution. The double layer force between

clay particles decrease as the VdW attractions dominates, this happens in a solution of very high ionic concentration. (LU, 1991).Figure 10 shows the potential curves of particles for the three different electrolyte content.

3.2.1. Double layer structure

Electrical negativity of clay minerals is balanced by counter ions which are strongly adsorbed to a clay surface. Excessive cations occur in the soil in the form of salt precipitate and electrical double layer is absent in dry clay minerals (Anderson, 2001).

When clay minerals interact with rain water, the salt dissociates into the solution. High Concentrations of cations can be observed near the clay surface and these cations diffuse towards bulk water solutions to neutralize the concentrations. But the free movement of these cations is restricted by electrostatic attraction of clay sheets.

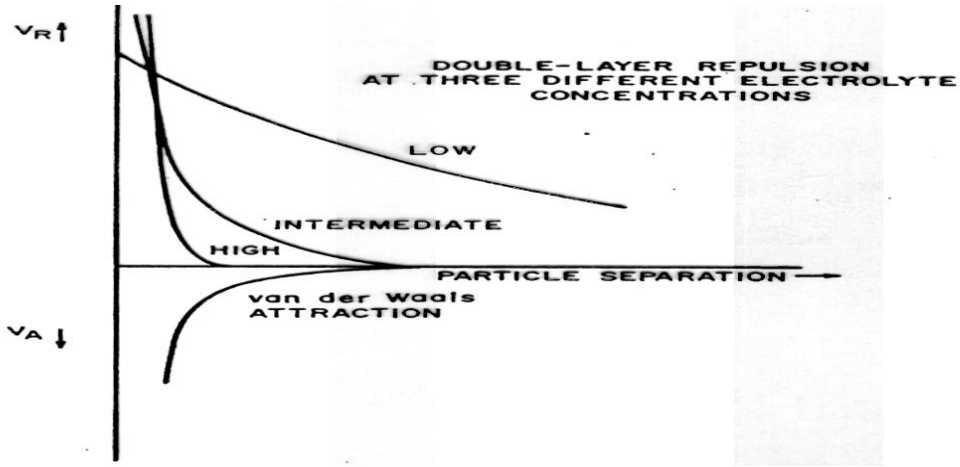

Figure 10. Potential curves of particles as a function of separation distance, for the three electrolyte content (Van Olphen, 1979)

The second layer is created by anions present in solutions, these anions are attracted to cations around the clay sheets, but these are loosely adsorbed to the first layer and they diffuse inside in bulk solution. These interactions create a non-uniform potential in the solution with

maximum potential on the clay surface and a zero potential at a large separation distance. Figure 11shows single double layer, a distribution of particles can be observed around the surface of a clay sheet. The balance between a charged surface and distributed ions around the surface creates a double layer (Chang and Sposito, 1996).

The thickness of the double layer can go up to 10^{-5} cm to 10^{-4} cm in dilute solutions. The thickness of a double layer is lesser in concentrated solutions (Van Olphen, 1979).

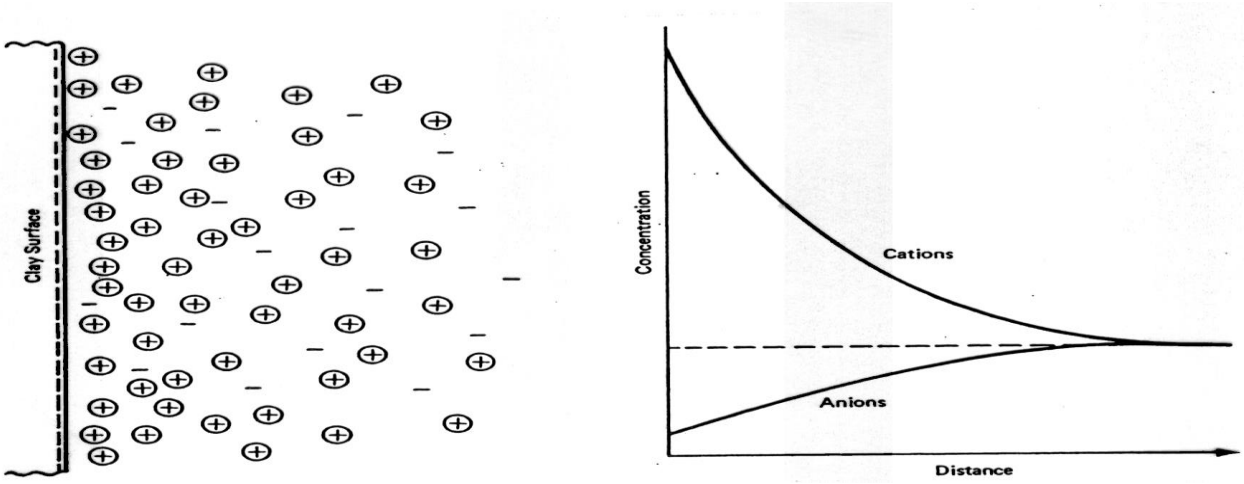

Figure 11. Ionic distributions around the clay sheet in a double layer (Mitchell, 1993)

Several theories have been proposed to explain the double layer theory with some basic assumptions. Solid clay minerals are assumed as sheets or spherical particles and charge on the surface is assumed to be homogeneous, the charges are assumed to be point charges and the first layer formed by these charged particles.

The second layer is formed by particles carrying opposite charges to the first layer charges. These charges are loosely adsorbed to the first layer and fluctuate due to thermal motions and Columbic interactions. As the distance increases the density of second layer decreases (McBride and Baveye, 2002).

Guoy-Chapman proposed one dimensional double layer theory, in which clay sheets are considered infinitely long sheets, size of double layer ions is neglected and considered as point charges and uniform distribution of the surface charges was assumed.

Stern further improved the existing model. The finite dimensions of clay sheets and finite distance between charged surfaces to the counter ion was considered in this model. Density of counter ions is higher than the second layer, size of counter ions also influence the thickness of a layer. According Stern's double layer theory most of counterions diffuse within 10 A° of charged surface. By applying Stern's theory Low identified that, in smectite minerals all the counterions reside in the double layer. This behavior explains that double layer theory is not well developed for smectite minerals. Bolt further developed Guoy-Chapman's theory and correction for distance was also included (Mitchell, 1993; Van Olphen, 1979).

However, pore water structure and swelling properties are generally explained using double layer theory.

3.3. Hydrogen Bonds

Hydrogen bonds are weak bonds between hydrogen atoms with other closely spaced electronegative atoms like Oxygen, Nitrogen or fluorine. Hydrogen bonds are also the combined interactions of electrostatic attractions and other intermolecular interactions. The stronger hydrogen bond H existing between any two atoms X and Y is normally represented as XH–Y; similarly weaker hydrogen bonds are represented as XH•••Y. The distance between atoms strongly influences the formation of hydrogen bonds. Hydrogen bond strength is normally higher between the hydrogen atom and the functional group of another species.

Hydrogen bonds normally exist near electronegative atoms. A Hydrogen bond length of ice is 2.76 A°. Typically, hydrogen bond length varies from 2-4.0 A°. Figure.12 below shows the

hydrogen bond formation in water. Strength of hydrogen bond energy varies from 10 to 40 kJ/mol, which is higher than typical Van der Waals interaction.

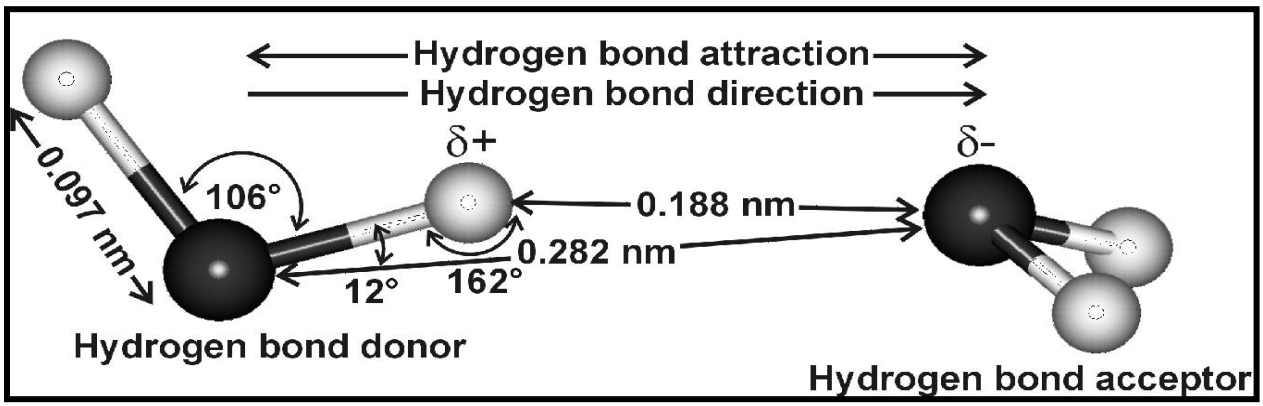

Figure 12. Formation of a hydrogen bond between water molecules (Chaplin, 2010)

A donor and an acceptor are required to form a hydrogen bond. Hydroxyls (OH) of water molecules are the donors and oxygen atom of the other water molecule is an acceptor in a hydrogen bond. An Electrostatic attraction between donor acceptor strongly influences hydrogen bond energy, 80% of hydrogen bond energy is the electrostatic attraction between donor and acceptor, VdW and other intermolecular forces influences the remaining portion of hydrogen bond energy. Hydrogen bonds affect the properties of water viscosity, density, electronic spectra and electrical conductivity (Chaplin, 2010; Pimentel, 1960).

3.4. Osmotic Model of Swelling

Montmorillonite swelling is explained in two phases, type1 swelling phase and type2 swelling phase. Type1 swelling phase is also referred as hydration swelling or crystalline swelling, this type of swelling occurs at the initial stage when clay minerals are in dry state and interacts with water. The attracted water molecules in the interlayer form a stack of water layers. The basal spacing varies from 9-20 A° and up to 4 mono layers of water forms in the interlayer.

Osmotic swelling or type2 swelling is the continuation of crystalline swelling. The basal spacing variation in osmotic swelling varies from 20-130 A°. Several layers of water molecules are observed between clay sheets (Jo et al., 2001; Mcbride, 1994).

When clay minerals are dispersed in a dilute salt solution, it creates an ionic in equilibrium between water -interlayer cations and lower free energy in water molecules. Cations are strongly bound to clay sheets and they don't diffuse out of the interlayer. To achieve an ionic balance water molecules diffuse into interlayer which leads to interlayer expansion. If the salt concentration is increased, water molecules move out of the interlayer causing shrinkage of clay minerals (Mcbride, 1994).Figure 13 and Figure 14 shows the osmotic swelling process.

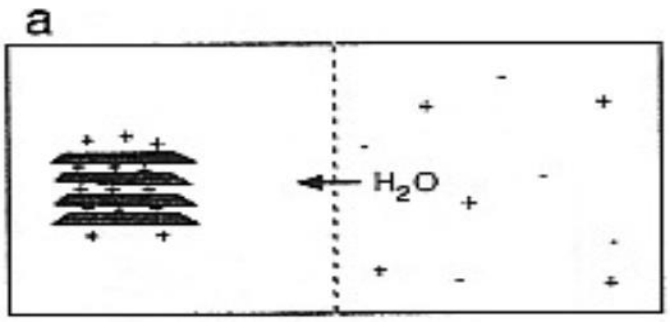

Figure 13. The movement of water molecules towards clay minerals or expansion mechanism of clay minerals (Mcbride, 1994)

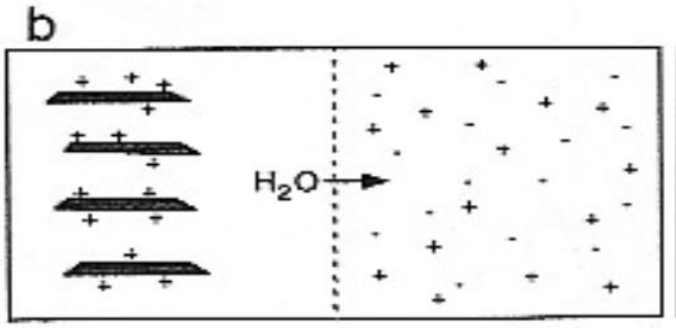

Figure 14. Shrinkage of clay minerals (Mcbride, 1994)

Generally, electrostatic, VdW and osmotic pressure influences this type of swelling. Density of charges, position of cations, electrolyte content and type of cations also affects osmotic swelling (Brindley, 1980) .

Magnitude of the water layer is directly proportional to the concentration of cations in the bulk water. Monovalent Cations of bulk water occupies exchange sites of clay minerals and influences the total bound water. When a divalent or trivalent ions occupy the exchange sites up to 4 monolayers of water forms between the sheets and restrict the swelling to the hydration phase or crystalline swelling phase e.g. calcium-betonies. The Osmotic model only explains the swelling above 20 A° of basal spacing, and this model only applied to low concentrated salt solutions (Mcbride, 1994).Figure 15 shows the variation of the basal spacing of Na and Ca smectites and different mechanisms involved while achieving osmotic swelling..

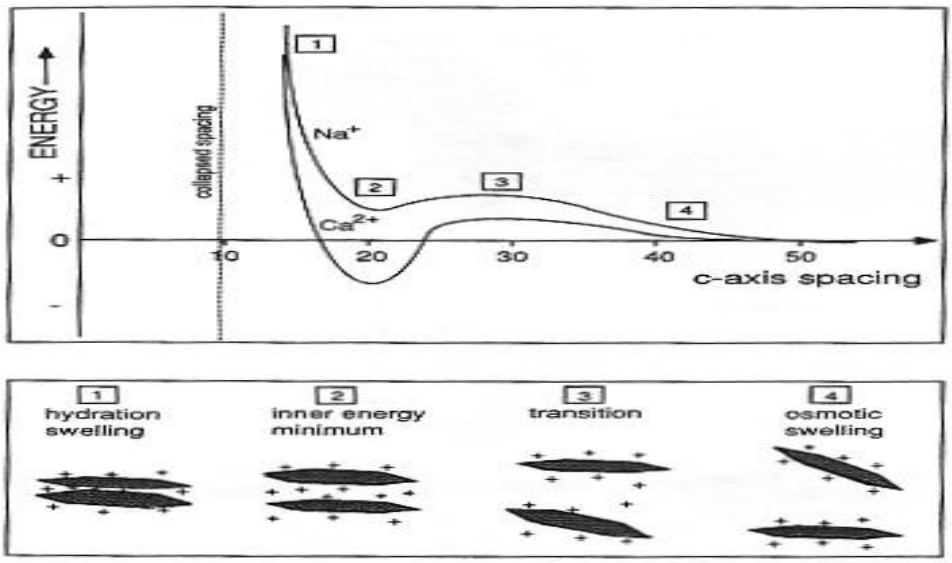

Figure 15. Variation of basal spacing and mechanism of swelling in Na and Ca smectites (Mcbride, 1994)

3.5. Microstructure Evolution

Most of the existing models explain macroscopic behavior clay minerals, and these models do not consider clay mineralogy, pore-water content, the structure and type of ions. Microstructure of expansive soils influences the macroscopic properties and stress-strain response of clay minerals. It is necessary to understand the fundamental mechanism of clay

swelling from molecular to the macroscopic level in order to model the physical properties (Katti and Shanmugasundaram, 2001)

A Controlled uniaxial swelling device was developed to measure swelling and scanning electron microscopy was used to observe microstructural changes. An increase in swelling pressure of dry bentonite from 120 kPa to160 kPa was observed over a period of 21 days. Swelling pressure was observed increasing rapidly to 120 kPa within 24 hours, a gradual increase of swelling pressure was observed from 120 to 160 kPa over a period of 9 to 10days. Figure 16 shows the swelling pressure variation with time. Significant change in swelling pressure was not observed after 10 days.

Clay samples were saturated for minimum 30 days and swelling pressure was recorded at 0, 1,2,4,10,17.5,25,50,75 and 100-percent swelling using controlled uniaxial swelling device. Relative swelling pressure was plotted with swelling percentage and void ratio. Figure 17 shows the variation of relative swelling pressure with swelling percentage and void ratio (Katti and Shanmugasundaram, 2001)).

SEM images were taken to observe the effect of swelling pressure on microstructure. Samples with 0%, 50% and 75% swelling were considered for this experiment. Figure 18, 19 and 20 shows SEM images of clay swelling.

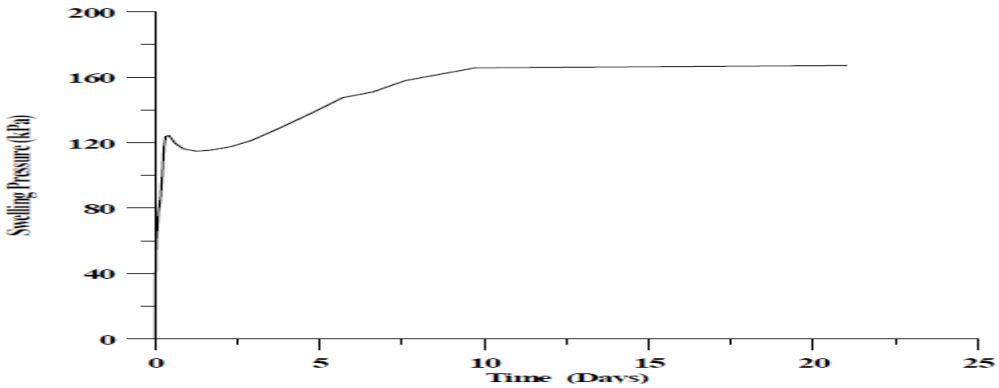

Figure 16. Swelling pressure variations with time (Katti and Shanmugasundaram, 2001)

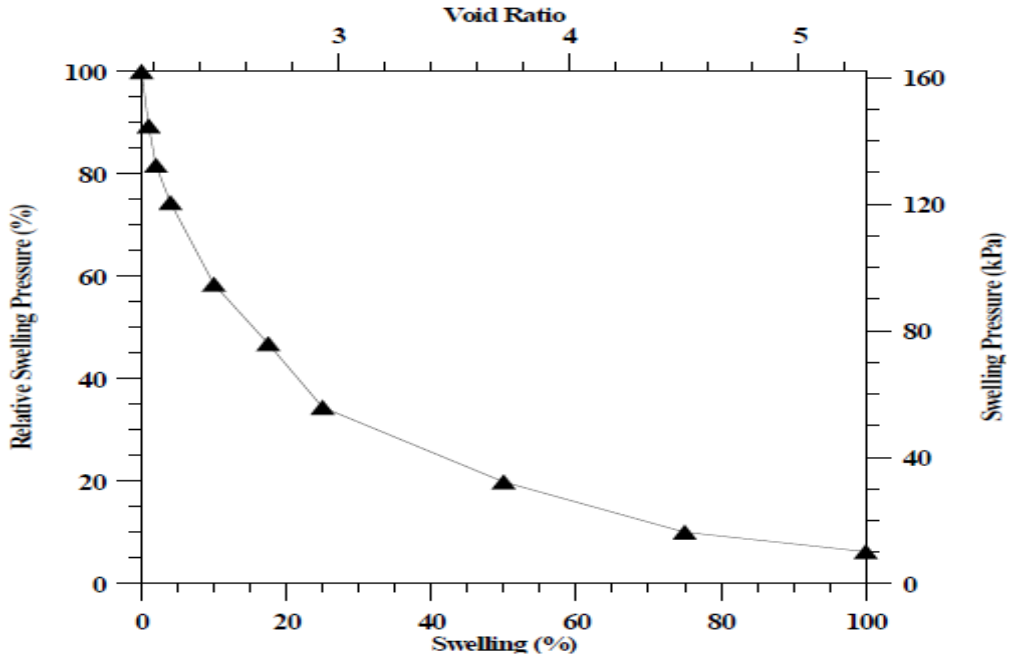

Figure 17. Variation of relative swelling pressure as a function of swelling percentage and void ratio (Katti and Shanmugasundaram, 2001)

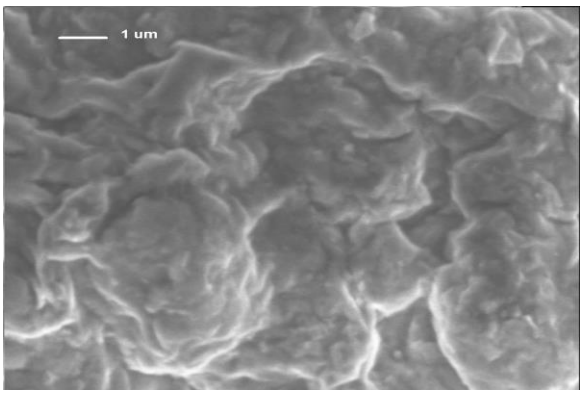

Figure 18. SEM image of the microstructure at 0% swelling

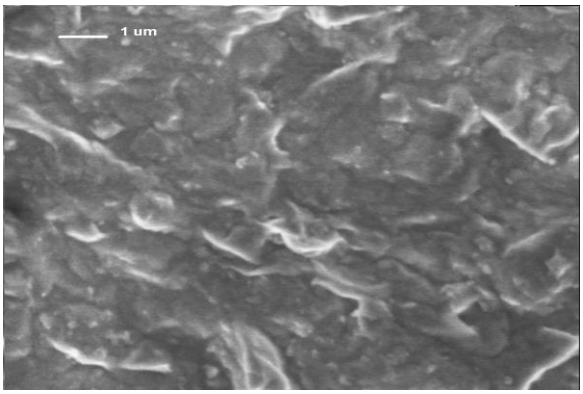

Figure 19. SEM image of the microstructure at 50% swelling (Katti, 2001)

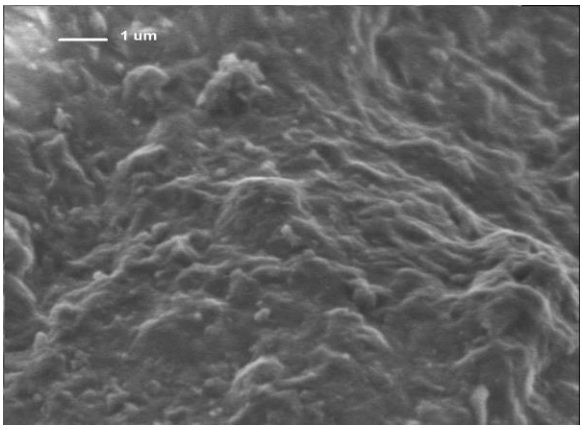

Figure 20. SEM image of the microstructure at 75% swelling (Katti and Shanmugasundaram, 2001)

Figure 21 shows larger sized clay particles at 0% swelling, particles size decrease as swelling progressed. Swelling pressure and particle sub-division increases as water enters to interlayer. Variation of swelling pressure and relative swelling with particle breakdown is shown Figure 21.

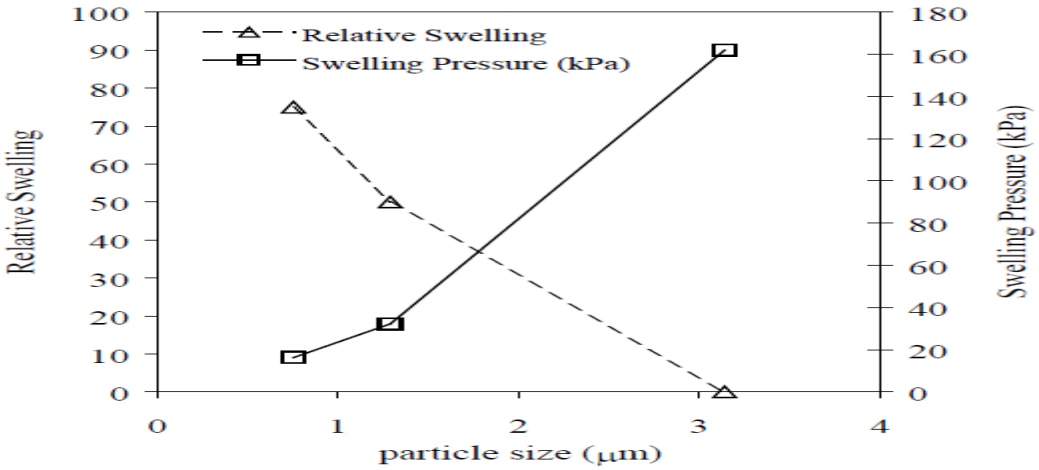

Figure 21. Variation of the relative swelling and swelling pressure with respect to particle size

3.6. Molecular Hydraulic Properties of Swelling Clays

FT-IR experiment s was performed over super saturated Na-Montmorillonite samples. Na-Montmorillonite- water slurries were prepared with 400% moisture content. The 3630 cm^{-1}

band was referred to O-H stretching vibration of the structural hydroxyl group. Broadening of these bands up to 3000 cm^{-1} was observed. This behavior is attributed to the strong hydrogen bond formation between structural hydroxyl group and water molecules. With the increase in clay-water interaction time, the O-H stretching band shift 3000-3500cm^{-1} to 3000-3400 cm^{-1} was observed in water and narrowing of the structural hydroxyl group O-H stretching was noticed. The Figure 22, 23 and 24 shows FT-IR spectra of Na-Montmorillonite slurries with time.

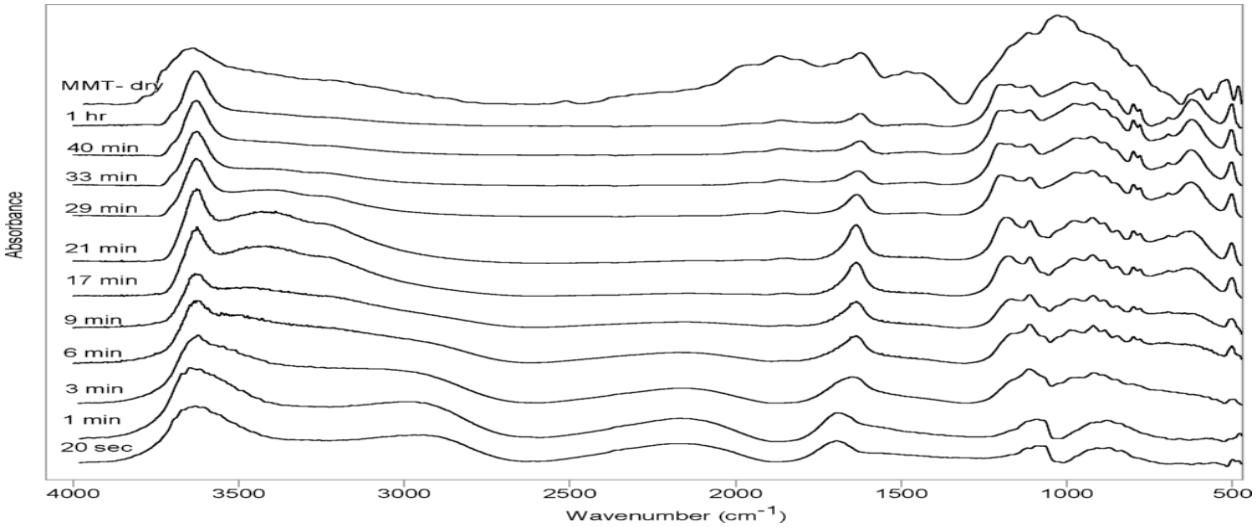

Figure 22. *p*-Polarized reflectance FT-IR spectra of clay-water slurry with the time

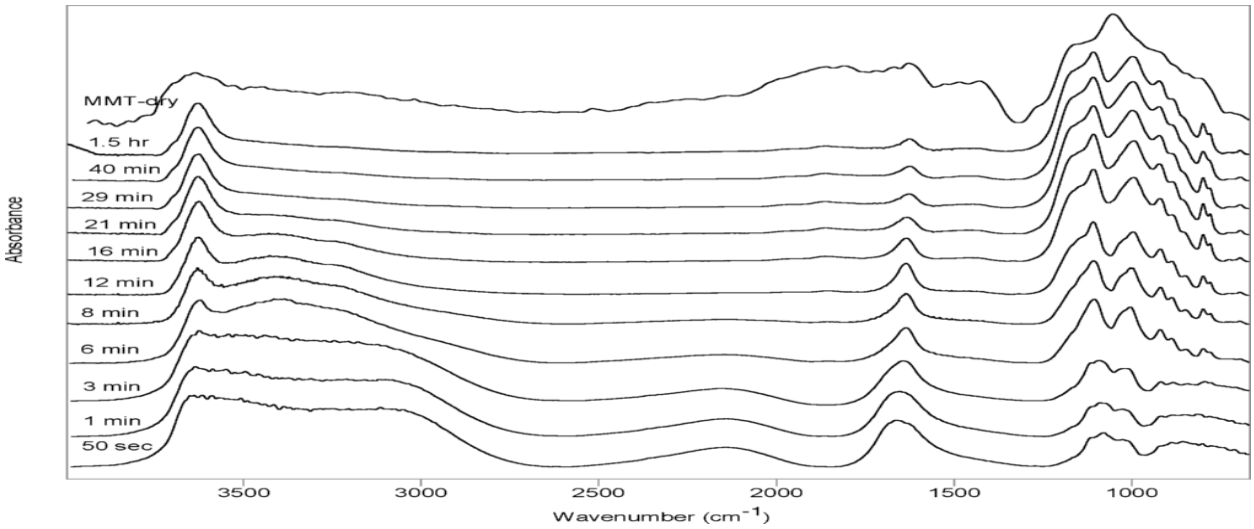

Figure 23. *s*-Polarized reflectance FT-IR spectra of clay-water slurry with the time

The H-O-H bending vibration of water molecules shifts to lower energy from 1694cm^{-1} to 1634cm^{-1}. This behavior was probably due to the lower degree of freedom for interlayer water molecules.

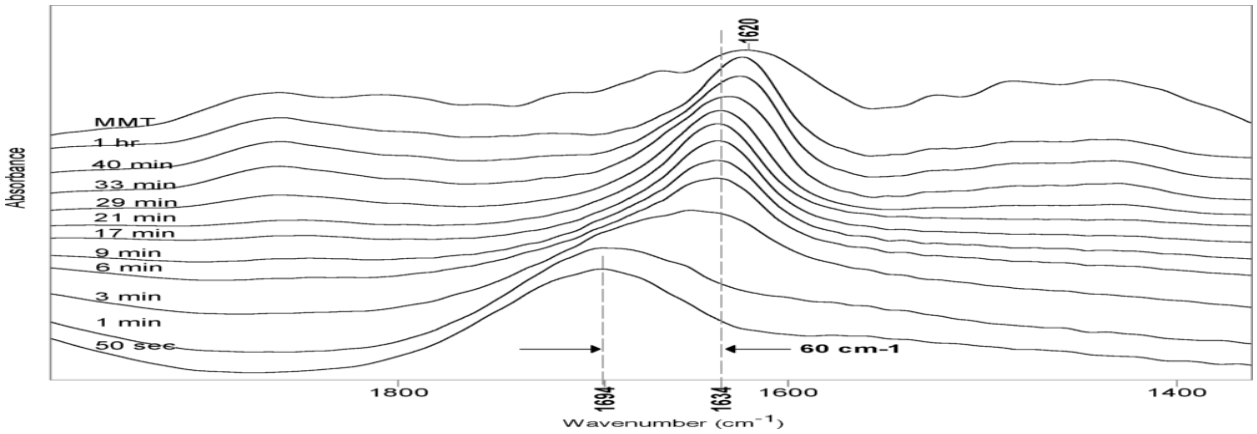

Figure 24. FT-IR spectra of H-O-H bending of bulk water to structural water

XRD experiments were performed to understand Na-Montmorillonite swelling process. Slurry of clay and water was prepared with different moisture content and soaked for 25minutes. Change in d-spacing was measured with an increase in time. Further these results were used in calculating flow rate. Figure 25 shows change in d-spacing of Na-Montmorillonite with time. The flow rate of water was reported as 3.22X10^{-9}cm/s.

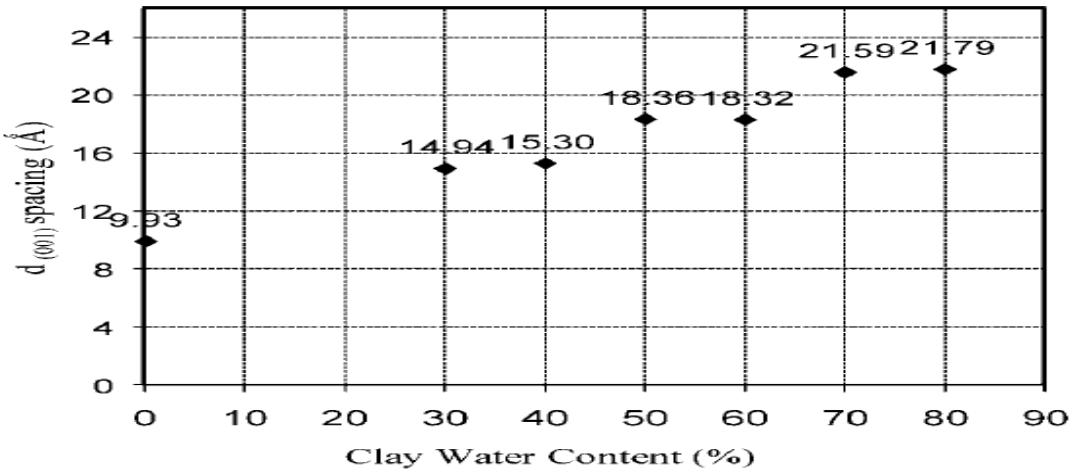

Figure 25. Na-Montmorillonite water slurry d-spacing variations with time

CHAPTER 4. MODELING BACKGROUND AND SIMULATION DETAILS

4.1. Discrete Element Modeling and Molecular Modeling

Discrete element modeling simulations are used to estimate the properties of particulate materials like sand, silt and clay minerals with no swelling behavior. Frictional forces, buoyancy and gravity are considered in these models. Physico-chemical forces like VdW force, double-layer repulsion is considered in this modeling approach.

Particle orientation in one dimensional compressed Montmorillonite was observed using discrete element modeling (Anandarajah, 1997a).Two dimensional DEM was used to understand the role of microscopic forces in the volumetric behavior of clay sediments. The microscopic forces like settling velocity of spherical particles, free swelling of kaolinite, Na-Montmorillonite and Ca-Montmorillonite was studied (Anderson, 2001). Yao and Anandarajah developed a 3-dimensional DEM model, which accounts Physico-chemical forces involved in the clay-water system (Anandarajah, 2002).

Several computational works on clay –water interactions have been appeared using molecular modeling (Chang et al. 1995; Delville 1991; Delville 1995; Hensen 2012; Shroll and Smith 1999; Skipper et al. 1995; Sposito et al. 1999; Teppen et al. 1997); (Hensen 2002). Most of these works addressed molecular interactions between clay sheets and interactions of interlayer sodium with water. Mechanical behavior of Sodium Montmorillonite was evaluated by Steven R. Schmidt et.al (2005) using Steered Molecular Dynamics (SMD) simulations. In this work mechanical response of Na-MMT with multiple layers of water was calculated. SMD simulations are also used to calculate stress-strain response of clay with amino acids (Katti et.al

2005b). Mechanical behavior of dry Na-MMT and slightly hydrated Na-MMT was estimated using SMD simulations (Katti et al. 2007).

4.2. Molecular Dynamics

Molecular Dynamics (MD) simulation is a computational method which is used to determine trajectories of atoms and molecular interactions using Newton's laws of motion. In this study MD simulation was used. MD simulations were first used by Stillinger and Rahman (1974) to simulate water. MD technique is based on Newton's second law of motion F = ma, where 'F' is the force exerted by on an atom, 'm' is the mass of an atom and 'a' is the acceleration of an atom. For the set of 'N' number of atoms, the second law of motion can be written as follows:

$$\mathbf{m_i a_i = -dU_{total}/dr_i = F_i} \quad \textbf{(3)}$$

Where m_i and a_i is the mass and acceleration of an atom i respectively; U_{total} is the total potential energy of the system, r_i is the position of an atom i and F_i is the force exerted on atom i. The acceleration and the velocity of an atom can be related as follows:

$$\mathbf{a_i = dv_i/dt} \quad \textbf{(4)}$$

$$\mathbf{v_i = dr_i/dt} \quad \textbf{(5)}$$

The knowledge of forces, atomic masses of atoms and by allowing atoms to interact for a very small time dt it is possible to calculate the find the position of an atom, hence the trajectory of an atom can be calculated as follows:

$$\mathbf{-dU_{total}/dr_i = m_i\, dr_i^2/dt^2} \quad \textbf{(6)}$$

Total potential energy of a system U_{total} can be represented by a following equation

$$\mathbf{U_{potential} = U_{bond} + U_{angle} + U_{dihedral} + U_{nonbonded}} \quad \textbf{(7)}$$

U_{bond} is the energy stored in a bond between two atoms, when a bond is stretched or compressed from a reference or equilibrium position. U_{angle} and $U_{dihedral}$ are the energy stored between three or four atoms when the atoms are allowed to move away from each other from an equilibrium position, the resulting change in angle and the dihedral position are represented by U_{angle} and $U_{dihedral}$ respectively.

Non-bonded energy ($U_{nonbonded}$) consists of Van-der-Waals (VdW) interaction and electrostatic interaction. Van der Waals interactions are long range interactions between atoms that show a dominant weak attraction at a very large distance 'r_{ij}' due to mutual polarization of atoms, at a very small distance 'r_{ij}' atoms strongly repel each other to avoid the overlap of electronic wave functions, this effect increases the total kinetic energy between atoms known as core repulsion. The electrostatic interaction is the short range interaction that decreases with an increase in the distance between atoms. Coulomb's equation was considered in this study to calculate the electrostatic interaction between atoms.

The Force field is a potential energy equation with parameters that describes the behavior of different molecules and atoms in a system. Consistent Force Field (CFF) and Chemistry at HARvard Molecular Mechanics (CHARMM) are widely used force fields. The parameters of these force fields are originally derived using computer simulations called the ab-initio molecular orbital theory. The potential energy expression of CFF is given as follows.

$$\cup_{\boldsymbol{potential}} = \sum_{\boldsymbol{bond}}\left[\mathbf{k}^{\mathbf{2(r-r_\circ)2}} + \mathbf{k}^{\mathbf{3(r-r_\circ)3}} + \mathbf{k}^{\mathbf{4(r-r_\circ)4}}\right] + \sum_{\boldsymbol{angle}}\left[\mathbf{k}^{\mathbf{2(\theta-\theta_\circ)2}} + \mathbf{k}^{\mathbf{3(\theta-\theta_\circ)3}} + \mathbf{k}^{\mathbf{4(\theta-\theta_\circ)4}}\right] + \sum_{\boldsymbol{dihedral}}\sum_{\boldsymbol{n=1}}^{\boldsymbol{3}}[\boldsymbol{V_n}^{\boldsymbol{D}}[\mathbf{1} - \mathbf{cos}(\boldsymbol{n\phi} - \boldsymbol{\phi_{\circ n}})] + \sum_{\boldsymbol{van\ der\ Waals}}\sum_{\boldsymbol{i\neq j}}\left[\frac{\boldsymbol{A_iA_j}}{\boldsymbol{r_{ij}^9}} - \frac{\boldsymbol{B_iB_j}}{\boldsymbol{r_{ij}^6}}\right] + \sum_{\boldsymbol{electrostatic}}\sum_{\boldsymbol{i\neq j}}\frac{\boldsymbol{q_iq_j}}{\boldsymbol{r_{ij}}} \quad \textbf{(8)}$$

Where k_2, k_3 and k_4 are force constants of bonds and angles, $V_n{}^D$ is the force constant of dihedral motion, $\mathbf{r}$, $\boldsymbol{\theta}$, and $\boldsymbol{\phi}$ are present values of bond lengths, bond angles and bond dihedrals; $\mathbf{r}_\circ$, $\boldsymbol{\theta}_\circ$ and $\boldsymbol{\phi}_{\circ n}$ are equilibrium values bond lengths, bond angles and bond dihedrals; $\boldsymbol{n}$ is the periodicity parameter of dihedral angle; $\boldsymbol{A_i}$ $\boldsymbol{A_j}$ and $\boldsymbol{B_i}$ $\boldsymbol{B_j}$ are van der Waals parameters of atoms i and j; $\boldsymbol{r_{ij}}$ is the separation distance between two atoms; $\boldsymbol{q_i}$ $\boldsymbol{q_j}$ are Columbic charges of atoms i and j respectively, the total potential expression of CHARMM force field is as follows.

$$\cup_{\boldsymbol{potential}} = \sum_{\boldsymbol{bond}}[\boldsymbol{k_b}(\mathbf{r}-\mathbf{r}_\circ)^2] + \sum_{\boldsymbol{angle}}[\boldsymbol{k_a}(\boldsymbol{\theta}-\boldsymbol{\theta}_\circ)^2] + \sum_{\boldsymbol{dihedral}}[\boldsymbol{V^D}[\mathbf{1}+\mathbf{cos}(\boldsymbol{n\phi}+\boldsymbol{\delta})] + \sum_{\boldsymbol{van\ der\ Waals}}\sum_{i\neq j}\mathbf{4}\boldsymbol{\varepsilon_{ij}}\left[\left(\frac{\sigma_{ij}}{r_{ij}}\right)^{\mathbf{12}} - \left(\frac{\sigma_{ij}}{r_{ij}}\right)^{\mathbf{9}}\right] + \sum_{\boldsymbol{electrostatic}}\sum_{i\neq j}\boldsymbol{\epsilon_{14}}\frac{\boldsymbol{Cq_iq_j}}{\boldsymbol{\epsilon r_{ij}}} \quad \textbf{(9)}$$

where $\boldsymbol{k_b}$,$\boldsymbol{k_a}$ and $\boldsymbol{V}^{\boldsymbol{D}}$ are force constants of bonds, angles and dihedrals respectively; $\boldsymbol{\delta}$ is the phase angle of dihedral motion; $\boldsymbol{\varepsilon_{ij}}$ and $\boldsymbol{\sigma_{ij}}$ are non-bonded van der Waals parameters of the atoms' pair i and j respectively.

4.3. Bonded Interactions

Bonded interactions involve 2-body, 3body and 4-body vibrational motion of atoms. The vibrational motion of covalently connected atoms (i, j) is represented by the equation shown below

$$\boldsymbol{U_{bond}} = \sum_{\boldsymbol{bond}}[\boldsymbol{k_b}(\mathbf{r}-\mathbf{r}_\circ)^2] \quad \textbf{(10)}$$

Where r_0 is the equilibrium bond length at unperturbed state, r is the bond length between two atoms at any given time instant $\vec{r} = \| \vec{r}_j - \vec{r}_i \|$ and k_b is the spring constant.

Angular motion between three covalently bonded atoms (i, j and k) is represented by the equation;

$$\boldsymbol{U_{angle} = \sum_{angle}[k_a(\theta - \theta_\circ)^2]} \quad \textbf{(11)}$$

Where θ_0 is the angle between atoms at unperturbed state and $\overrightarrow{r_{ij}} = \| \vec{r_j} - \vec{r_i} \|$ and $\overrightarrow{r_{jk}} = \| \vec{r_j} - \vec{r_k} \|$ is the angle $\boldsymbol{\theta}_\circ$ between the vectors in radians.

The torsional motion of 4 atoms (i, j, k and l) connected consecutively to one other is represented by the following equation

$$\boldsymbol{U_{dihedral} = \sum_{dihedral}[V^D[1 + \cos(n\phi + \delta)]} \quad \textbf{(12)}$$

4.4. Non Bonded Interactions

Bonded interactions are further classified as Van der Waals and Electro static interaction.

4.4.1. Van der Waals interactions

Van der Waals interaction between any two neutral atoms is explained by using the Lennerd-jones potential system.

4.4.2. Lennerd–Jones potential system

The potential energy between two electrically neutral molecules can be calculated using the first principles of quantum mechanics and it can be applied for modeling purposes, but constructing such a model and calculating forces by the first principles of quantum mechanics for a large system would be tedious and too complex. So it is usually better to choose a simple form of potential. The prominent features of this form of the equation is when (r) is small it shows a strong repulsion between molecules and an attraction when the (r) is sufficiently large, this can be Explained by using Pauli's exclusion principle. That is the electron wave function should

distort to avoid overlap at a small separation distance r. This effect increases the Kinetic energy and an effective repulsion between the atoms; this is known as “core repulsion”. The dominant weak attraction at a large (r) is known as the Van-der-Waals attraction, which is caused due to mutual polarization of molecules(Gould, 2007).The Figure 26 shows a typical L-J curve for neutral atoms.

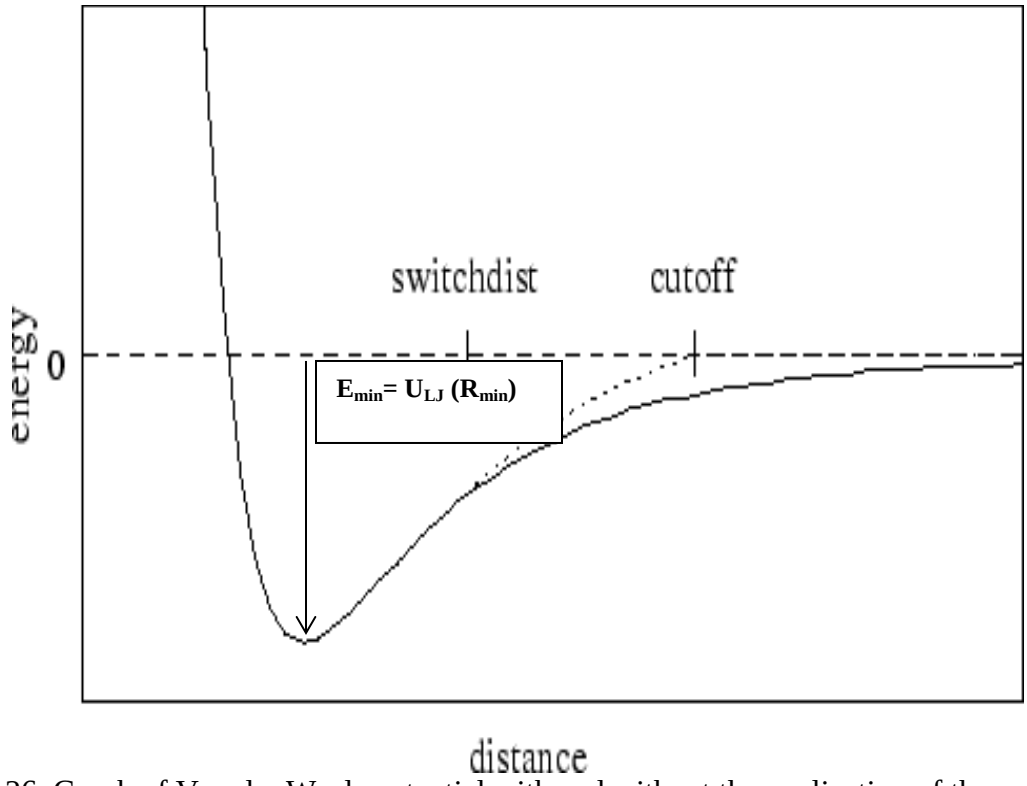

Figure 26. Graph of Van der Waals potential with and without the application of the switching function (Phillips et al., 2005)

$$\boldsymbol{U_{VdW} = \sum_{van\ der\ Waals} \sum_{i \neq j} 4\varepsilon_{ij} \left[\left(\frac{\sigma_{ij}}{r_{ij}} \right)^{12} - \left(\frac{\sigma_{ij}}{r_{ij}} \right)^{9} \right]} \qquad \textbf{(13)}$$

The equation above describes the Van der Waals attraction and repulsion, where $\boldsymbol{r_{ij} = \| \overrightarrow{r_J} - \overrightarrow{r_\iota} \|}$ is the distance between a pair of atoms, $E_{min}= U_{LJ} (R_{min})$ is the minimum energy between two atoms also depth of the potential well. L-J potential approaches to zero with the increase in the separation distance r.

4.4.3. Electrostatic interaction

Electro static interaction between any two atoms with the same sign or the opposite sign varies with distance. The equation below describes the electrostatic interaction between two atoms

$$\boldsymbol{U_{Electrostatic} = \sum_{electrostatic} \sum_{i \neq j} \epsilon_{14} \frac{C q_i q_j}{\epsilon_o r_{ij}}} \quad \textbf{(14)}$$

Where $r_{ij} = \| \overrightarrow{r_j} - \overrightarrow{r_i} \|$the distance between a pair of atoms qi and qi, C is the Coulombs constant and $\boldsymbol{\epsilon_o}$is the dielectric constant and $\boldsymbol{\epsilon_{14}}$ is the dimensionless scaling factor with value 1.

4.5. Force Field Parameters

Table 1. Bonded interaction parameters conversion from CFF force field to CHARMM (Katti et al., 2005; Teppen et al., 1997)

Bond stretching		CFF			CHARMM	
I	J	K_2^B(kcal/mol A°^{2})	K_3^B(kcal/mol A°^{2})	K_4^B(kcal/mol A°^{2})	K^B(kcal/mol A°^{2})	R^2
ao	ocl	328.70	341.0	2189.0	382.617	0.975
ocl	hcl	656.80	-1627.50	-3684.20	827.209	0.876
sz	oss	459.10	-672.40	443.40	492.387	0.935
sz	ocl	494.10	-36.70	2150.70	558.593	0.995

Angle bending			CFF			CHARMM	
I	J	K	K_2^B(kcal/mol rad°^{2})	K_3^B(kcal/mol rad°^{2})	K_4^B(kcal/mol rad°^{2})	K^B(kcal/mol rad°^{2})	R^2
ao	ocl	hcl	44.00	-53.40	103.40	34.933	0.968
sz	ocl	ao	195.300	48.90	185.30	155.754	0.988
oss	sz	ocl	88.10	-57.00	92.50	97.493	0.90
ao	ocl	ao	195.30	48.90	185.30	198.27	0.998
ocl	ao	ocl	-40.00	0.00	32.40	80.0	0.957

Torsion			CFF				CHARMM	
I	J	K	L	V_1^D(kcal/mol)	V_2^D(kcal/mol)	V_3^D(kcal/mol)	V^D(kcal/mol)	R^2
oss	sz	ocl	ao	0.160	1.790	0.200	0.200	0.589

Atom type descriptions
ao Aluminum in Octahedral sheet
ocl Oxygen in octahedral sheet (in coordination with Al)
hcl Hydrogen in the octahedral sheet(OH-group)
sz Silicon in the tetrahedral sheet
oss Surface oxygen

Table 2. Conversion of non-bonded from parameters from Teppen et al.(1997) to CHARMM parameters (Katti et al. (2005)

I	A_i(((kcal/mol)$A^{\circ 6}$)$^{1/2}$)	B_i(((kcal/mol)$A^{\circ 6}$)$^{1/2}$)	σ_i(kcal/mol)	ε_i(A°)
sz	775.000	0.010	0.001	7.400
ocl	790.000	190.000	6.000	2.800
ao	2800.000	0.010	0.150	6.300
oss	635.000	140.000	1.000	3.000
hcl	2.000	0.400	0.0001	2.400
Na	79	3.89	0.25	2.500

Atom type descriptions
ao Aluminum in Octahedral sheet
ocl Oxygen in octahedral sheet (in coordination with Al)
hcl Hydrogen in the octahedral sheet(OH-group)
sz Silicon in the tetrahedral sheet
oss Surface oxygen

NAMD(Phillips et al., 2005) version2.8 package was used for MD simulations. NAMD uses CHARMM force field parameters to integrate the equation of motion. CHARMM force field parameters for Montmorillonite developed by Katti et al (2005a).CFF force field parameters for Clay sheets were developed by Teppen et al (1997), these CFF force field parameters were converted to CHARMM force field using regression analysis by Katti et al (2005a). Converted force field parameters are given in the Table 1.

4.6. Model Construction

Experimental studies on Na-MMT ((Katti and Shanmugasundaram, 2001) were performed in previous work, Na-MMT used for these experiments belongs to SW_y-1 group, this clay was acquired from a clay repository of the University of Missouri, Columbia. The chemical formula of SW_y-1 group Na-MMT is as follows $(Ca_{0.12}\ Na_{0.32}\ K_{0.05})\ [Al_{3.01}\ Fe\ (III)_{0.41}\ Mn_{0.01}\ Mg_{0.54}\ Ti_{0.02}][Si_{7.98}\ Al_{0.02}]O_{20}(OH)_4$ (Van Olphen, 1979). Due to the limitation of model construction the chemical formula was reduced to $NaSi_{16}(Al_6FeMg)O_{20}(OH)_4$ (Schmidt et al., 2005).As mentioned earlier the clay sheets are negatively charged particles , the negative charge of clay sheets is balanced by positively charged sodium (Na) cations. These cations reside in the interlayer and they carry equal or lesser charge. Due to the charge imbalance clay sheets carry a net negative charge. Van der Waals interaction between Na^+ ions and clay sheets holds Na-MMT together (Cornelis and Dutrow, 2007). The unit cell of this model carries 0.5e charge due to isomorphic substitution. This charge was balanced by adding 0.5 Na cations per unit cell in the interlayer.

4.6.1. 4X2 Na-MMT model construction

The Na-MMT 4X2 model was used for previous simulation studies (Katti et al., 2007; Schmidt et al., 2005). The unit cell dimension of this model is 5.28A° X 9.14 A° (10^{-10}m; A°=0.1nm). The bigger model was constructed using this unit cell, which consists of two clay layers, 4 unit cells in x direction and 2 unit cells in y direction. The thickness of an individual clay sheet is 6.56A° and the final dimensions of 4X2 Na-MMT model before minimization is 21.12A°X18.28A°X6.56A°. For the solvation analysis interlayer spacing of 3.44A° was considered for dry Na-MMT solvation, interlayer spacing 6.44A°, 7.44A°, 8.44A° and 9.44A° were considered for slightly hydrated models. Interlayer spacing distance and thickness of the

individual clay sheet resulted in the basal spacing of 10 A°, for dry Na-MMT solvation basal spacing of 13 A°, 14 A°, 15 A° and 16 A° were considered. Basal spacing is the distance from the bottom of the top clay sheet to the bottom of bottom clay sheet. Figure 27 (a) and (b) shows the plan and side view of 4X2 Na-MMT model.

The Initial coordinates of pyrophyllite clay mineral was given by Skipper et al (1995a). The structure of pyrophyllite clay mineral is similar to the structure of Montmorillonite clay mineral, so the coordinates proposed by Skipper et al (1995a) were substituted for 4X2 Na-MMT model. In this model one out of every Al^{3+} ion was replaced by Mg^{2+} ion and Fe^{3+} ion. An atomic charge of every atom was taken from Teppen et al (1997). Coordinates and charges of one unit cell of 4X2 Na-MMT model is given in the Table 2. All these atomic charges are calculated using ab-initio quantum mechanics modeling.

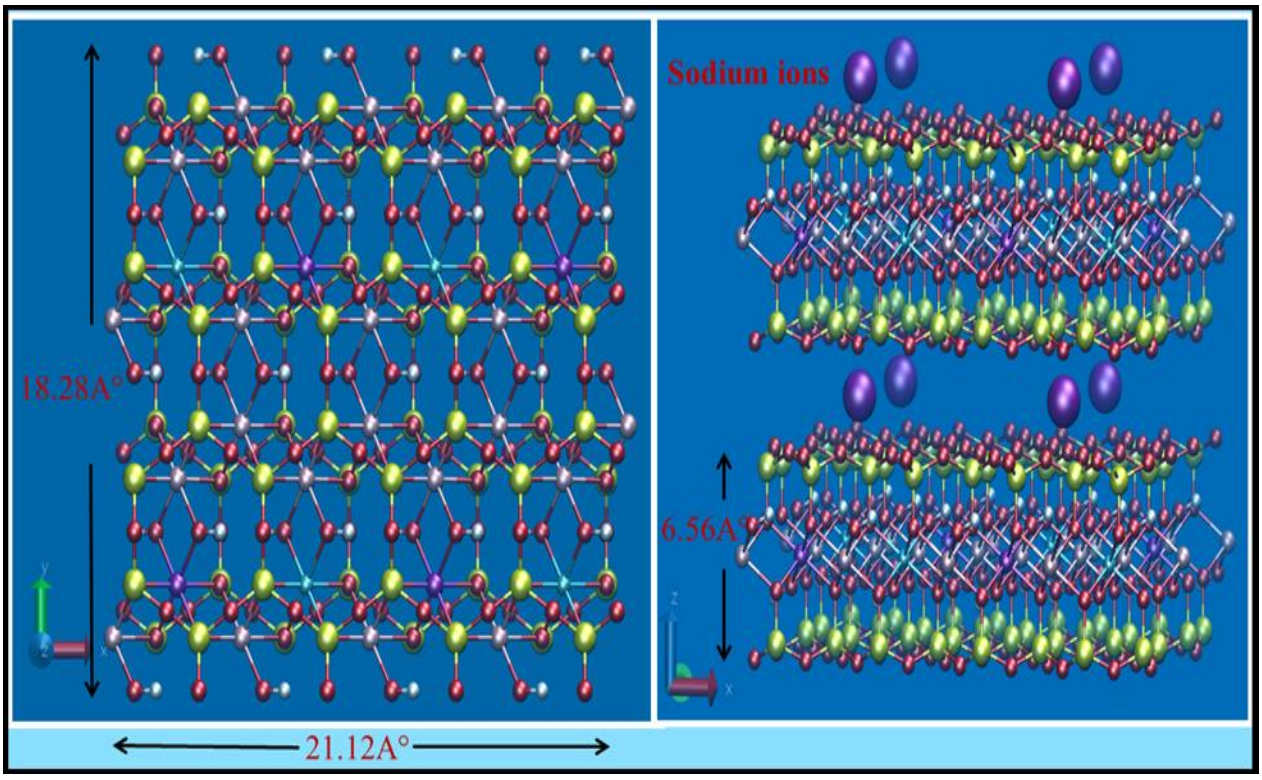

Figure 27 (a) Plan of 4X2 Na-MMT model and b) Side view of 4X2 Na-MMT model

Table 3. Na-MMT unit cell coordinates and charge (Katti et al., 2005)

no	atom	x(A°)	y(A°)	z(A°)	q_i	no	atom	x(A°)	y(A°)	z(A°)	q_i
1	AL1	-0.053	-14.956	-15.442	1.68	21	O11	2.189	-20.295	-18.679	-0.70
2	FE2	2.587	-16.486	-15.404	1.68	22	O12	4.829	-20.295	-18.645	-0.70
3	AL3	2.587	-19.526	-15.396	1.68	23	O15	0.346	-15.717	-12.155	-0.70
4	AL4	5.227	-21.055	-15.358	1.68	24	O16	2.986	-15.716	-12.121	-0.70
5	SI1	0.862	-19.534	-18.148	1.40	25	O18	4.306	-17.996	-12.098	-0.70
6	SI2	0.862	-16.494	-18.156	1.40	26	O20	0.346	-20.286	-12.141	-0.70
7	SI3	3.501	-14.964	-18.127	1.40	27	O21	1.666	-22.566	-12.118	-0.70
8	SI4	3.502	-21.064	-18.110	1.40	28	O22	2.986	-20.286	-12.108	-0.70
9	SI5	4.312	-16.478	-12.652	1.40	29	O1	3.481	-18.009	-16.449	-0.96
10	SI6	1.673	-14.948	-12.690	1.40	30	O2	1.694	-18.003	-14.351	-0.96
11	SI7	4.313	-19.518	-12.644	1.40	31	O3	0.841	-19.529	-16.478	-0.91
12	SI8	1.673	-21.048	-12.672	1.40	32	O4	0.841	-16.489	-16.487	-0.91
13	H1	4.367	-18.010	-16.812	0.40	33	O6	3.480	-14.959	-16.458	-0.91
14	H2	0.807	-18.002	-13.988	0.40	34	O10	3.481	-21.059	-16.440	-0.91
15	H3	3.449	-22.571	-13.942	0.40	35	O13	4.334	-16.482	-14.322	-0.91
16	H4	1.727	-13.440	-16.858	0.40	36	O14	1.694	-14.953	-14.360	-0.91
17	O5	3.508	-13.445	-18.682	-0.70	37	O17	4.334	-19.522	-14.313	-0.91
18	O7	2.189	-15.725	-18.692	-0.70	38	O19	1.694	-21.053	-14.342	-0.91
19	O8	4.828	-15.725	-18.659	-0.70	39	O23	4.334	-22.572	-14.304	-0.96
20	O9	0.869	-18.016	-18.702	-0.70	40	O24	0.840	-13.439	-16.495	-0.96

4.6.2. Clay-water solvation model construction

The Na-MMT model built for previous work was used for Solvation analysis of Na-MMT and water. Solvation of any substance is a stabilizing interaction of solute and solvent or it can be an interaction between solvent and groups of an insoluble material. Generally these interactions are driven by Electrostatic forces, Van der Waals forces and hydrogen bond

formation. In this work Na-MMT model kept at the center and the net negative charge of clay sheets are balanced by adding an appropriate number of Na^+ ions, so each clay sheet carries 4e of charge and it was balanced by adding 4 Na^+ ions. The dry Na-MMT solvation box was built by keeping dry Na-MMT at the center and water box was built around clay sheets. The Basal spacing of 10A° was chosen for dry Na-MMT and no interlayer water molecules were present in the dry Na-MMT solvation box. For slightly hydrated solvation analysis for 4 solvation models of Na-MMT with different water molecules or moisture content were considered. The final solvation models had 13 A°, 14 A°, 15A° and 16A° of basal spacing with 13, 23, 34 and 43 water molecules in the interlayer respectively, 13 interlayer water molecules with 13 A° basal spacing of Na-MMT represents 4% of moisture content, 14 A°, 15A° and 16A° Na-MMT models with 23, 34 and 43 interlayer water molecules represent 7%, 10.6% and 13% moisture content. All these models were surrounded by 2128 TIP3 water molecules. The final dimensions of these models were 44A°X 42A°X 44A°. For this study TIP3 water model was used, each water molecule carries three interaction sites which correspond to 3 atoms of a water molecule. The bond length of TIP3 molecule is 0.96A° and angle between hydrogen atoms of a water molecule is 104.5°.

For the purpose of simulating the above-mentioned system Molecular dynamics or Monte Carlo simulation techniques are suitable techniques to use. The molecular dynamics simulations were performed using NAMD(Phillips et al., 2005) version2.8 package. For interactive studies and post process VMD version1.9.2 (Humphrey et al., 1996) package was used. NAMD and VMD were developed by Theoretical and Computational Biophysics Group in the Beckman Institute for Advanced Science and Technology at the University of Illinois at Urbana-Champaign.

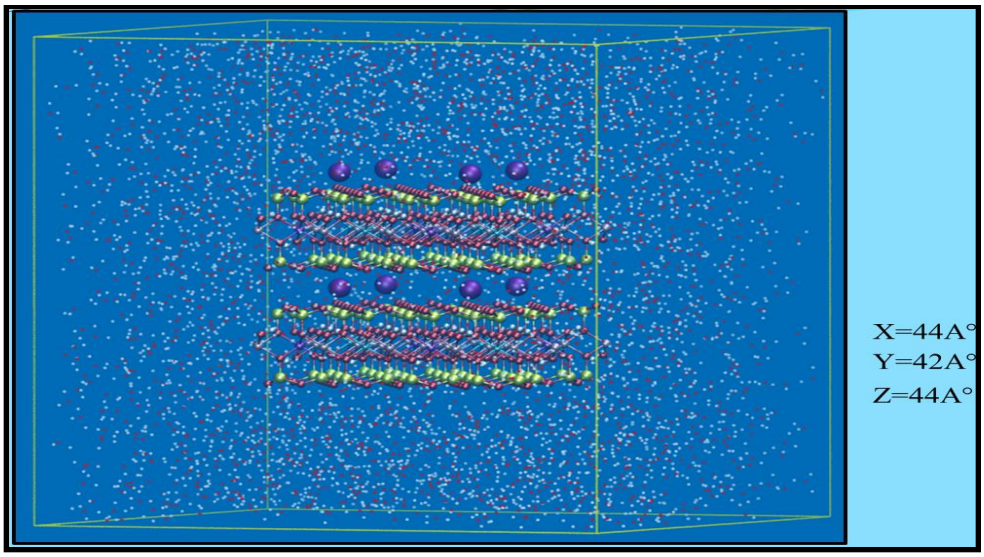

Figure 28**.** Solvation box with 2128 TIP3 water molecules (every point around clay sheets inside the box is a water molecule)

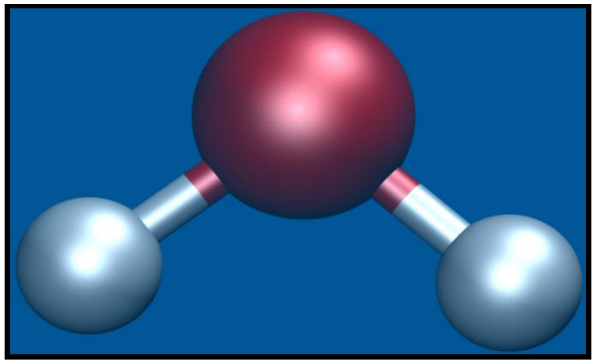

Figure 29**.** TIP3 water molecule

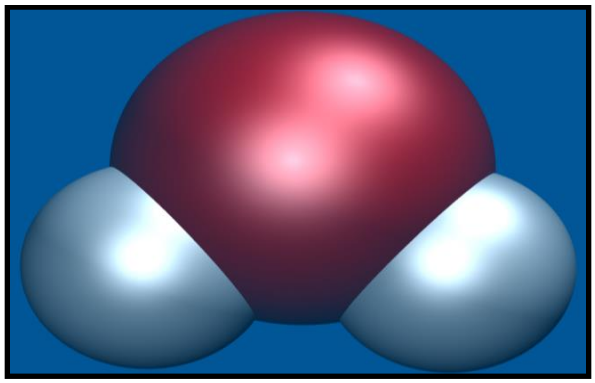

Figure 30. TIP3 water molecule with Van der Waals radius

4.7. Simulation Details

NAMD (Phillips et al., 2005) version2.8 package was used to perform simulations and Virtual Molecular Dynamics (VMD) version1.9.2 (Humphrey et al., 1996) package was used for

the post process and interactive studies. MD simulations were performed using 128-node/1024-core cluster with 2.66Ghz 5550 Nehalem parallel processing computer systems at Center for Computationally Assisted Science and Technology, North Dakota State University.

Energy minimization and equilibration are two major steps in MD simulations. Energy minimization is the first step involves searching local energy minima of a molecule which is free in all directions. NAMD uses the conjugate gradient algorithm to perform energy minimization, local energy minima of the system was found by calculating energy and varying positions of atoms.

Minimization confirms that the model is stable; this step avoids instability of the system while performing dynamics simulations. Each solvation model was minimized using 100000 iterations. First time models were minimized by allowing atoms to move freely in all directions, the same models were minimized again by restraining clay sheets and Na^+ ions in X-Y directions and keeping them free in Z- direction. Throughout the simulation water molecules were kept free in all directions. Total minimum potential energy of the system was observed after 50000 iterations; these simulations were carried at simulated conditions vacuum and 0 K temperature.

Equilibration is the second step in molecular simulations; this step involves molecular dynamics and solves Newton's second law of motion for every atom to trace its trajectory in a system. A system with proper distribution of velocities, pressure, etc. over a given amount of time can be considered as an equilibrated system.

Swelling of clay minerals is a natural phenomenon which occurs at atmospheric condition, this work is to mimic the initial hydration of the Na-MMT, it is necessary to bring all minimized solvation models from 0K to 300K and 1 atm pressure. It is suitable to increase temperature and pressure of simulation models gradually. The temperature was increased from 0

K to 300 K in three equal increments, each time the simulation was performed for 100000 time steps. The total energy, velocities and temperature of the system was observed carefully at the end of every simulation. Langevin dynamics was used to regulate the temperature and to heat the system up to 300K; In Langevin dynamics temperature can be carefully regulated by adding friction and random forces.

NAMD uses Nosé-Hoover piston method (Martyna et al., 1994) to increase the pressure in constant pressure simulations; in this study pressure was increased form 0 bar to 1 bar in four equal increments. Periodic boundary conditions are required to perform NPT simulations. The pressure of the system was maintained carefully by adjusting periodic cell dimensions and rescaling the coordinates of all atoms. Once desired temperature and pressure was achieved then the model is ready for long MD simulation.

Verlet algorithm was used by NAMD to integrate Newton's equation of motion. It is one of the widely used time integration algorithm in molecular simulations. Verlet algorithm is two-third expansion of Taylor's series for the position r (t).Periodic boundary Conditions (PBC) were applied with cell dimensions of 50 A°X 50 A° X 50 A°. These boundary conditions were applied to avoid problems caused by boundary effects due to finite dimensions of the model. PBC creates infinite copies of a central simulation cell in all the directions. Whenever a molecule or an atom crosses the left-hand side of the PBC, it appears at the right-hand side of the simulation, due to the PBC it is possible to maintain the constant number of atoms (N), temperature (T) and pressure (P) throughout the simulation. Time step of 0.5fs (10^{-15}s) was considered for this work. Time steps required for 1ns simulation was 2000000 steps. Out of all the simulation models one of the models was considered for a longer simulation about 100ns ($20X10^{7}$-time steps).

Non-bonded interactions decrease as the distance between a pair of atoms increases. To save the computational time a cutoff distance of 10 A° was selected for non-bonded interactions, the interactions beyond this distance were neglected.

The position of an atom was identified by selecting an atom and calculating its center of mass for the last 20ps (20000 steps) of the simulation, this data was averaged and considered for the basal spacing calculations. Every 10ns of simulation took 120h using 24 processors on the 1024 processor system.

CHAPTER 5. RESULTS AND DISCUSSION

5.1. Dehydrated Clay-Water Simulation

The simulation results of dry Na-MMT (10A° initial basal spacing) were analyzed after 15ns (30000000 steps). Figure 31, 32 and 33 shows movement of water molecules inside the solvation box. Clustering of water molecules around clay sheets was observed at the end of 15ns of simulation. Basal spacing was calculated after every 2000000 steps (1ns). All the data extracted once after simulation reaches 300K and 1 bar pressure, for the convenience this point is considered as 0ns.

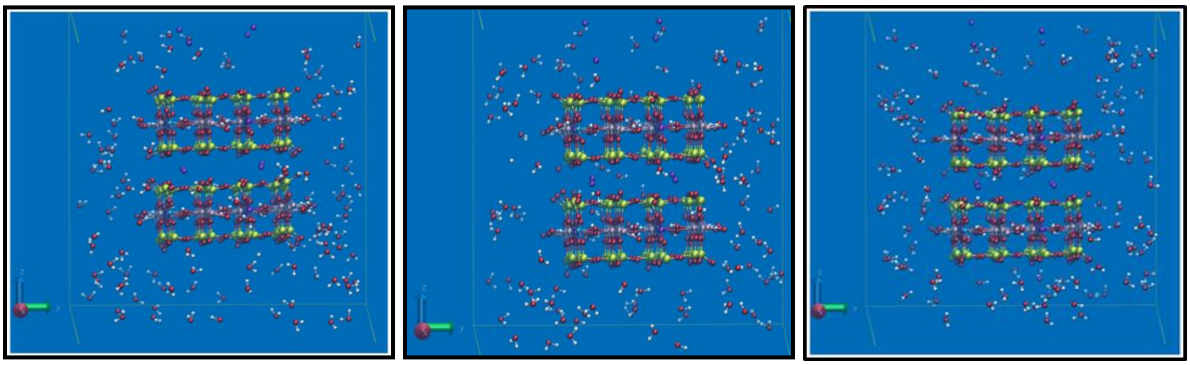

Figure 31. Positions of water molecules at 0, 1 and 2 ns respectively

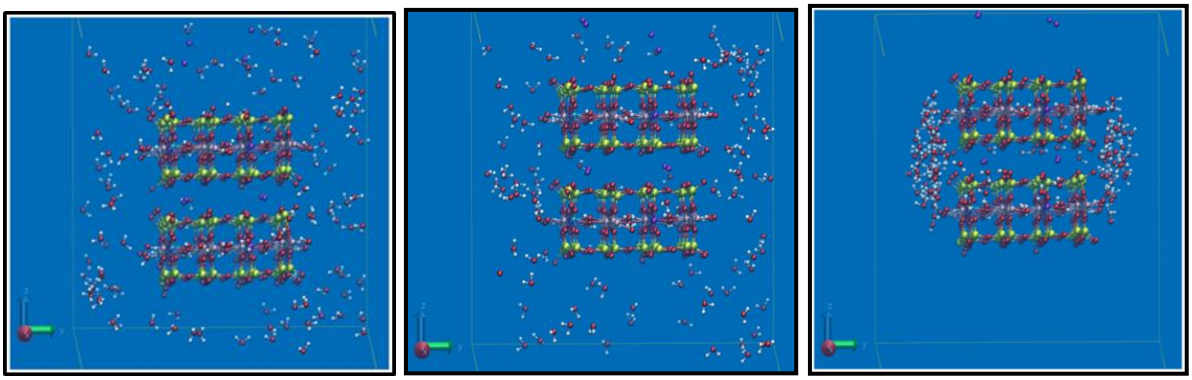

Figure 32. Positions of water molecules at 5, 10 and 15 ns respectively

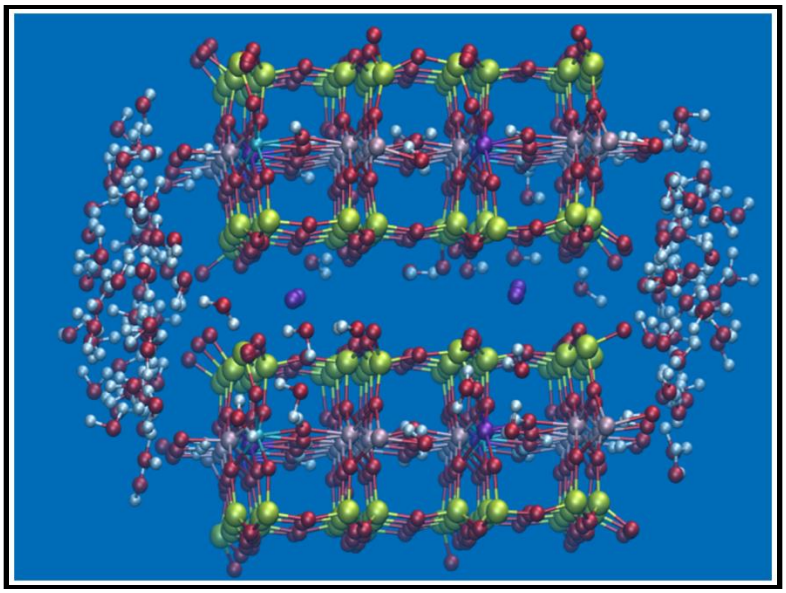

Figure 33. Clustering of water molecules around clay sheets after 15ns of simulation

Figure 34 shows the variation of basal spacing with respect to time. At 0 ns the basal spacing was 11.00A° and throughout the simulation significant change in basal spacing was not observed.

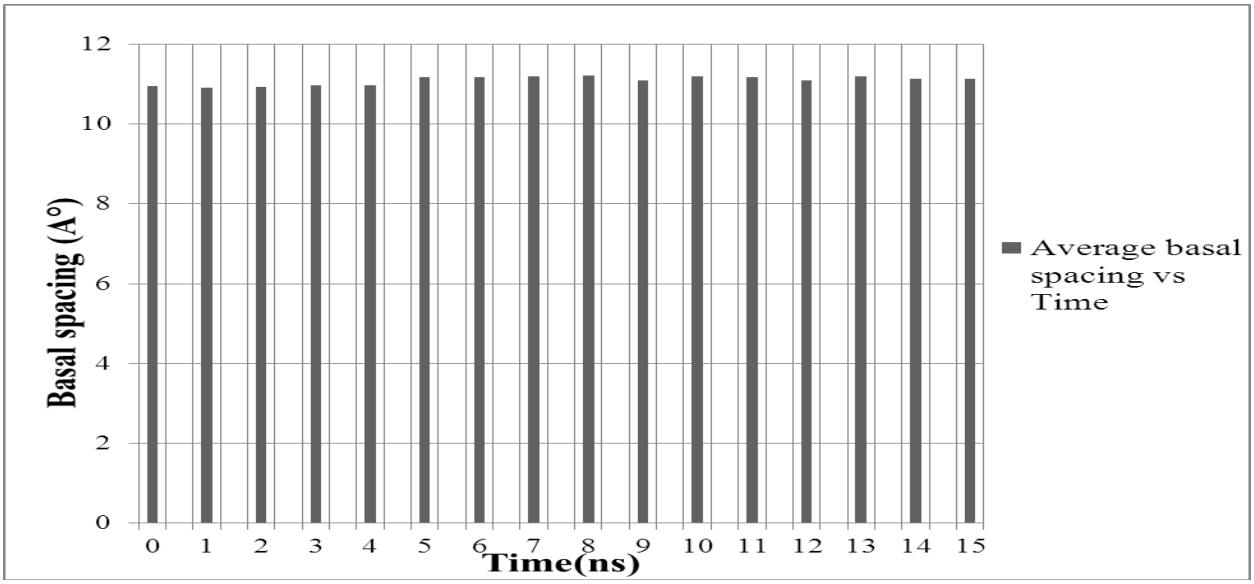

Figure 34. Plot showing the average Basal spacing with time

Figure 35 shows the non-bonded interaction energy between clay sheets. A strong Van der Waals (VdW) interaction can be observed and a weak electrostatic attraction was observed between clay sheets.

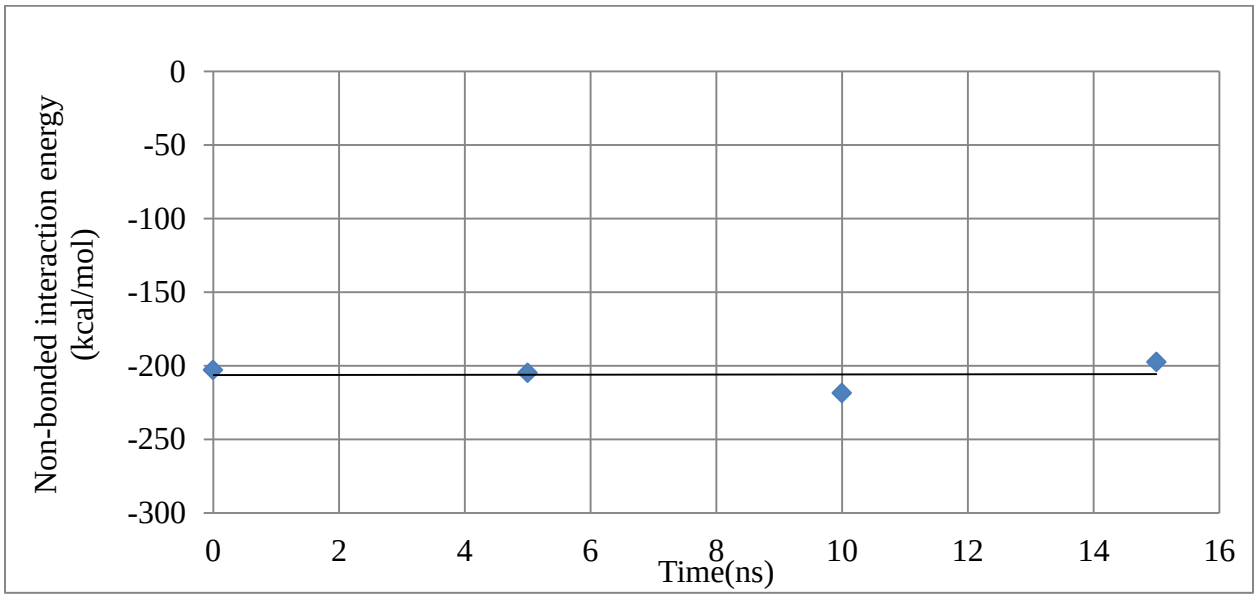

Figure 35. Plot showing average interaction energies between dehydrated clay sheets

Non-bonded interaction between interlayer Na ions and clustered water molecules is shown in Figure 36. Weak VdW interaction was observed between interlayer Na^+ ions and water molecules. With time electrostatic attraction between water molecules and interlayer Na^+ ions was observed decreasing.

Interlayer Na^+ ions hold clay sheets together; the non-bonded interaction between these Na+ ions and clay sheets is shown in Figure 37. Constant strong electrostatic attraction was observed and the weak VdW interaction was observed between interlayer Na ions and clay sheets. These energy plots describe the intensity of interaction from 0ns to 15ns.The non-bonded energies were recorded for each time step. The recorded values are averaged over every Nano second and later considered values at 0, 5,10 and for plotting. This method describes the overall trend of energy behavior and also reduces the thermal-fluctuations.

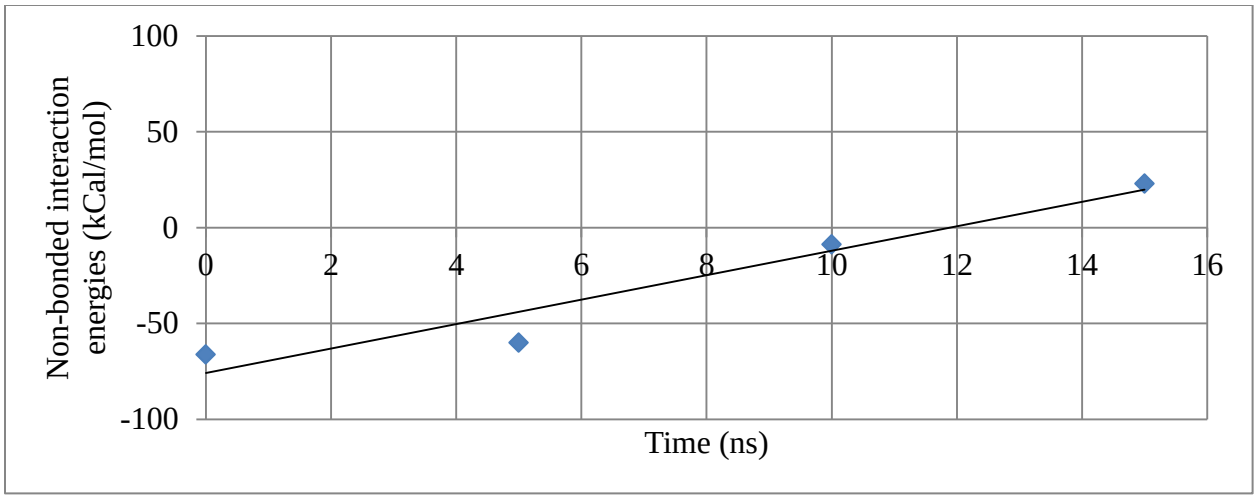

Figure 36. Average interaction energies between interlayer sodium ions and clustered water molecules around clay sheets

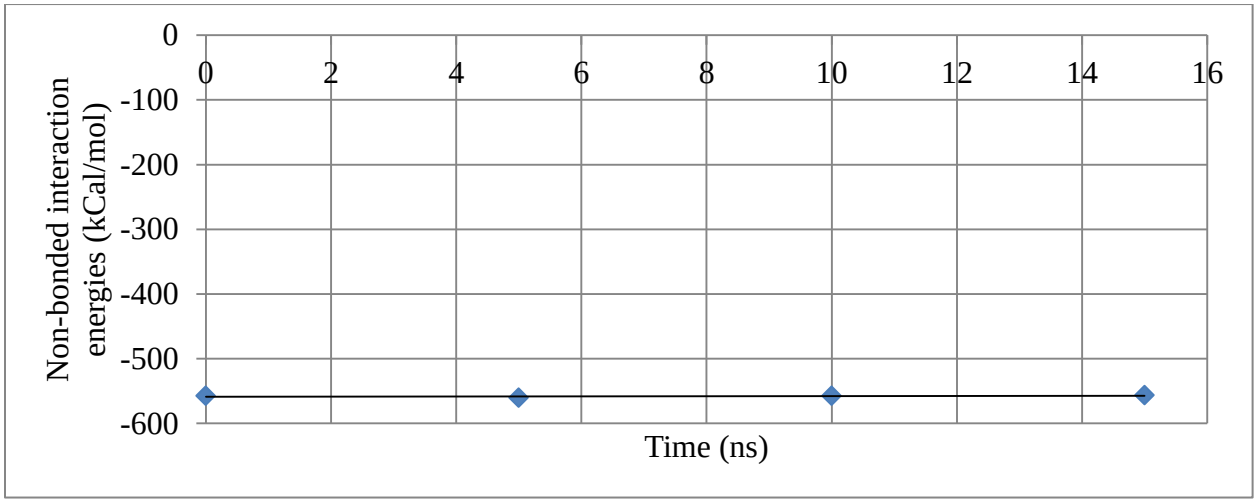

Figure 37. Plot showing average interaction energies between dehydrated clay sheets and interlayer sodium ions

The Figure 38 shows non-bonded interaction between clay sheets and the cluster of water molecules around clay sheets is. Electrostatic attraction between water and clay sheets was observed increasing with time and no significant change in VdW interaction energies between clay sheets and water molecules was observed throughout the simulation.

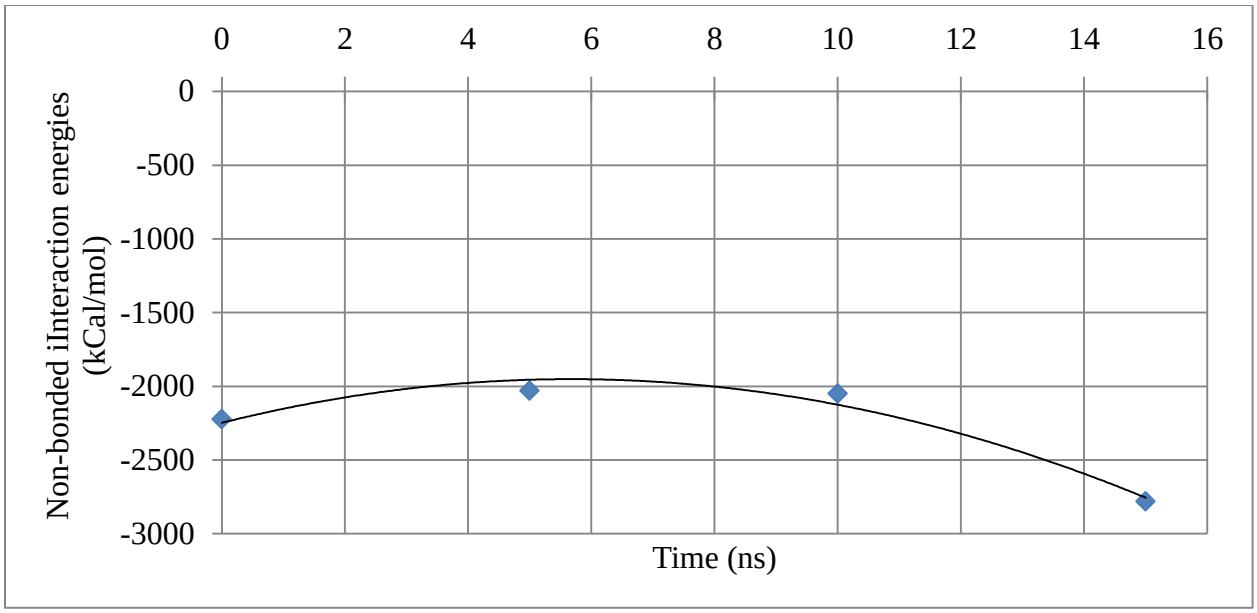

Figure 38. Plot showing average interaction energies between dehydrated clay sheets and water molecules clustered around clay sheets

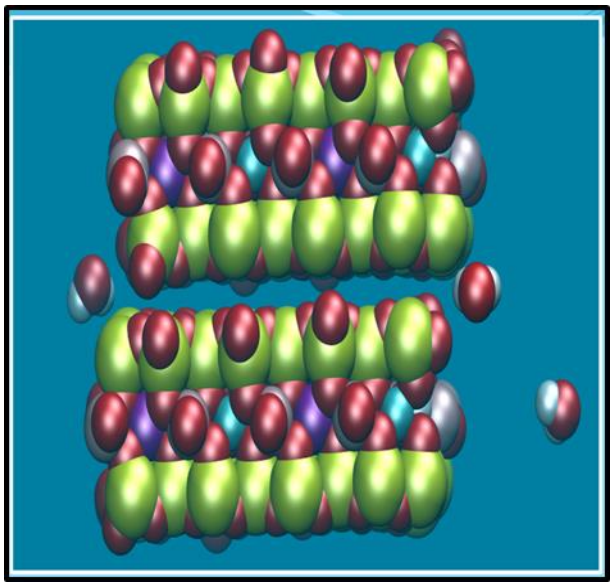

Figure 39. Collapsed Na-MMT sheets with VdW radius

From the interaction energy plots it can be inferred that there is a strong attraction between clay sheets, interlayer Na ions and water molecules. Interaction energies and basal spacing results reveals that there is no flow of water molecules in to the interlayer, hence swelling was not observed in dry Na-MMT solvation analysis. To understand the non-swelling

behavior of Montmorillonite Van der Waals interaction of clay sheets and water molecules is explained here.

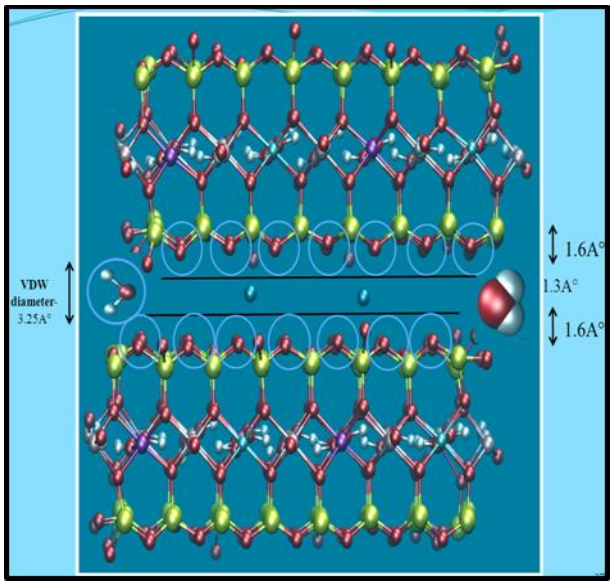

Figure 40. VdW radii of water molecules and oxygen atoms of clay sheets

Figure 39 and 40 shows VdW representation of clay sheets and water molecules. The VdW diameter of water molecules, VdW radii of oxygen atoms located at the bottom of the top clay sheet and oxygen atoms located at the top of the bottom clay sheet were measured. The VdW radius is one half of equilibrium internuclear distance between any two atoms.

The average total basal spacing between two clay sheets after 15ns simulation was 11.06A°, the basal spacing is the sum of interlayer spacing and thickness of a single clay sheet. In this case interlayer spacing was 4.5A°. A major portion of the interlayer spacing is occupied by VdW radii of oxygen atoms; the effective interlayer spacing excluding VdW radii of oxygen atoms was 1.3A°. This effective interlayer spacing is the empty space between two clay sheets. The measured VdW diameter of a water molecule is 3.25A°. The Van der Waals radius of oxygen atoms avoids the flow of water molecules in to the interlayer and also reduces the

interaction between water molecules and interlayer Na ions. The total effect results in the non-swelling behavior of dry Na-MMT.

Generally, non-swelling behavior of completely dehydrated clay sheets is due to collapse of the interlayer. Fig. 42 shows the VdW representation of the bottom clay sheet with locations of interlayer Na ions. The Complete collapse of interlayer avoids interactions between interlayer Na ions and water molecules; this is because interlayer Na^+ ions reside in the ditrigonal cavities of Na-MMT sheet. Figure 41 shows the interaction between interlayer Na ions and oxygen atoms of ditrigonal cavities of Na-MMT. A significant electrostatic attraction was observed between interlayer Na ions and oxygen atoms of ditrigonal cavities. This could be one of the important observations which explain the interlayer collapse of completely dehydrated Na-MMT or dry Na-MMT. Dehydration above 90°C is normally referred as stage II dehydration. This stage of dehydration leads to a primary collapse of interlayer. Complete dehydration of interlayer cause collapse of the interlayer, 2:1 tetrahedral: octahedral sheets remain intact but the interlayer Cations reside in ditrigonal cavities of clay sheets.

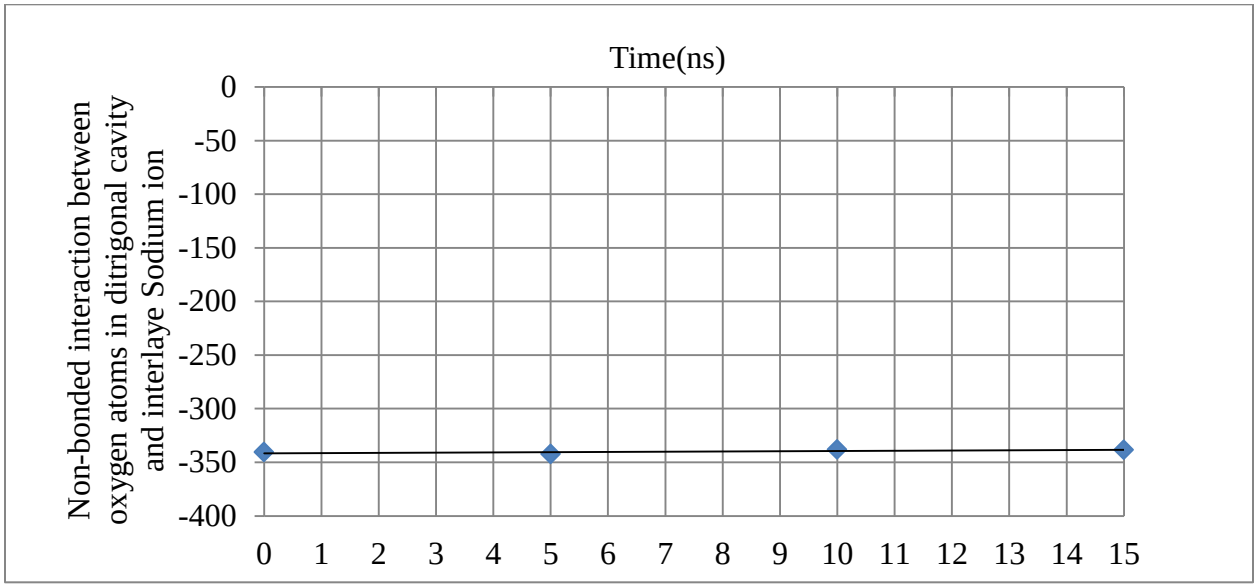

Figure 41. Plot showing average electrostatic interaction attractions between oxygen atoms in ditrigonal cavity and interlayer sodium ion

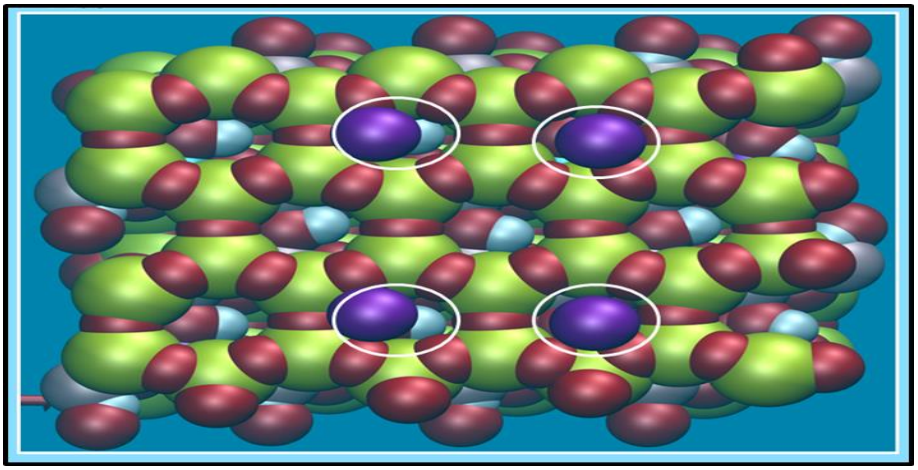

Figure 42. Positions of Na ions residing inside the collapsed Na-MMT sheets

5.2. Slightly Hydrated Clay-Water Solvation

Several attempts were made to initiate the swelling mechanism of Na-MMT. One layer and two layers of water molecules were introduced inside interlayer; water box was built around slightly hydrated Na-MMT. The Interlayer collapse was observed after 4ns of simulation and interaction and no significant change was observed in interaction energies. For all the cases mentioned above (dry Na-MMT, slightly hydrated Na-MMT) pressure was increased up to 100 bars and simulation was performed for 4ns. These simulations were discontinued after observing interlayer collapse.

The objective of this work is to explain the initial swelling mechanism of clay minerals. The simulation results of dry Na-MMT indicates that there should be an enough interlayer spacing between clay sheets to generate interaction between interlayer Na ions and water molecules. Experimental works refer initial swelling as hydration swelling (McBride 1994) and the basal spacing of 13A° to 15 A° is required to initiate the swelling. Six simulation models were built to understand the mechanism of swelling with different moisture content and different basal spacing. The basal spacing used in this work starts from 11A°to 16A°, .Water box was built around clay sheets. Because of the different basal spacing different moisture content was

observed inside the interlayer of solvation models. Six solvation boxes with different basal spacing 11A°, 12A° 13A° 14A° 15A° and 16A°, number of water molecules found inside the interlayer of clay sheets before minimization are 5(1.56% Moisture content), 7(2.19% Moisture content), 13(4.06% Moisture content), 23(7.19% Moisture content), 34(10.63% Moisture content) and 46(14.38% Moisture content) respectively. Figure 43 to 46 shows solvation models with different interlayer moisture content. All the solvation models were minimized and brought to room temperature and pressure, after 4ns of simulation, models with the initial basal spacing of 11A° and 12A° were discontinued because swelling was not observed in these models. Rest of the solvation models were considered for 10ns of long simulation.

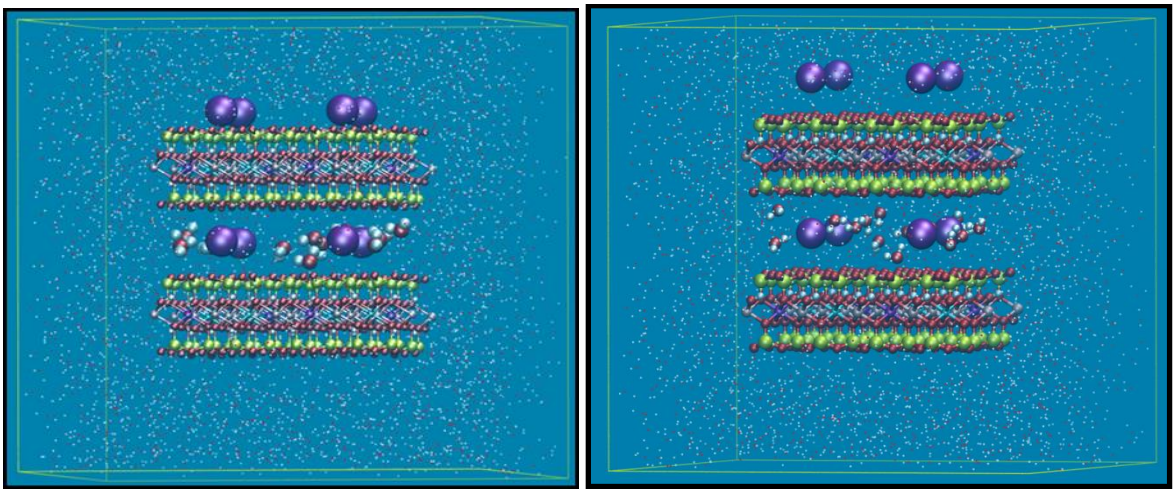

Figure 43. A solvation models with 13 A° initial basal spacing and 14 A° initial basal spacing respectively

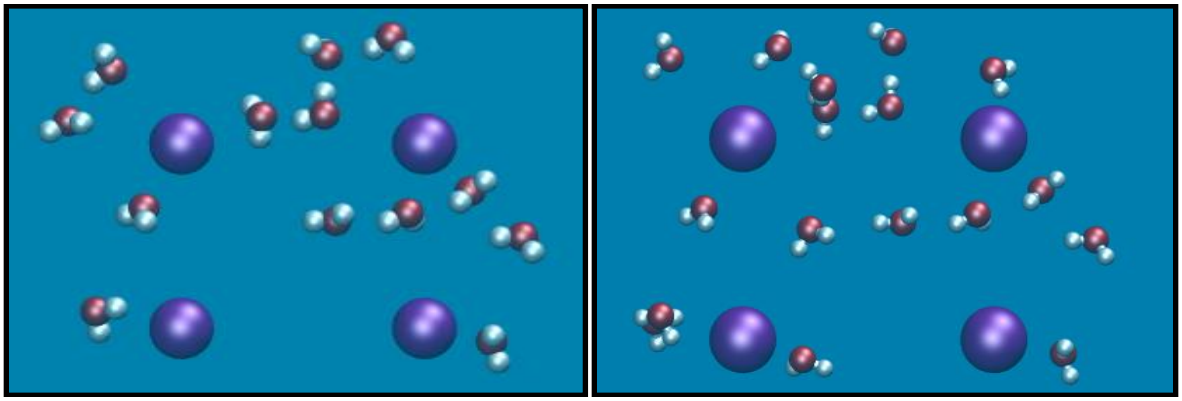

Figure 44. Interlayer configuration of 13 A° and14 A° respectively

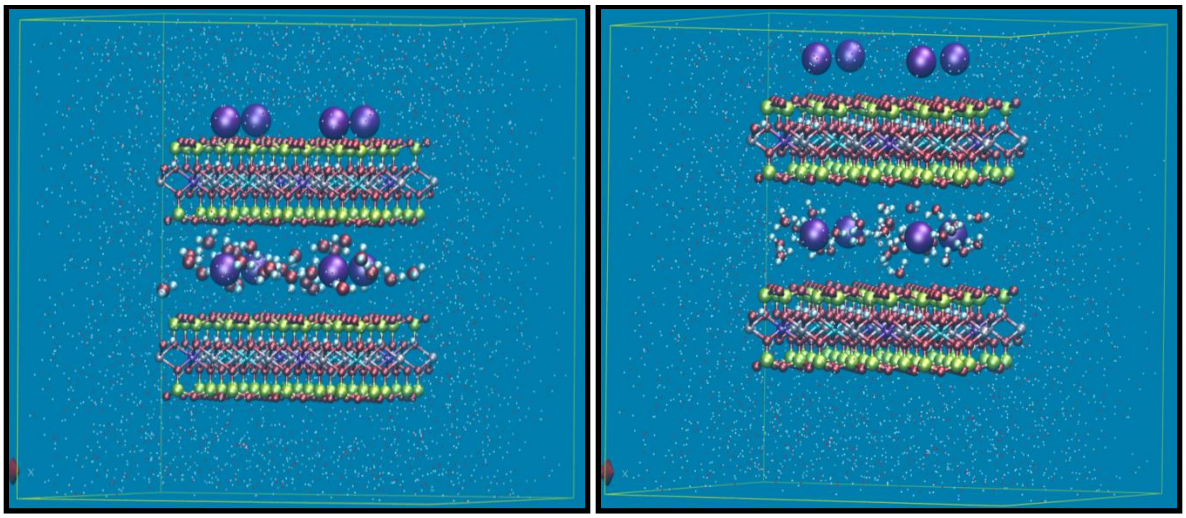

Figure 45. A solvation models with 15 A° initial basal spacing and 16 A° initial basal spacing respectively

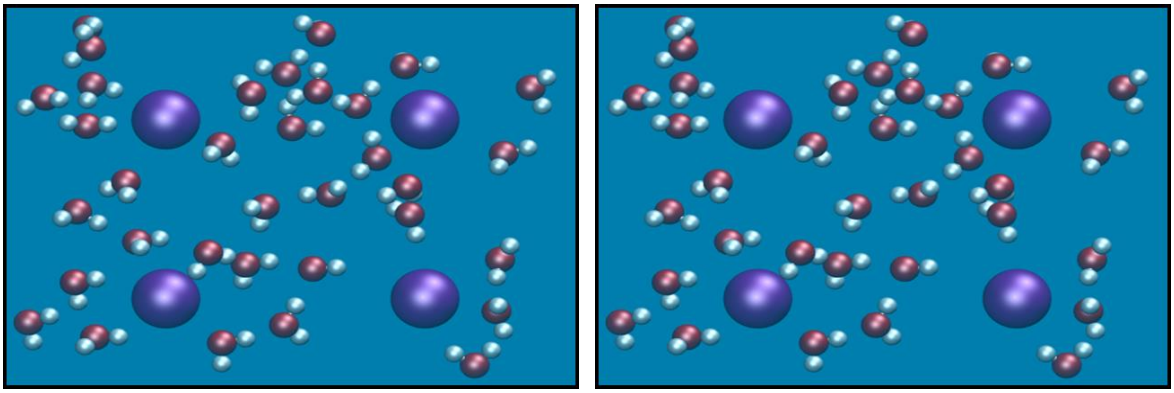

Figure 46. Interlayer configuration of 15 A° and16 A° respectively

Figure 47 and 48 shows results after 10ns of simulation. Figure 47 shows the variation of basal spacing after every 1ns of simulation, at the time of the atmospheric condition basal spacing of all the models was approximately between 13.4A° to 13.5A°. At the end of 10ns basal spacing was increased from 13.4A° to 14.00A°. Figure 48 shows change in the number of water molecules inside the interlayer with time.

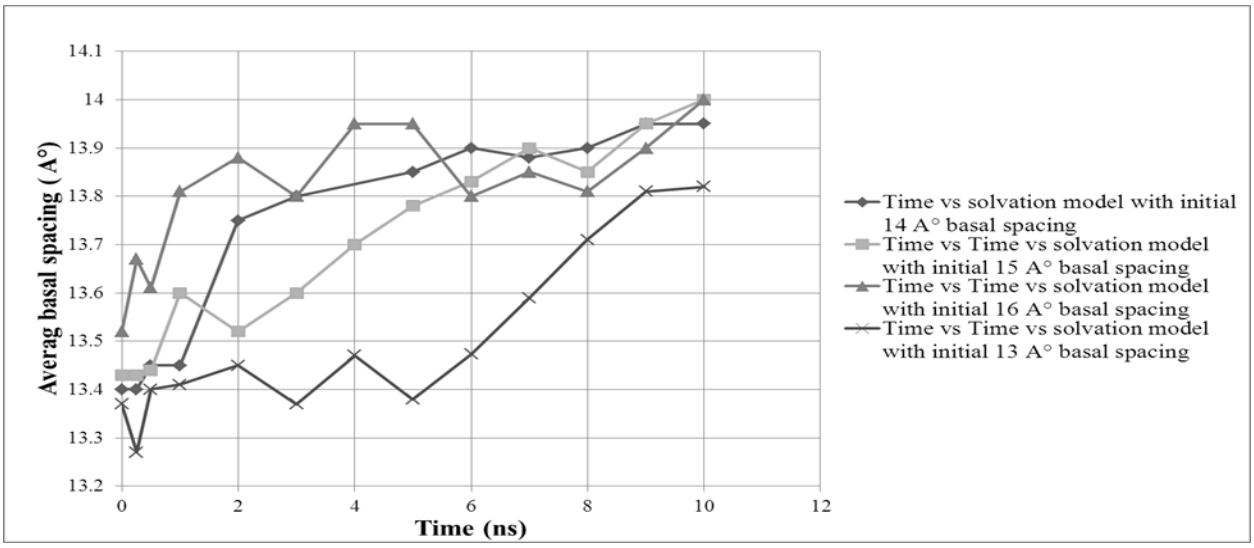

Figure 47. Plot showing basal spacing variations of slightly hydrated solvation models

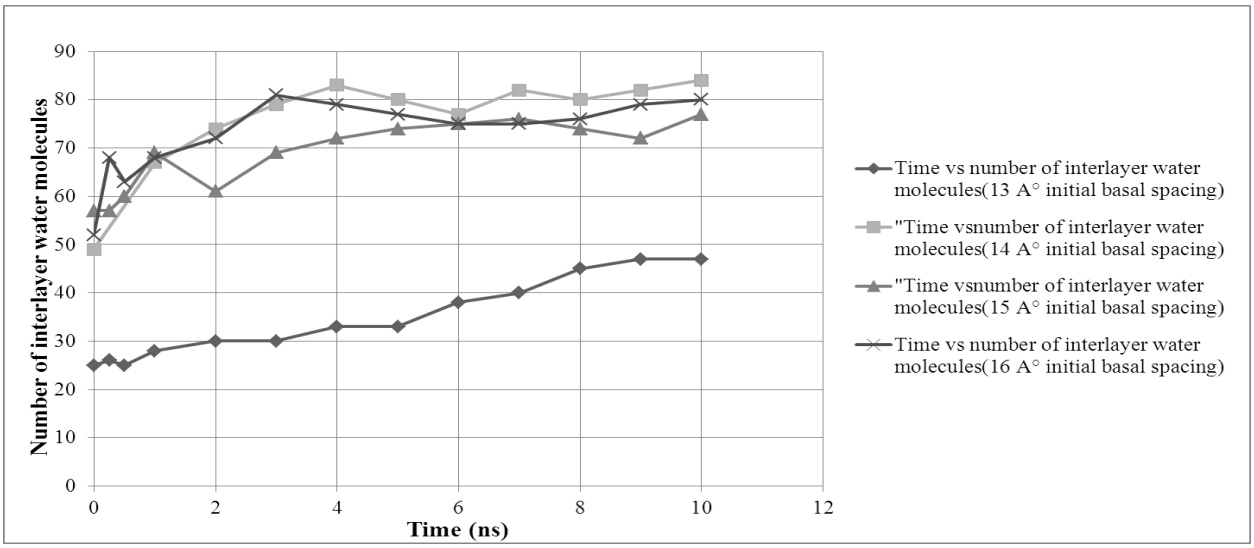

Figure 48. Plot showing number of interlayer water molecules with time

Approximately 50-60 water molecules were observed inside the interlayer at the time of atmospheric temperature and pressure. The total number of water molecules was counted after every 1ns of simulation, at the end of 10ns of the simulation number of molecules was increased from 20 to 85 water molecules. Increase in the basal spacing and number of water molecules in the interlayer indicates the beginning of the swelling process. A solvation model (14A° initial basal spacing) showing better configuration was further considered for long simulation up to

100ns. Figure 49to 54 shows the organization of water molecules in the interlayer with time, 53, 85 and 92 water molecules were found in the interlayer at 0, 5, 10, 30 and 100ns of simulation respectively.

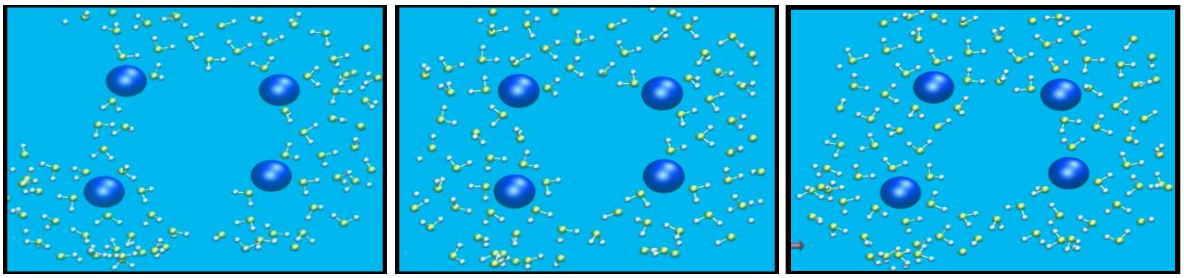

Figure 49. Interlayer water molecules arrangement after 0, 1 and 2ns respectively

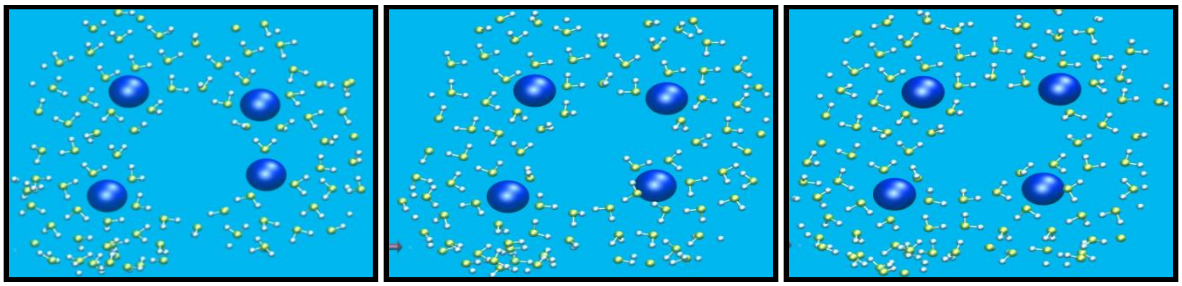

Figure 50. Interlayer water molecules arrangement after 3, 4 and 5ns respectively

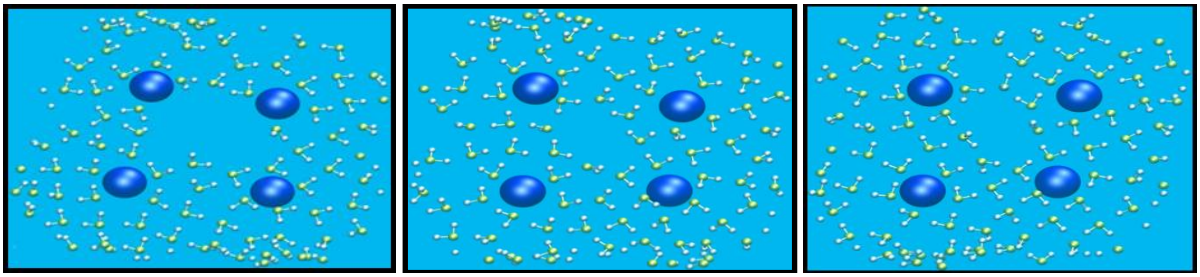

Figure 51. Interlayer water molecules arrangement after 10, 15 and 20ns respectively

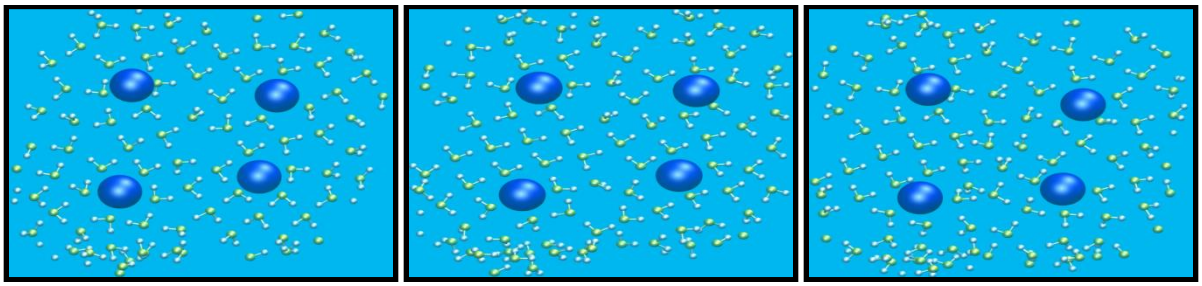

Figure 52. Interlayer water molecules arrangement after 30, .40 and 50ns respectively

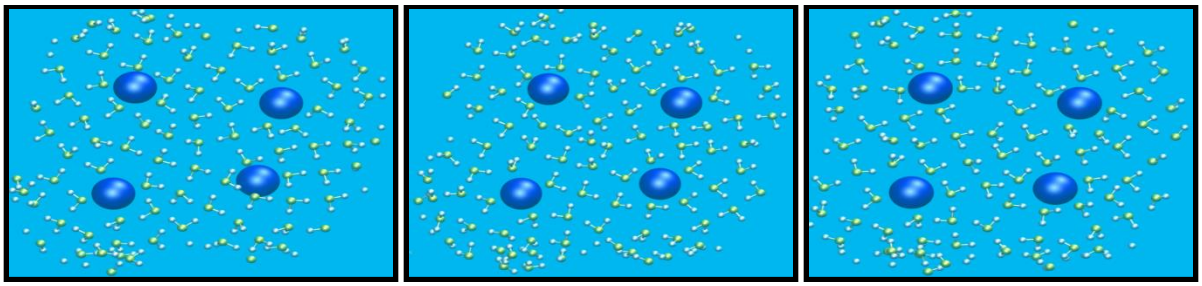

Figure 53. Interlayer water molecules arrangement after 60, 70 and 80ns respectively

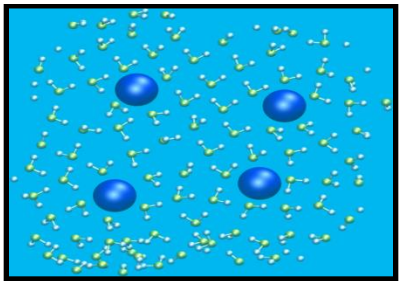

Figure 54. Interlayer water molecules arrangement at 100ns

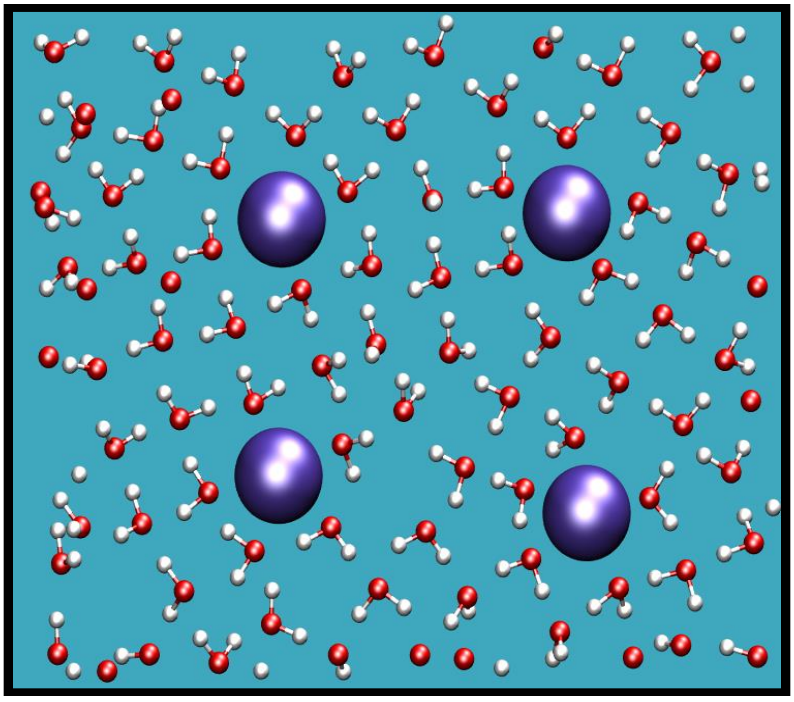

Figure 55. Organization of water molecules inside the interlayer

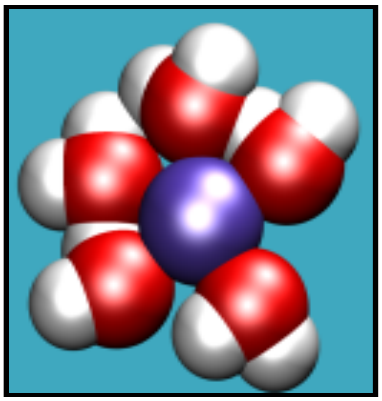

Figure 56. First solvation shell around Na ion

Around the interlayer Na ions cluster of water molecules was observed, oxygen atoms of water molecules pointing towards Na ions, this indicates the interaction between Na^+ ions and water molecules. Around interlayer Na^+ ion a shell of water molecules was observed, the shell approximately contains 5 water molecules at the distance of 2.4A° from the Na^+ ion, this shell is referred as the first solvation shell. Figure 55 and 56 shows interlayer water organization and the first solvation shell.

Figure 57 describes the variation of basal spacing from 0ns to 100ns with time. At 0ns basal spacing was observed around 12A° and spacing was increased from 12A° to 14A, the change basal spacing clearly indicates flowing of water molecules inside the interlayer.

Figure 58, 59 60 61 and 62 shows non-bonded interaction energies between clay sheets, interlayer Na ions, interlayer water and water surrounding clay sheets, these energy plots describe the intensity of interaction from 0ns to 100ns.The non-bonded energies were recorded for each time step. The recorded values are averaged over every Nano second and later considered values at 0, 20,40,60,80 and 100ns for plotting. This method describes the overall trend of energy behavior and also reduces the thermal-fluctuations. Figure 58 shows the non-

bonded interaction between clay sheets, a negligible electrostatic attraction and VdW interaction was observed between clay sheets.

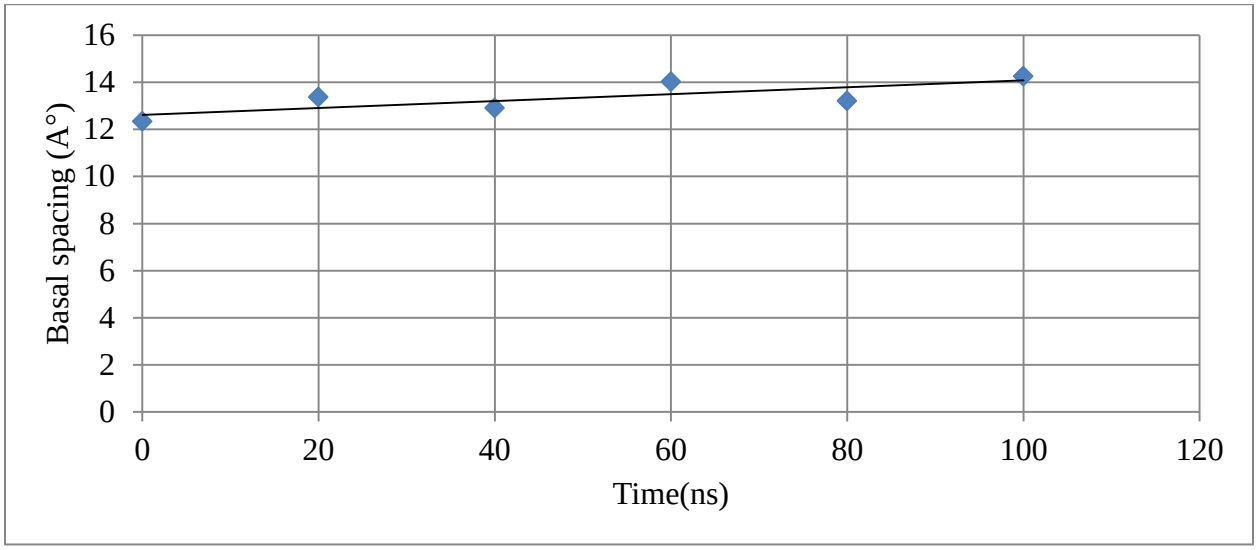

Figure 57. Plot showing average change in basal spacing with time (14 A° initial basal spacing)

The non-bonded interaction between clay sheets reduced significantly when compared to the dry Na-MMT simulation Figure 59 describes the non-bonded interaction between clay sheets and interlayer Na ions. Generally a strong electrostatic attraction exists between clay sheets and cations. In this case also a dominant electrostatic attraction and the weak negligible VdW interaction were observed throughout the simulation. However, the electrostatic attraction decreases as the distance between any atoms increases; here also the intensity of electrostatic attraction between cations and Na-MMT sheets were decreased as compared to dry Na-MMT results. Interaction energies between clay sheets and water surrounding clay sheets were described in Figure 60 with time. The dominant electrostatic attraction and VdW interaction was observed between clay sheets and water molecules. Figure 61 also describes that water molecules always attracted towards clay sheets also the intensity of interaction between clay sheets and water molecules in slightly hydrated Na-MMT simulation is almost similar with dry Na-MMT simulation. The electrostatic attraction and weak VdW interaction between cations and water

molecules around the clay sheets is described in Figure 62. Intensity of interaction energies between cations and water molecules around clay sheets are similar with dry Na-MMT simulation. The electrostatic attraction and VdW interaction between cations and interlayer water molecules is explained in Figure 63. The increase in Electrostatic attraction between interlayer water molecules and cations were observed with time. A jump in the electrostatic attraction observed at the end of simulation. The closed packing of interlayer water molecules within the range of cations could be a reason for this kind of behavior VdW interaction between interlayer and water molecules was weak throughout the simulation. Interaction energy maps and simulation results of slightly hydrated Na-MMT describe a nature of the Na-MMT swelling.

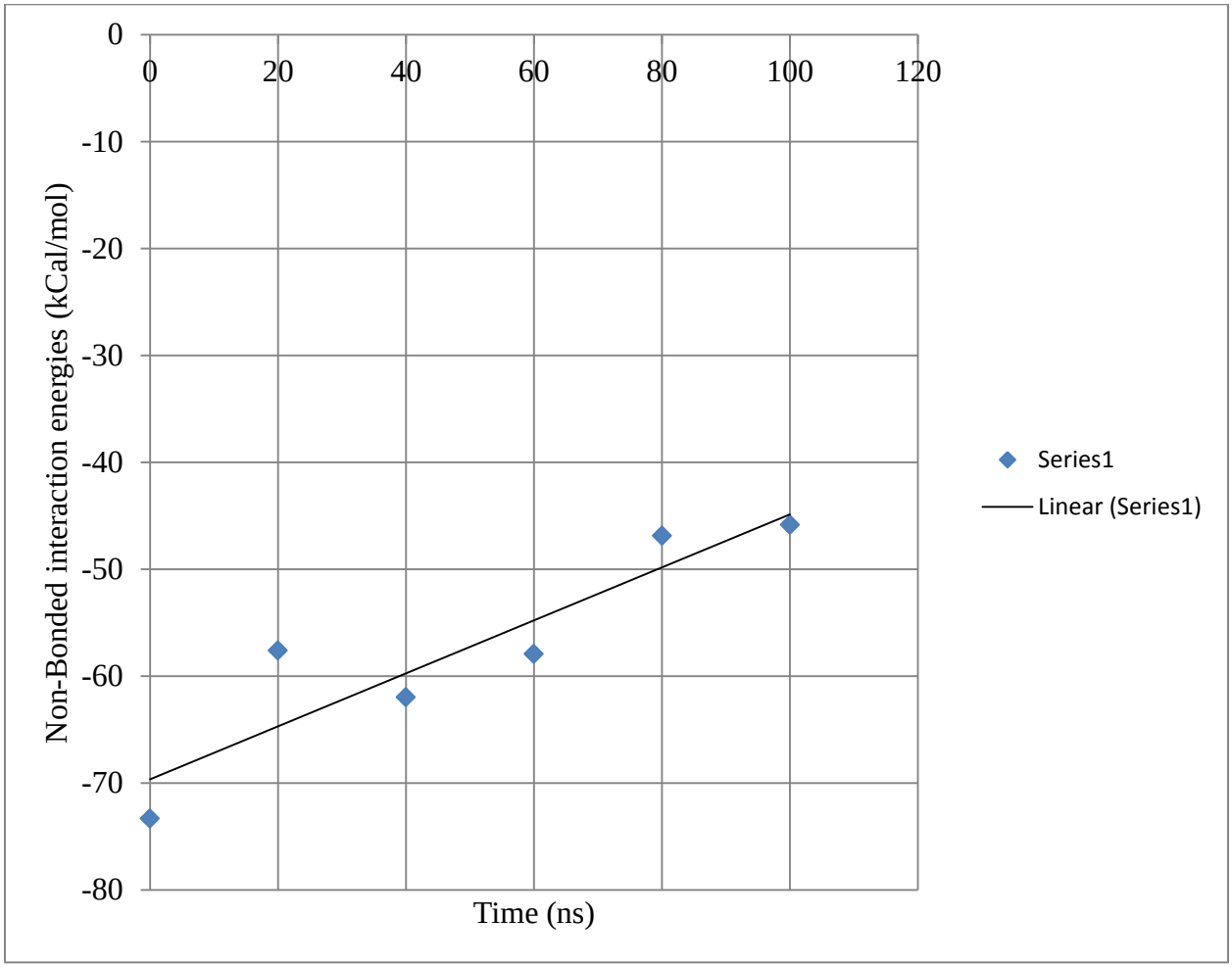

Figure 58. Plot showing average interaction energies between hydrated clay sheets

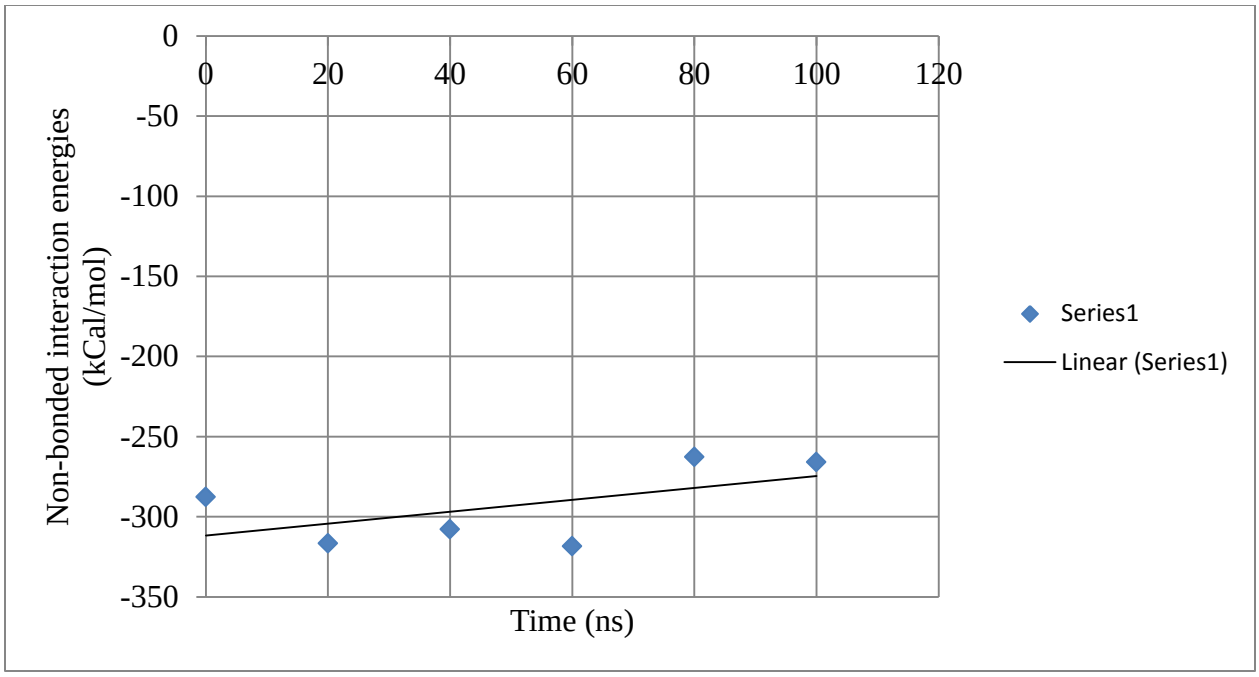

Figure 59. Average interaction energies between interlayer sodium ions and clay sheets

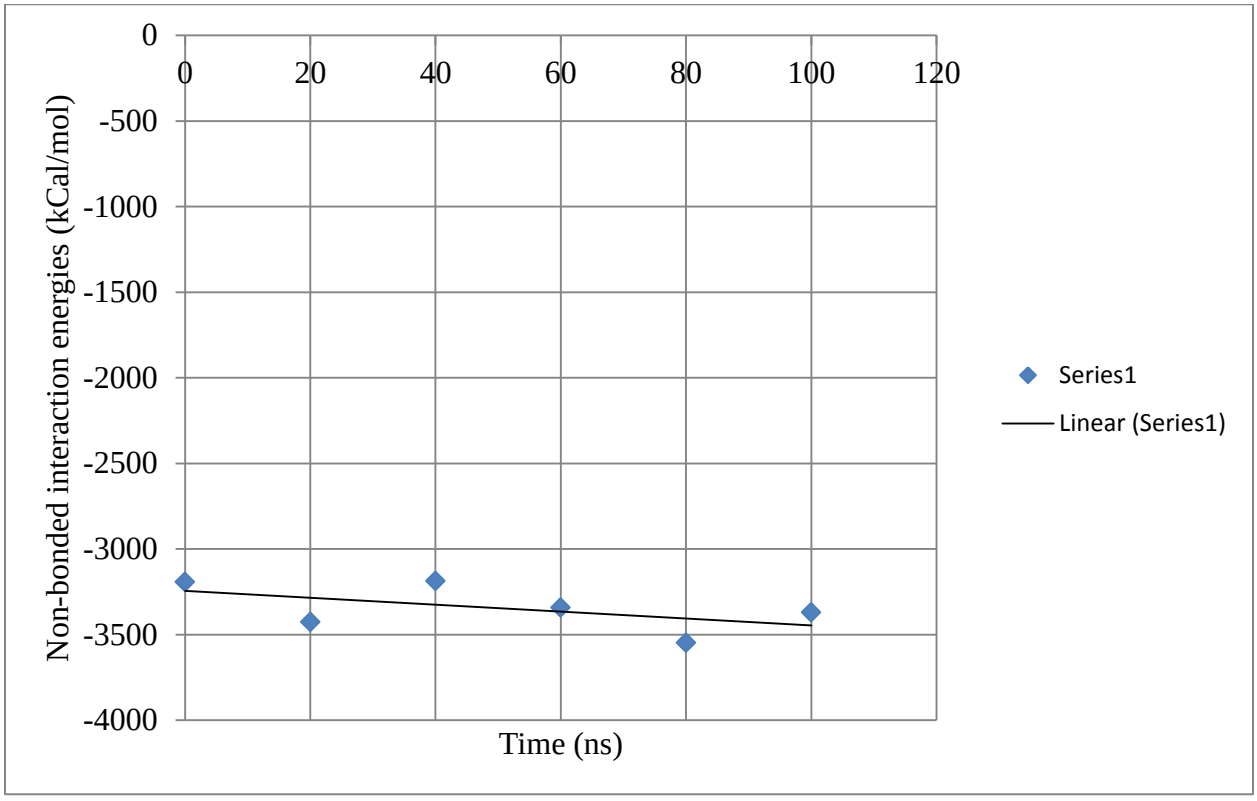

Figure 60. Plot showing average interaction energies between slightly hydrated clay sheets and water molecules

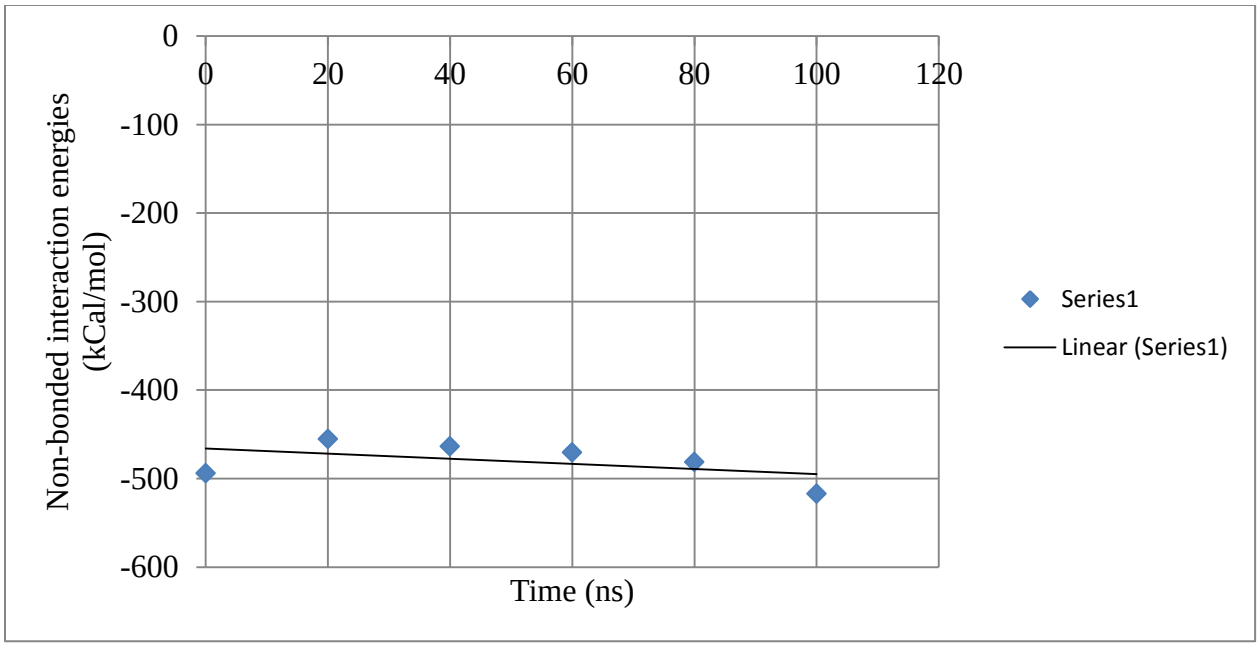

Figure 61. Average interaction energies between interlayer sodium ions and water molecules

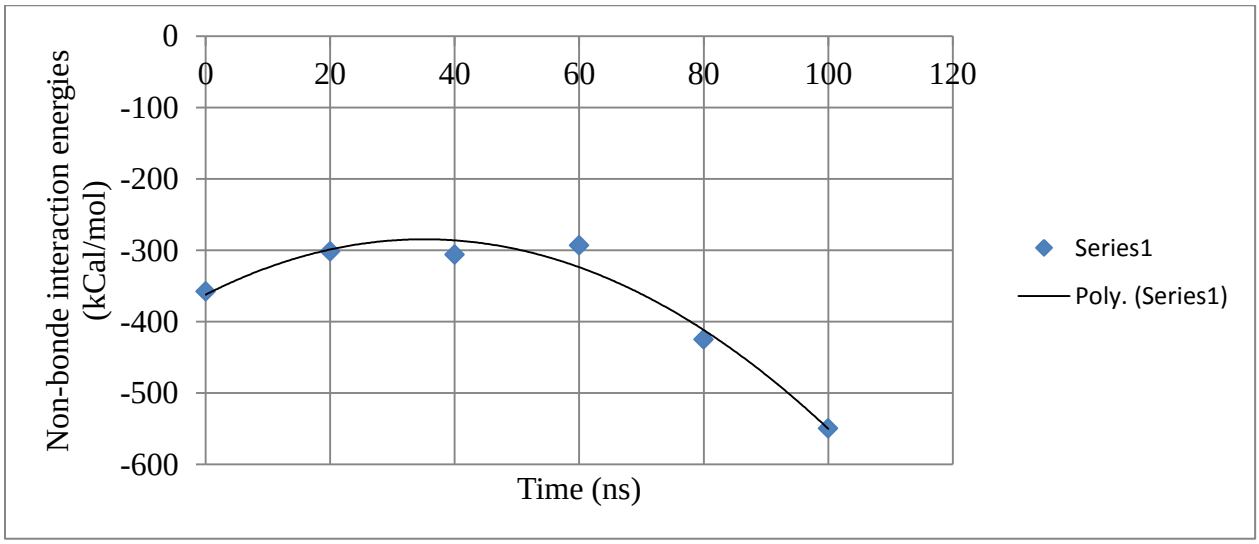

Figure 62. Average interaction energies between interlayer sodium ions and interlayer water molecules

The Radial Distribution Function (RDF) or Pair Correlation Function is used to find the density of water molecules around an interlayer Na ion. In a homogeneous and isotropic system of atoms/molecules, RDF gives the probability of finding an atom/molecule in a shell of thickness dr at a separation distance r from a chosen reference point. RDF can be used to find the

number of atoms or molecules at a distance from the reference point; this is a common technique used to find the density of fluid around charged species. The shortest center to center distance between any two atoms is the sum of equilibrium internuclear distance between two atoms. The probability of finding an atom near the reference atom is normally higher, at larger separation distances, the system would be more diffused and the probability of finding an atom would be 1, which is a uniform probability. RDF can be calculated by knowing the total number of atoms in a system and the total number of atoms in a shell dr at a separation distance r from a reference atom, dividing these numbers by total volume of the system and total volume of the shell respectively. Obtained numbers were considered as the number density of a system and number density of shell. A ratio of number density a shell to the number density of a system results in RDF. Generally, RDF depends on the density and temperature of a system; the general form of RDF is given below.

$$\mathbf{g\,(r) = \rho(r)/\,\rho} \qquad \mathbf{(15)}$$

g(r) = Radial distribution function

ρ= $N_{\text{Total number of atoms in a system}}/V_{\text{Total volume of a system}}$

ρ(r)= $N_{\text{Number atoms in the shell at a distance r}}/V_{\text{Volume of the shell}}$

$$\textbf{Volume of the shell} = 4/3*\pi*r^2*(dr) \qquad \mathbf{(16)}$$

dr=thickness of the shell in Angstroms

r= separation distance in Angstroms

Figure 63 and 64 shows the radial distribution of oxygen atoms of water molecules and water molecules around a reference interlayer Na^+ ion. The first peak was observed at a distance of 2.4A° (internuclear equilibrium distance between Na and Oxygen atoms) from Na ion, the probability of finding an oxygen atom and a water molecule around a Na ion is 6.5 and 2.5 times

more than anywhere else in the solvation box respectively. A sharp peak describes the closed packing of water molecules around Na ion and a coordination or solvation shell around Na ions. The second peak was observed in both the plots at a distance of 4A° and 3A°. The second peak shows the second layer of organization in the interlayer. At a larger separation distance a uniform probability of around 0.5 was observed. The obtained results indicate a possibility of very high density of water molecules in the interlayer. The density of water molecules inside the interlayer is higher than bulk water, the obtained results also indicates the formation of a "quasi-crystal" phase of water molecules inside the interlayer. Further studies on density calculation interlayer water molecules are documented in this work.

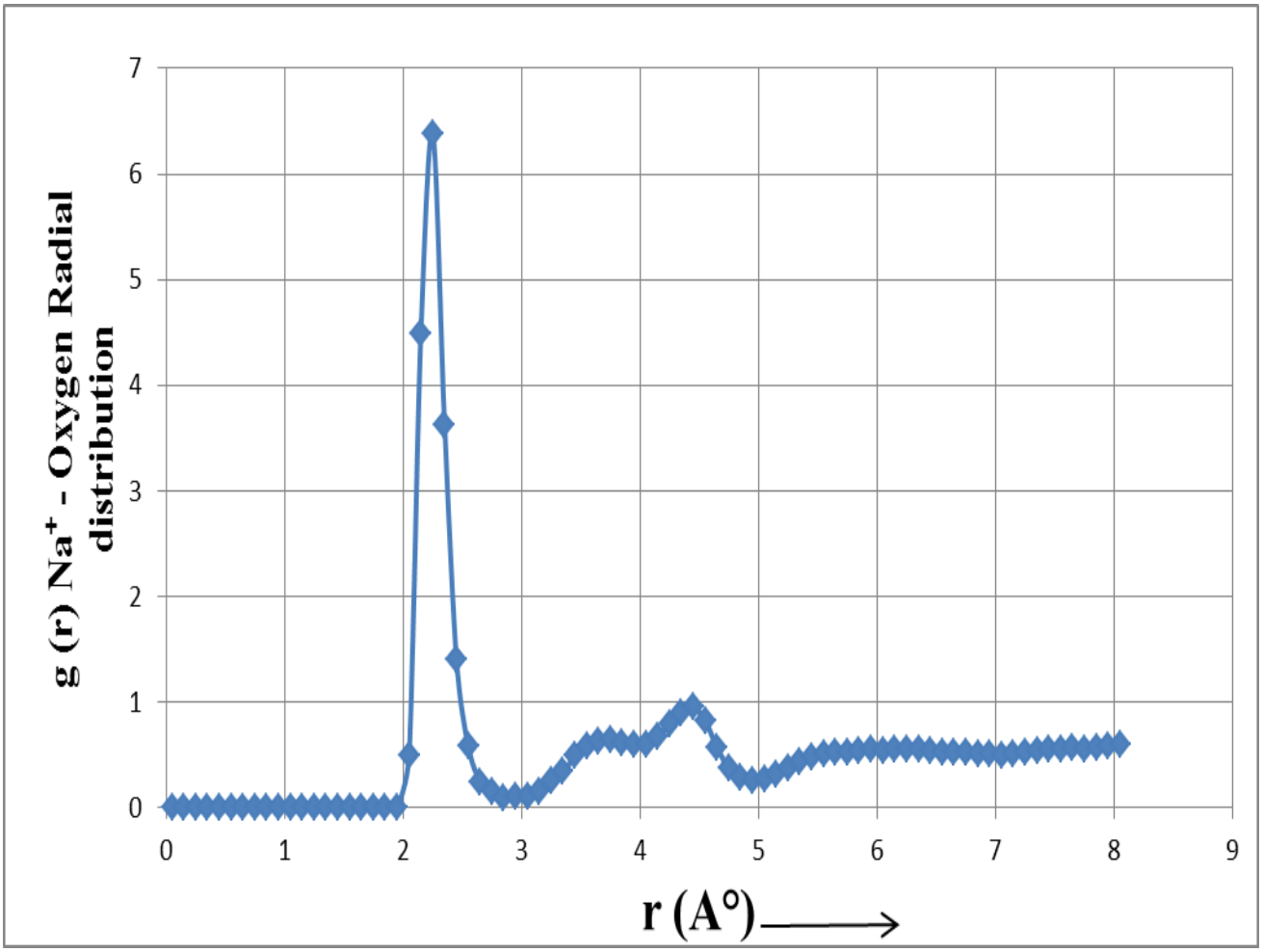

Figure 63. Radial distribution of oxygen atoms around interlayer sodium ions

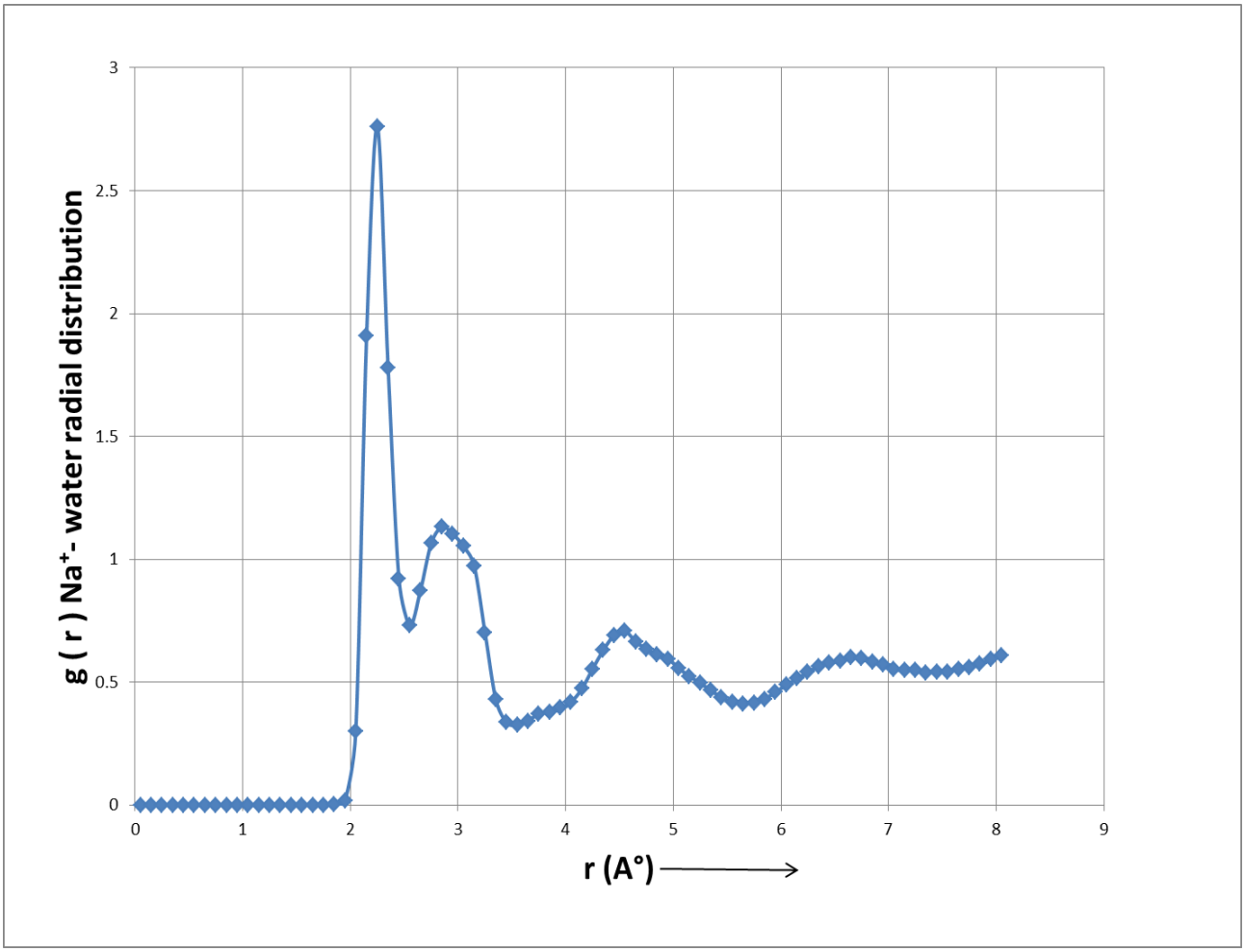

Figure 64. Plot showing radial distribution function of interlayer sodium ion and interlayer water molecules

The density of water inside the interlayer was calculated by tracking the position of oxygen atoms of clay sheets facing interlayer. The variation of Z coordinates of oxygen atoms located in the clay sheets was estimated and averaged over 100 ns. The difference between Z coordinates of the top clay sheet and Z coordinate of the bottom sheet of oxygen atoms were tracked to estimate the interlayer spacing, the obtained interlayer spacing (Z_{total}) 6.87A° is an average of interlayer spacing over 100ns. The effective interlayer spacing (Z_{eff}) 3.5A° was calculated by deducting the VdW radius of oxygen atoms from Z_{total}. Interlayer volume (V_{total}) was estimated by multiplying X Y dimensions of a single clay sheet and Z_{eff}. The VdW volumes

of interlayer ions were deducted from V_{total} to get effective interlayer volume (V_{eff}). The calculations are given below.

Total interlayer volume = 21.12A°X18.28A°X3.5A° = 1352.15A°³

VdW volume of 4 interlayer Na^+ ions= 4*(4/3)*π* (Rvdw) ³

$$(Rvdw)^3 = 4*(4/3)*\pi*(1.4030)^3$$

$$(Rvdw)^3 = 46.27A°^3$$

Effective interlayer volume =1352.15A°³ - 46.27 A°³ = 1305.88A°³

It is a common practice in MD simulations to calculate the number density of a system, which is the number of atoms per unit volume. Figure 65 describes increases in interlayer water molecules with time and Figure 66 describes interlayer density variations with time. The estimated number densities of interlayer are represented in the form of mass density and associated calculations are given below.

1 gram of water occupies 1 cc of volume

H = 1.00794 g/moles

O = 15.9994g/ moles

Water (H_2O) = 18.00988 grams/moles (two parts of hydrogen and one part of oxygen)

1 gram of water = 1/18 = 0.05556 mole

1 mole = $6.023*10^{23}$ molecules

1 g of water contains = $0.05556* 6.023*10^{23} = 3.3346*10^{22}$ molecules

1 cc = (10^8 A° * 10^8 A° * 10^8 A°)

1 g/cc= $3.3346*10^{22}$ molecules/ (10^8 A° * 10^8 A° * 10^8 A°)

1 g/cc= 0.03346 molecules/A°³

1 g/cc= 0.03346*3 = 0.1 atoms/A°³

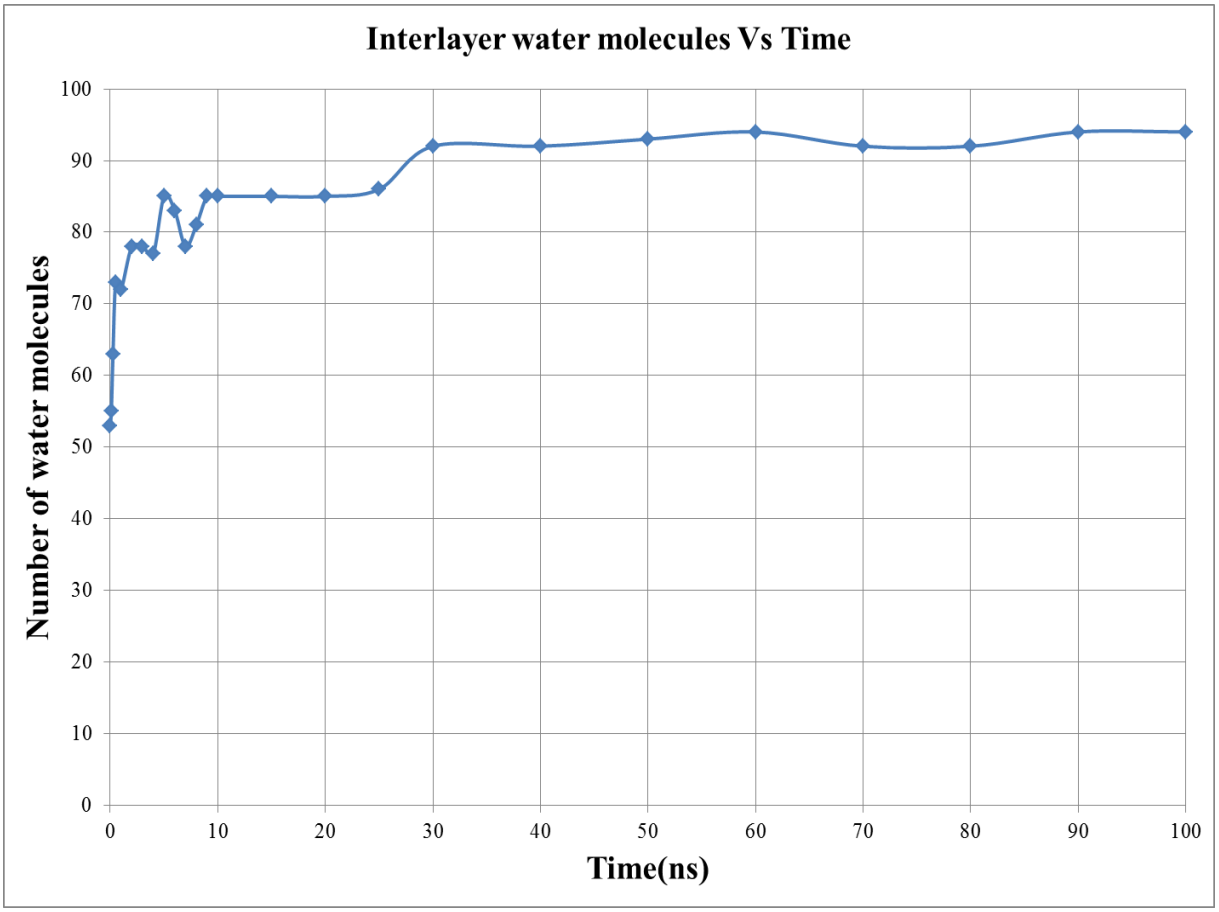

Figure 65. Plot showing the number of interlayer water molecules as function of time

Water density inside the interlayer was observed higher than bulk water density, and interlayer water density was observed 2.25g /cc at the end of 100ns of simulation. This behavior of water was observed in several clay-water simulation works. Figure 67 shows the increase in interlayer water density as a function of the number of interlayer water molecules. The structure of interlayer water and hydrogen bonding was evaluated to understand quasi-crystalline behavior of water inside the interlayer. The Hydrogen bond is a strong attractive intermolecular force between molecules. Hydrogen bonds can be observed between hydrogen atoms and electronegative atoms of other molecules. Water molecules have charged ends, hydrogen atoms are positively charged and oxygen atoms are negatively charged. In order to form a hydrogen bond a hydrogen donor and a hydrogen acceptor must exist.

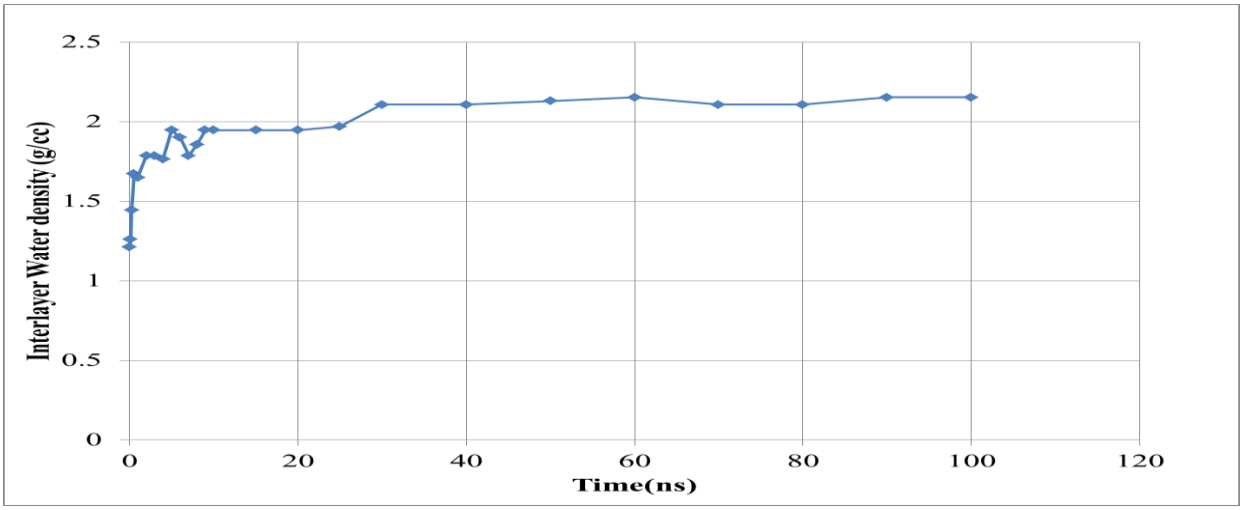

Figure 66. Plot showing change in interlayer water density with time

A hydrogen donor in a hydrogen bond is the charged species to which hydrogen atom has a covalent bonded. Hydrogen acceptor is any electronegative atom or ion neighboring hydrogen donor. Typically OH^{-} part of a water molecule acts as a hydrogen donor and oxygen atoms of neighboring water molecules acts as hydrogen acceptor.

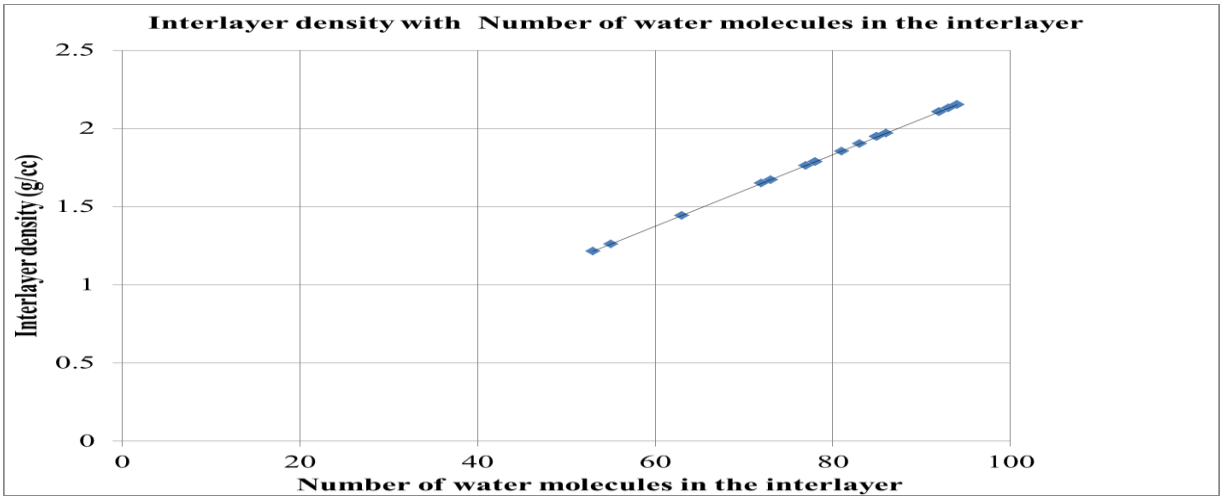

Figure 67. Plot showing change interlayer water density as a function of the increase in number of interlayer water molecules

Generally hydrogen bond cutoff distance between a donor and an acceptor is 2-4A°. The hydrogen bond is stronger than intermolecular forces like VdW interaction, Borns repulsion etc. and weaker than ionic and covalent bonds. Generally hydrogen bond energy between water

molecules varies between 3-6 Kcal/mole. Water molecules show the strong hydrogen bonding network and they form different water structures like dimers, trimers and pentamers etc.

The number of Hydrogen bonds of water molecules with time is shown in Figure 68. A 3.5A° cutoff distance between donors and acceptors and cutoff angle 20 degrees between donors and acceptors was used in this calculation. Approximately 50 hydrogen bonds between water molecules were observed inside interlayer at 0ns (300K and 1 bar pressure), a gradual increase in number of hydrogen bonds were observed with time, at the end of 90-100ns 100-120 hydrogen bonds between water molecules were observed inside interlayer. A network of hydrogen bonds shows several water structures, generally these structures are classified as dimers, trimers and pentamers. Hydrogen bonds between two, three and five water molecules are referred as dimers, trimers and pentamers respectively. The hydrogen bond energy increases as the number of hydrogen bonds increase. For example, hydrogen bond energy in the water pentamer structure is his higher than dimer and trimer. Figure 69 and 70 shows the hydrogen bond network inside the interlayer and different water structures formed inside the interlayer.

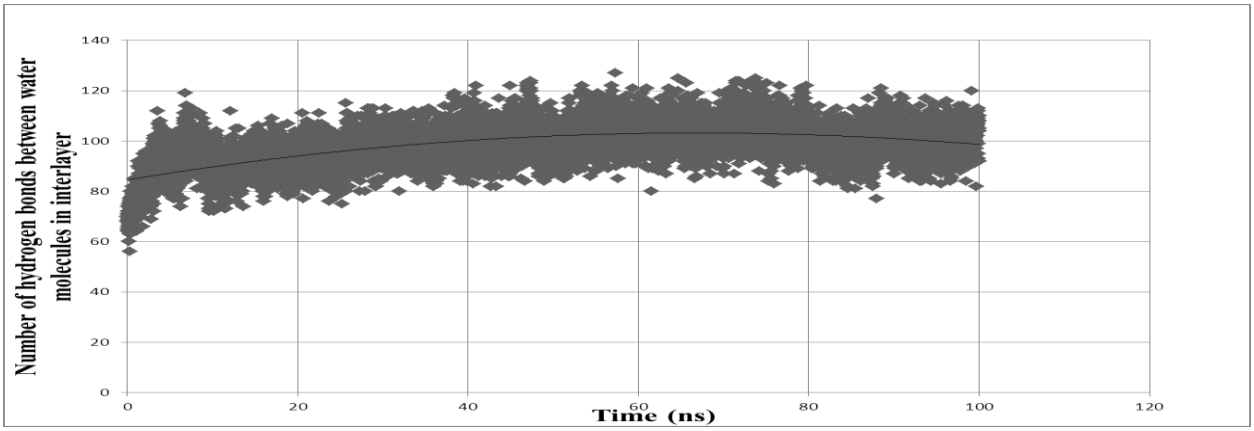

Figure 68. Plot showing hydrogen bond formations between interlayer water molecules with time

Figure 71 and 72 shows the interlayer hydrogen bonds from 95 ns to 100ns. These hydrogen bonds were considered for hydrogen bond energy calculation and no significant movement of water molecules was observed within in the area of Na ions. Figure 73 shows a plot

of comparison between the interlayer electrostatic attraction between cations –water and Hydrogen bond energy between water molecules. A strong hydrogen bonding energy was observed between water molecules. This could be a reason behind no movement of water molecules. Trajectories of water molecules were plotted to analyze the movement of water molecules and velocity of a water molecule entering interlayer. These trajectories are captured from 0ns to 100ns of simulation and consists 10000 frames.

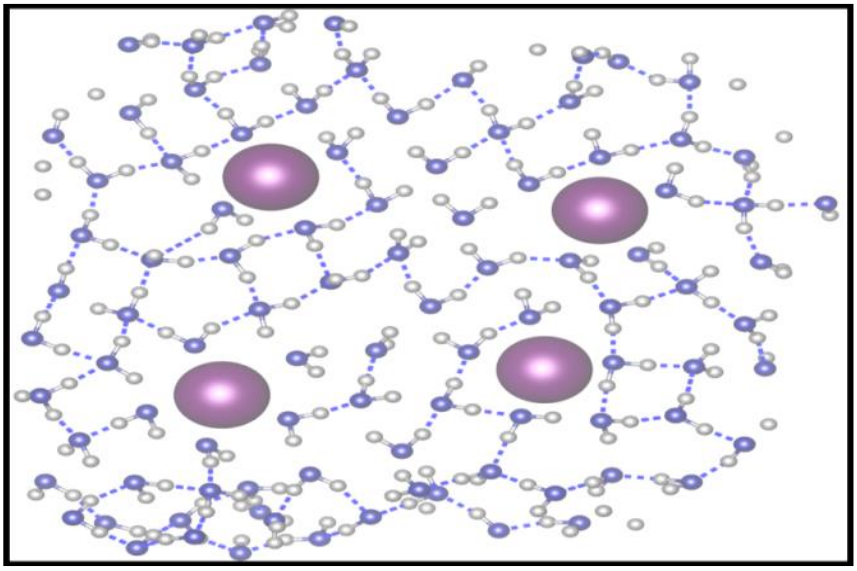

Figure 69. Interlayer water hydrogen bonds

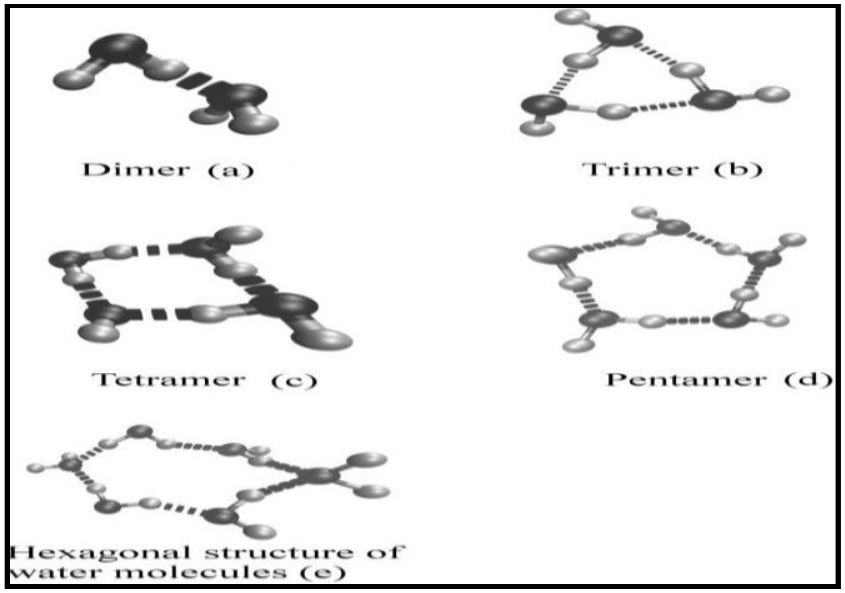

Figure 70. Different water structures inside interlayer

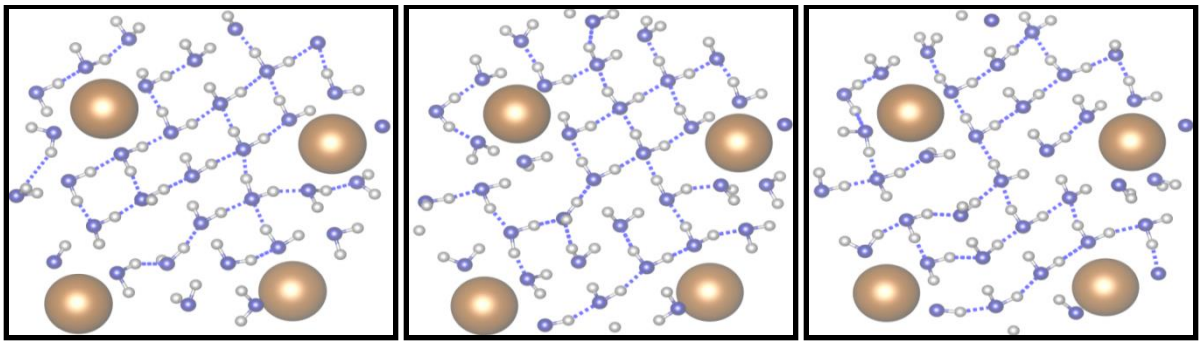

Figure 71. Formation of hydrogen bonds in the interlayer at 95, 96 and 97 ns respectively

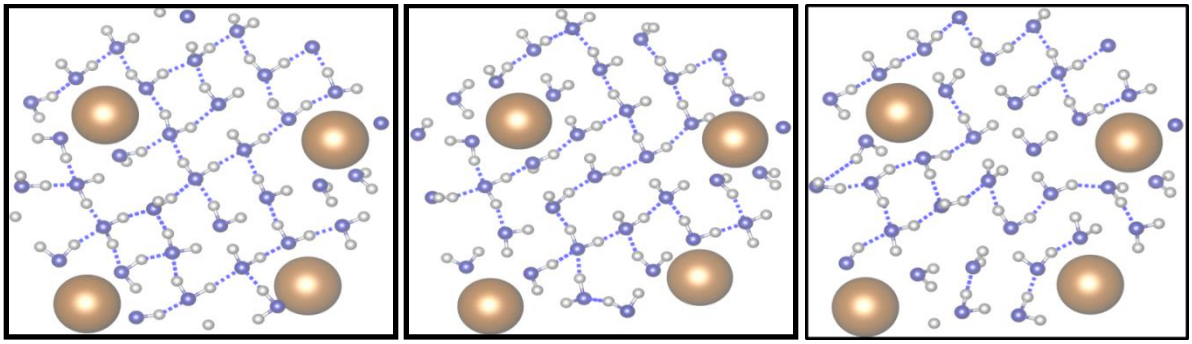

Figure 72. Formation of hydrogen bonds in the interlayer at 98, 99 and 100 ns respectively

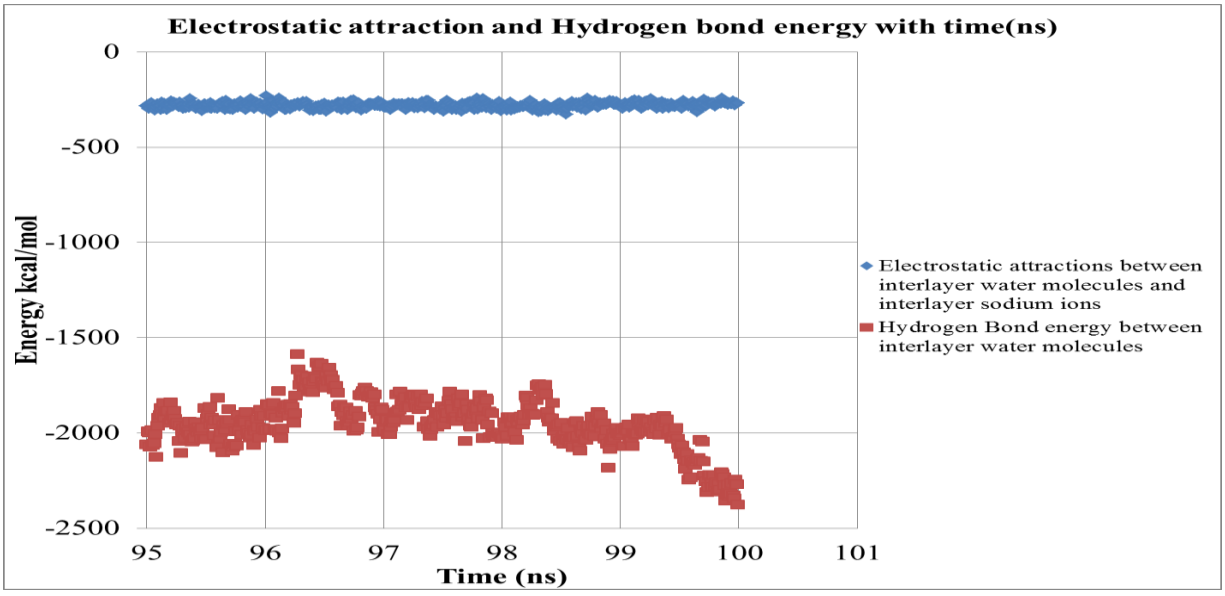

Figure 73. Plot showing comparison of interlayer electrostatic and hydrogen bond energies

Trajectories are captured to observe the movement of water molecules towards interlayer. The distance travelled by these water molecules was estimated by calculating the center of mass

of a water molecule at the end of a frame. The ratio of distance to time gives velocity of a water molecule. Figure 74 and 75 shows the trajectory of a water molecule from the interlayer edge to the interlayer center of a clay sheet from 0 ns to 100 ns. The average speed of a water molecule from the edge to center of the clay sheet is $8X10^{-5}$m/sec. Speed of a water molecule reduces once it starts flowing from the edge to center. Figure 76 shows a plot of speed of the water molecule versus time from 0ns to 100ns. The speed of water molecule decreases with time as water molecule moves from the edge to center. This could be due to high density of interlayer water molecules. The Experimental flow rate $3.22X10^{-11}$m/sec (Amarasinghe et al., 2008) of water was estimated using AFM (Atomic Force Microscopy) and XRD studies.

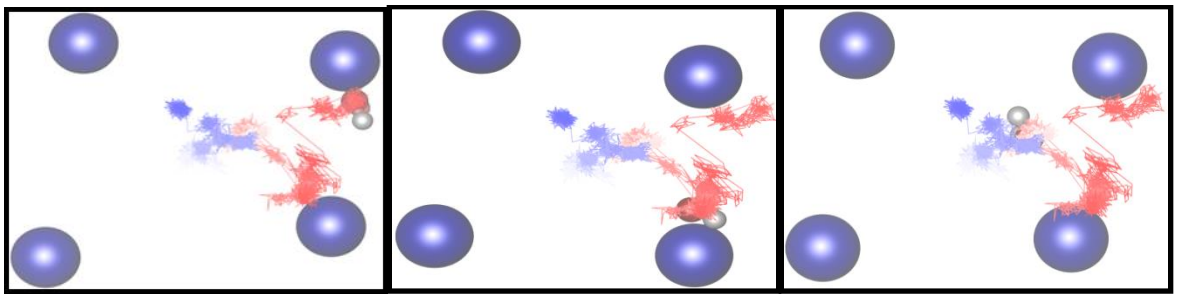

Figure 74. Position of a water molecule along its trajectory from 0ns, 10ns and 25nsrespectively

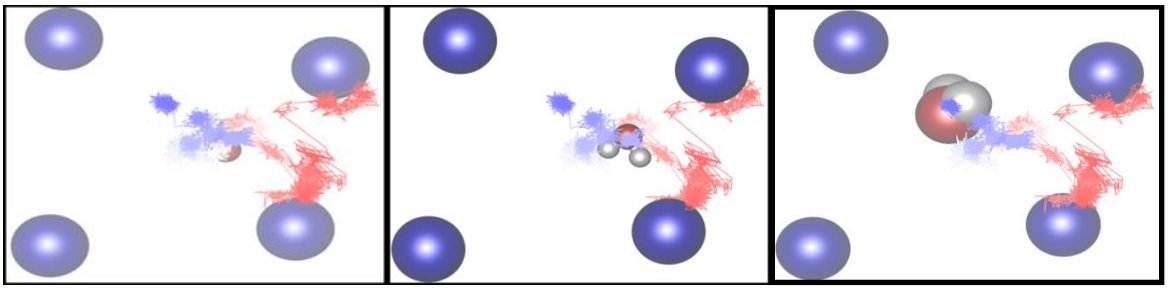

Figure 75. Position of one water molecule along its trajectory from 50ns, 75ns and 100ns respectively

5.3. Solvation without Electrostatic Attraction between Na ions and Water Molecules

The electrostatic attraction between interlayer Na ions and hydrogen bonds between water molecules are the two major factors that control initiation of swelling. Two more

simulations were performed to understand the role of electrostatic attraction and hydrogen bonds. First set of simulation carries no electrostatic attraction between Na ions and water, Figure.77 an 78 shows the configuration of interlayer Na ions and interlayer water molecules without electro static attraction between sodium and water molecules from 0ns (300K and 1bar) to 50ns.At the beginning of simulation 50 interlayer water molecules were observed, all the interlayer water molecules started flowing out of interlayer, this is due to no electrostatic interaction between sodium and water molecules. Figure 79 and 80 shows the configuration of interlayer water molecules and interlayer sodium ions, in this simulation electrostatic attraction between Na and water molecules was considered for the first half of the simulation (0ns to 50ns), from 50 to 100ns no electrostatic attraction between Na and water molecules.

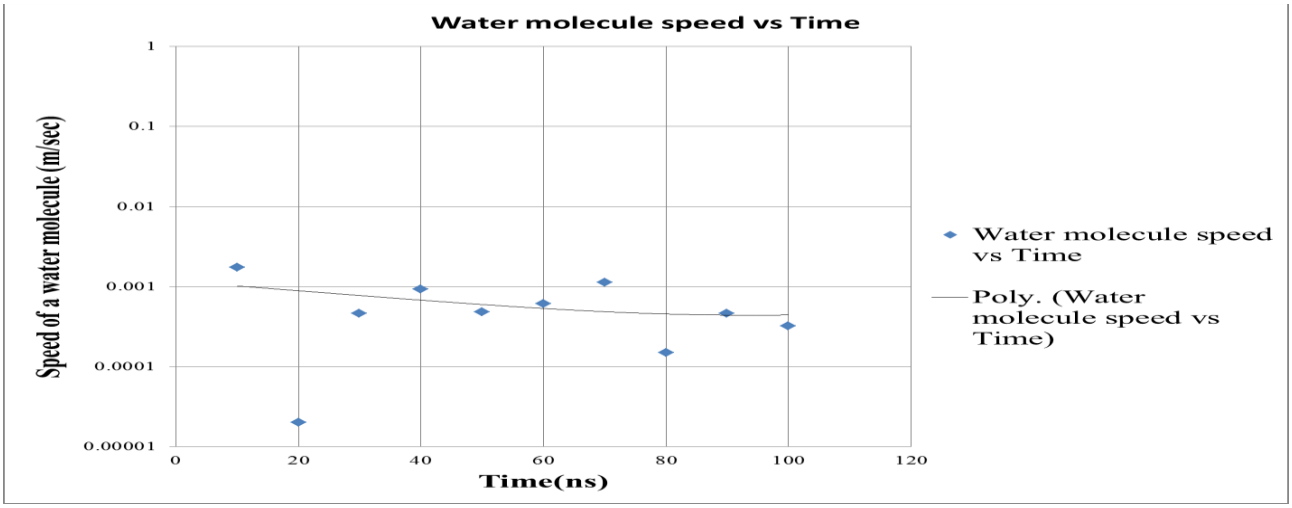

Figure 76. Plot showing change in speed of water molecule with time

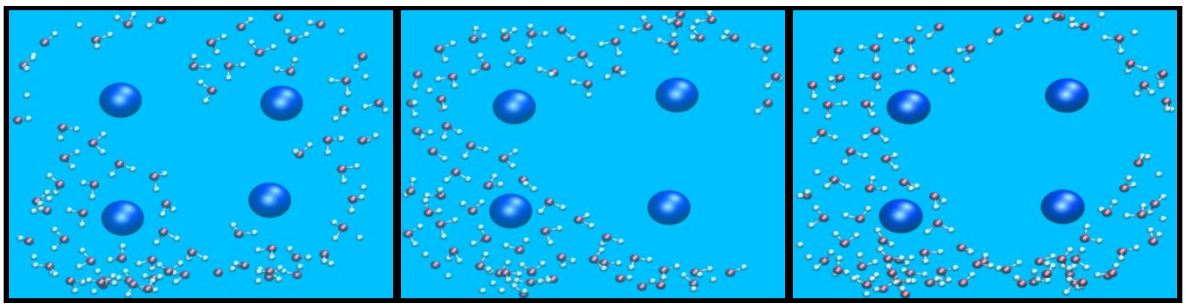

Figure 77. Arrangement of water molecules in the interlayer at 0, 10 and 20ns respectively

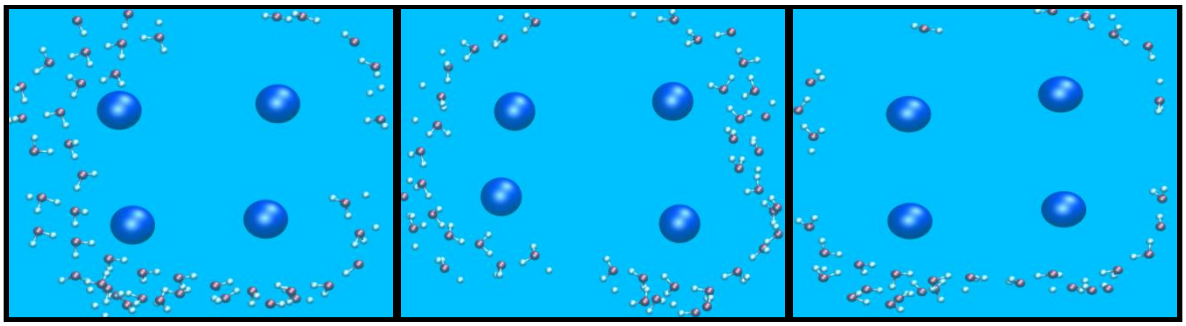

Figure 78. Arrangement of water molecules in the interlayer at 30, 40 and 50ns respectively

Flow of water molecules towards interlayer Na ion and attraction between water molecules and Na ions was observed for first 50ns. For the next 50ns there was no electrostatic attraction between sodium and water molecules but the flow of water molecules towards interlayer was observed. This is behavior is due to strong hydrogen bonding between water molecules which keeps swelling process under constant progress, also oxygen atoms were pointing towards Na ions during first 50ns of simulation and oxygen atoms are pointing away from Na ions from 50-100ns of simulation. Figure 81 and 82 describes the variation of average electrostatic, VdW and total non-bonded interaction energies between clay sheets and clay sheets-interlayer Na ions as a function of increase in interlayer water molecules. In Figure 81 Electrostatic attraction between clay sheets did not vary much throughout the simulation but VdW interaction and non-bonded interaction between clay sheets reduced as the number of water molecules increased inside the interlayer.

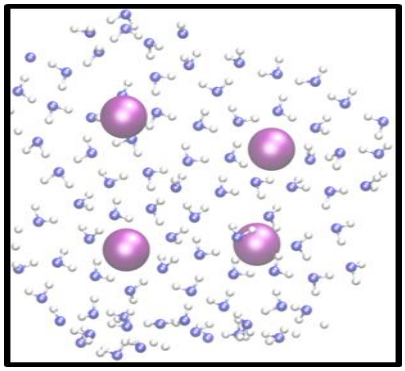

Figure 79. Arrangement of interlayer water molecules at 50ns

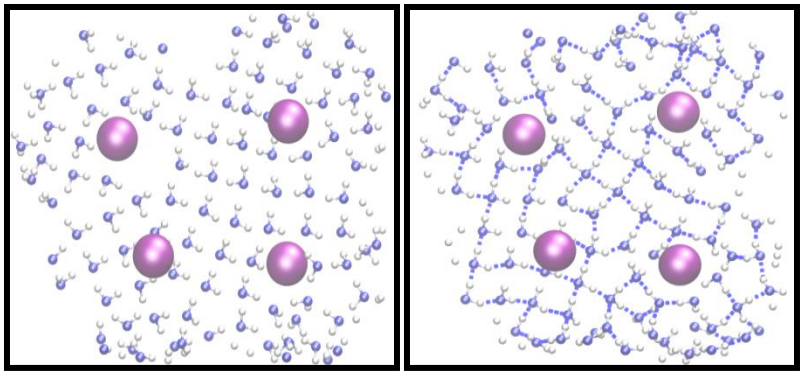

Figure 80. Arrangement of interlayer water molecules and interlayer hydrogen bond network at 75 and 100ns respectively

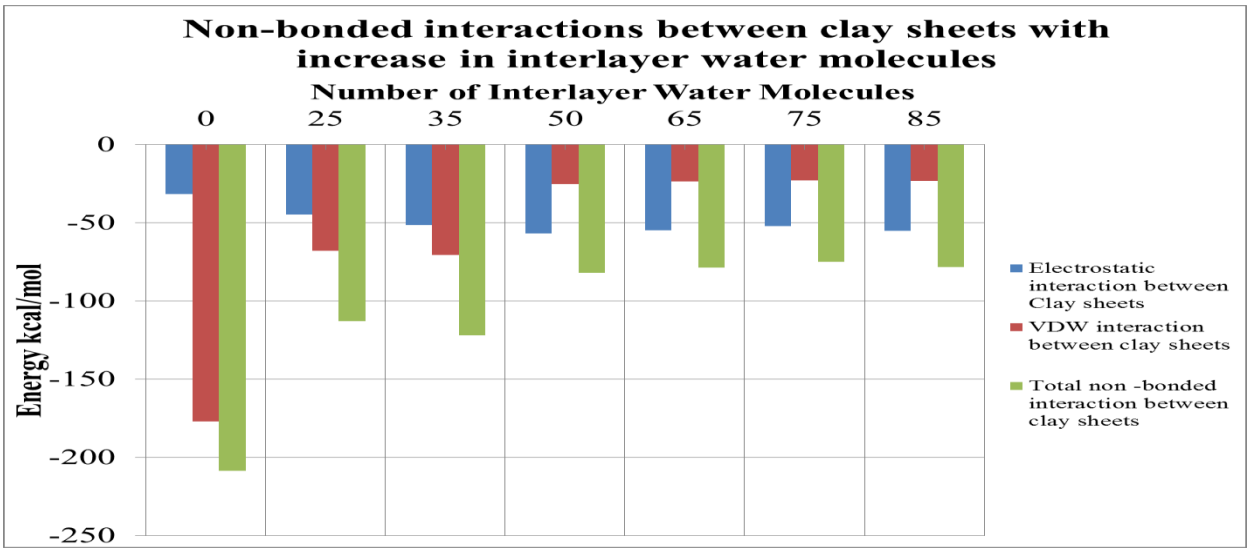

Figure 81. Plot showing change in average interaction energies between clay sheets with increase in number of interlayer water molecules

Figure 82 explains change in interaction energies between interlayer Na ions and clay sheets. A weak VdW interaction was observed between clay sheets and Na ions. Electrostatic attraction and total non-bonded interaction energy between clay sheets and interlayer Na ions decreased as the number of water molecules increased inside the interlayer. The strong electrostatic attraction between water molecules and Na ions could be an important factor for this behavior. The reduction in interaction energies like electrostatic and VdW describes that clay sheets are moving apart and also moving away from interlayer Na ions. This behavior clearly

indicates swelling of Na-MMT, as the clay sheets separate and interlayer Na ions interact with water more water molecules move inside the interlayer, hydrogen bonding between water molecules keeps this phenomenon under constant progress.

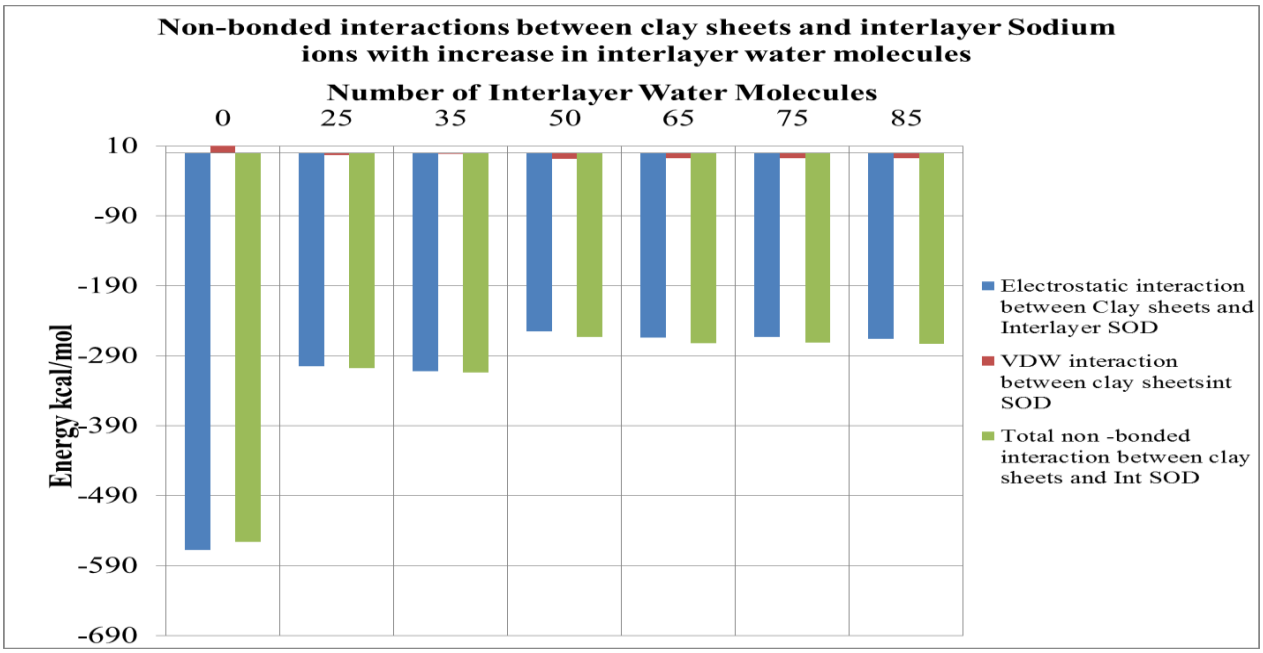

Figure 82. Plot showing change in average interaction energies between clay sheets and interlayer sodium ions with increase in number of interlayer water molecules

RDF plots and density calculations explain the higher density of water molecules around Na ions. Trajectory plots and velocity calculations describe the movement of water molecules inside the solvation box.

CHAPTER 6. CONCLUSION

- Solvation models for the clay- water system were built for the first time and trajectory of a water molecule moving from outside to inside the interlayer was captured.
- Solvation models were built both dry Na-MMT and slightly hydrated Na-MMT models. Molecular Dynamics simulations were performed on these models for several Nano seconds.
- Interaction energies between clay sheets, Na ions and water molecules were extensively studied. Variation basal spacing was plotted to estimate the swelling of clay sheets. Radial distribution functions and density calculations were performed to evaluate the behavior of water molecules around interlayer Na ions and in the interlayer.
- Trajectories of water molecules were captured to observe the movement of a water molecule and velocities of water molecules were calculated using trajectory plots.
- Hydrogen bonding forming and several structures of water molecules was observed in the interlayer to distinguish between the role of electrostatic interaction and hydrogen bond network in the swelling process.
- The results of dry Na –MMT simulation describes the mechanism of non-swelling behavior and interlayer collapse of Na-MMT after complete dehydration of interlayer.
- Swelling was not observed in dry Na-MMT simulation after 10ns of simulation. Clay layers did not show any structural deformation and remain intact during the simulation progress. Interlayer Na ions attracted towards ditrigonal cavities of clay sheets and resided in cavities, which eventually avoided the interaction between water molecules to

restrict the swelling process. Attraction between clay sheets, Sodium ions and water molecules was observed but change in basal spacing was negligible.

- The results of slightly hydrated Na-MMT simulations describe the initial hydration or the initial swelling mechanism of Na-MMT clay minerals.
- Pre-existing moisture content of 8 to 10% and basal spacing of 12-13A° is required to trigger the hydration process of Na-MMT.
- Dominant electrostatic attraction was observed between interlayer cations and water molecules. VdW interaction between clay sheets and electrostatic attraction between interlayer was significantly decreased during hydration of interlayer.
- Hydrogen bonding between water molecules is necessary for the constant flow of water molecules and it keeps swelling under constant progress. Electrostatic attraction between interlayer cations and water molecules plays a key role in the initial hydration of Na-MMT.
- Radial Distribution plots explain the arrangement and orientation of water molecules around cations. RDF plots also show the greater possibility of finding water molecules around cations.
- First and second coordination shells were quantitatively described using RDF plots. Larger density of interlayer water describes the closed packing of water molecules in the interlayer.
- The electrostatic attraction between cations-water and hydrogen bonding between water molecules is probably one of the reasons for closed packing of interlayer water molecules. The thickness of the interlayer water remained constant.

- Water structures around cations showed the behavior of water molecules in the interlayer. The water molecules oriented with oxygen atoms towards the interlayer cation shows one more possibility of electrostatic attraction between cations and water molecules.
- The first solvation shell of five water molecules was observed around cations from images. The average basal spacing of clay sheets increased from 12-14A° which is a clear indication of the beginning of swelling. Trajectories of water molecules were captured to describe the movement and the speed of water molecules.
- The speed of a water molecule decrease in the interlayer due closed packing of water molecules. The movement of interlayer water molecules also captured using trajectories and velocities. Water molecules take more time to reach the center from the edge of the clay sheets.
- Solvation simulations with and without electrostatic attraction between water molecules and interlayer Na ions describe the role of non-bonded interactions in the interlayer.
- A molecular Dynamics simulation is a powerful tool to evaluate the molecular properties of the clay-water system at atomic scale. This system need to be further developed to explain the osmotic swelling and Double layer theories. The Molecular Dynamics technique can be used in the future along with other computation techniques like Discrete element modeling and the Finite element modeling to develop a multiscale model of the clay-water system, which explains the swelling process from molecular to Macroscopic scale.

REFERENCES

Gould. H. e., 2007, Introduction to Simulation Methods: Applications to Physical Systems.

Amarasinghe, P. M., K. S. Katti, and D. R. Katti, 2008, Molecular Hydraulic Properties of Montmorillonite: A Polarized Fourier Transform Infrared Spectroscopic Study: Applied Spectroscopy, v. 62, p. 1303-1313.

Anandarajah, A., 1995, Single correction function for computing retarded van der Waals attraction, *in* J. Chen, ed., J. colloid and Interface Science, p. 519-523.

Anandarajah, A., 1997a, Influence of particle orientation on one-dimensional compression of montmorillonite, J. Colloid and Interface Science, p. 44-52.

Anandarajah, A., 1997b, Influence of particle orientation on one-dimensional compression of montmorillonite: Journal of Colloid and Interface Science, v. 194, p. 44-52.

Anderson, M. T., 2001, Role of microscopic physicochemical forces in large volumetic strins for clay sediments, *in* N. Lu, ed., Journal of Engineering Mechanics, ASCE.

Birkeland, P. W., 1999, Soils and geomorphology, Newyork, Oxford University press.

Brindley, G. W., and Brown, G., 1980, Crystal structures of clay minerals and their x-ray identification, London, Mineralogical Society.

Chang, F. R. C., and G. Sposito, 1996, The electrical double layer of a disk-shaped clay mineral particle: Effects of electrolyte properties and surface charge density: Journal of Colloid and Interface Science, v. 178, p. 555-564.

Chaplin, M. F., 2010, Water and life, The unique Properties of H2O, CRC press, p. 69-86.

Chen, J., 1996, Physico-chemical analysis of contaminated clays, Johns Hopkins University, Baltimore, MD., Dept. of Civil Engineering.

Cornelis, K., and B. Dutrow, 2007, Manual of Mineral Science, John Wiley & Sons, Inc.

De Boer, J. H., 1936, The influence of van der Waals forces and primary bonds on binding energy, strengrth and orientation, with special reference to some artificial resins, Transacttions of the Faraday Society, p. 10-32.

Dixon, J. B., and Weed, S.B., eds., 1989, Minerals in soil environments, Madison, Wisconsin, Soil Science Society of America.

Gillot, J. E., 1987, Clay in engineering geology, Amsterdam, Elsevier.

Grim, R. E., Clay mineralogy, Newyork, McGraw Hill.

Hamaker, H. C., 1937, The London-van der Waals attraction between spherical particles, Physica, p. 1058-1072.

Humphrey, W., A. Dalke, and K. Schulten, 1996, VMD: Visual molecular dynamics: Journal of Molecular Graphics, v. 14, p. 33-&.

Israelachvili, J. N., 1985, Intermolecular and surface forces, Orlando, Academic Press.

Jackson, M. L., 1953, Chemical weathering of minerals in soil: Advances in agronomy, *in* G. D. Sherman, ed., Newyork, Academic press.

Jo, H. Y., T. Katsumi, C. H. Benson, and T. B. Edil, 2001, Hydraulic conductivity and swelling of nonprehydrated GCLs permeated with single-species salt solutions: Journal of Geotechnical and Geoenvironmental Engineering, v. 127, p. 557-567.

Katti, D., and V. Shanmugasundaram, 2001, Influence of swelling on the microstructure of expansive clays: Canadian Geotechnical Journal, v. 38, p. 175-182.

Katti, D. R., S. R. Schmidt, P. Ghosh, and K. S. Katti, 2005, Modeling the response of pyrophyllite interlayer to applied stress using steered molecular dynamics: Clays and Clay Minerals, v. 53, p. 171-178.

Katti, D. R., S. R. Schmidt, P. Ghosh, and K. S. Katti, 2007, Molecular modeling of the mechanical behavior and interactions in dry and slightly hydrated sodium montmorillonite interlayer: Canadian Geotechnical Journal, v. 44, p. 425-435.

London, F., 1937, The general theory of molecular attractive forces between solids, Transactions of the Faraday Society, p. 8.

LU, N., 1991, Numerical study of the electrical double-layer repulsion between nonparallel clay particles of finite length, Johns Hopkins University, Baltimore, MD, Dept. of Civil engineering.

Glenn J. Martyna, Douglas J. Tobias and Michael L. Klein,1994, Constant Pressure Molecular Dynamics Algorithms.

Mcbride, M. B., 1994, Envionmental Chemistry of Soils, New York, Oxford university Press.

McBride, M. B., and P. Baveye, 2002, Diffuse double-layer models, long-range forces, and ordering in clay colloids: Soil Science Society of America Journal, v. 66, p. 1207-1217.

Mitchell, 1993, fundamentals of soil behavior.

Newman, A. C. D., 1987, Chemistry of clays and clay minerals, London, Mineralogical Society.

Overbeek, J. T. G., 1952, Colloid Science, *in* e. H.R. Kruyt, L. C. Jackon, ed., Amsterdam, Elsevier.

Phillips, J. C., R. Braun, W. Wang, J. Gumbart, E. Tajkhorshid, E. Villa, C. Chipot, R. D. Skeel, L. Kale, and K. Schulten, 2005, Scalable molecular dynamics with NAMD: Journal of Computational Chemistry, v. 26, p. 1781-1802.

Pimentel, G. C., 1960, The hydrogen bond, *in* McClellan, ed., San Francisco and London, W. H. Freeman and Company.

Schmidt, S. R., D. R. Katti, P. Ghosh, and K. S. Katti, 2005, Evolution of mechanical response of sodium montmorillonite interlayer with increasing hydration by molecular dynamics: Langmuir, v. 21, p. 8069-8076.

N.T. Skipper, Garrison Sposito and Fang-Ru Chou Chang, Feller

1995, Montecarlo simulations of Interlayer Molecular Structure in Swelling Clay Minerals . 2. Monolayer Hydrates.

Sposito, G., 1989, The Chemistry of Soils, New York, Oxford University Press, Inc.

Sposito, G., N. T. Skipper, R. Sutton, S. H. Park, A. K. Soper, and J. A. Greathouse, 1999, Surface geochemistry of the clay minerals: Proceedings of the National Academy of Sciences of the United States of America, v. 96, p. 3358-3364.

Teppen, B. J., K. Rasmussen, P. M. Bertsch, D. M. Miller, and L. Schafer, 1997, Molecular dynamics modeling of clay minerals .1. Gibbsite, kaolinite, pyrophyllite, and beidellite: Journal of Physical Chemistry B, v. 101, p. 1579-1587.

Van Olphen, H. a. F., J. J, 1979, *Data handbook for clay materials and other non-metallic minerals*, Pergamon Press, New York.

Velde, B., ed., 1992, Origin and mineralogy of clays, Newyork, Springer.

APPENDIX

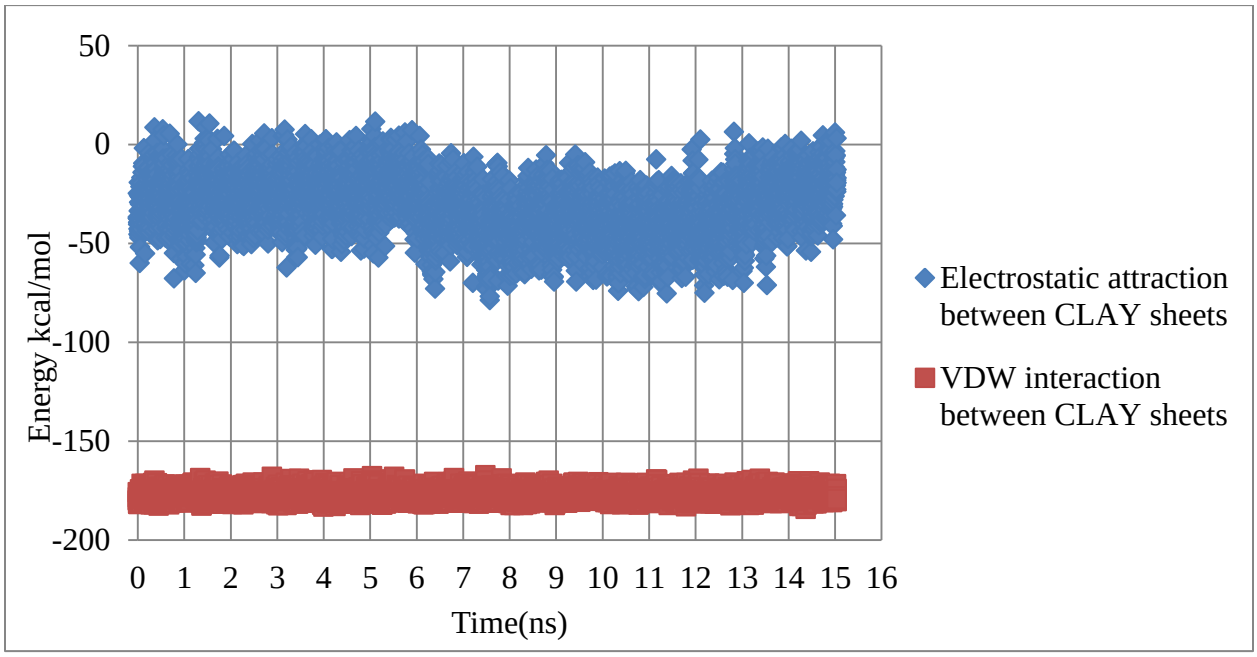

Figure A1. Interaction between clay sheets

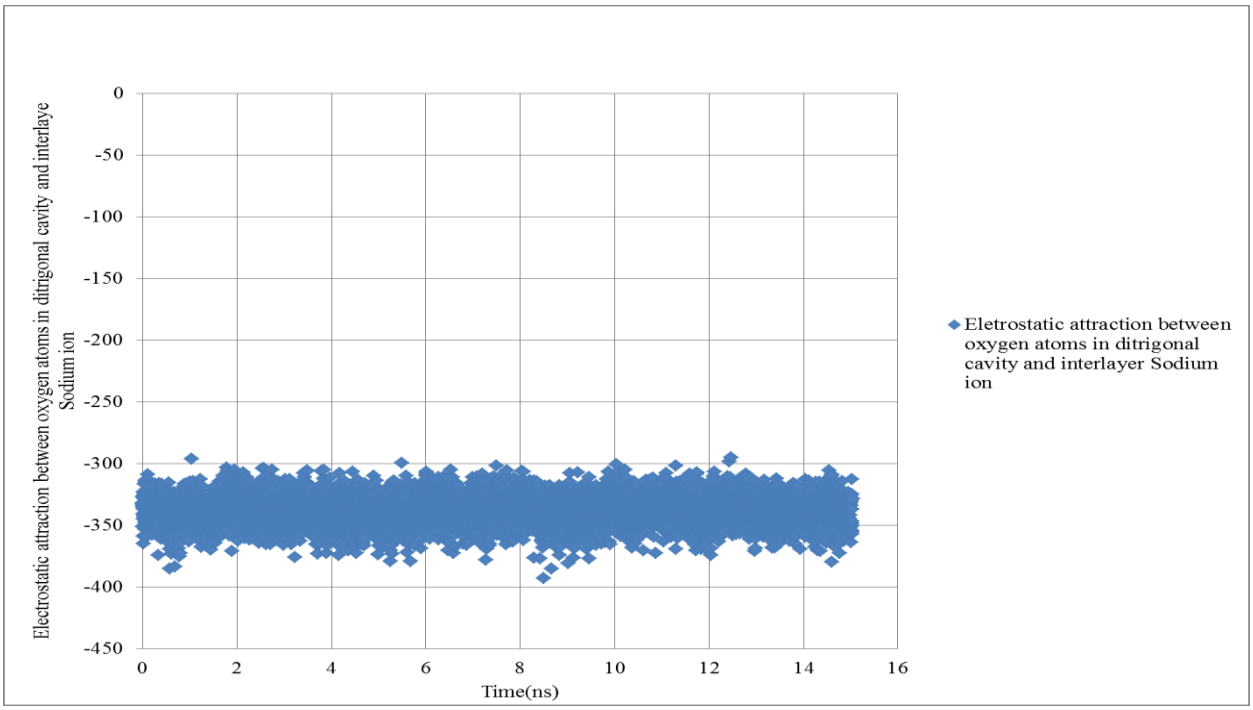

Figure A2. Electrostatic attraction between oxygen atoms in ditrigonal cavity and interlayer sodium ion

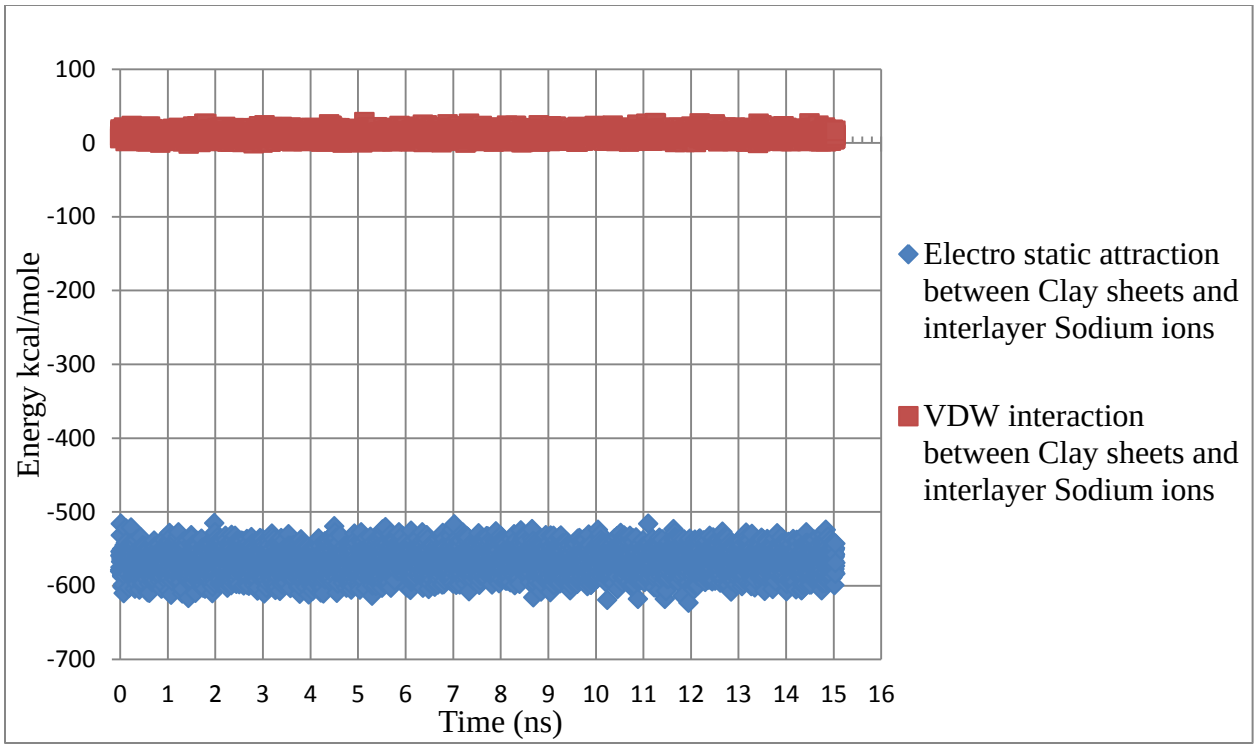

Figure A3. Interaction between clay sheets and interlayer sodium ions

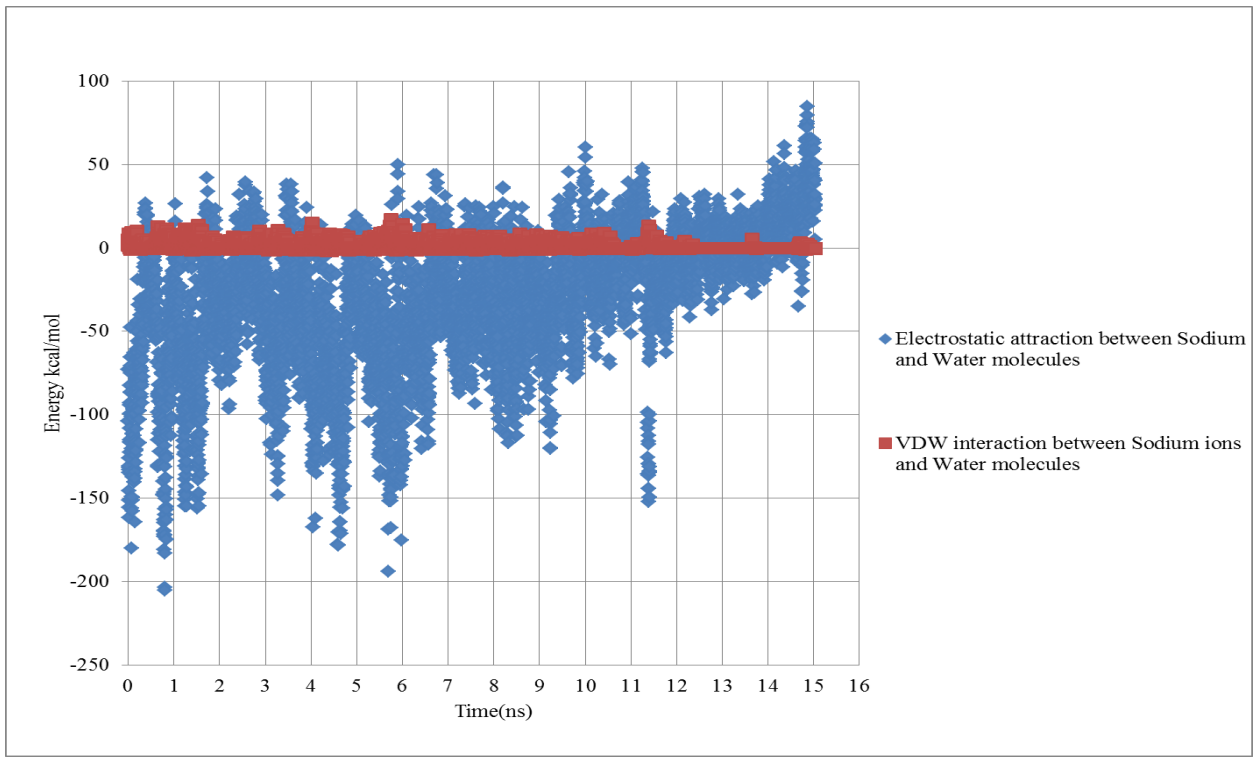

Figure A4. Interaction between interlayer sodium ions and claustered water molecules around clay sheets

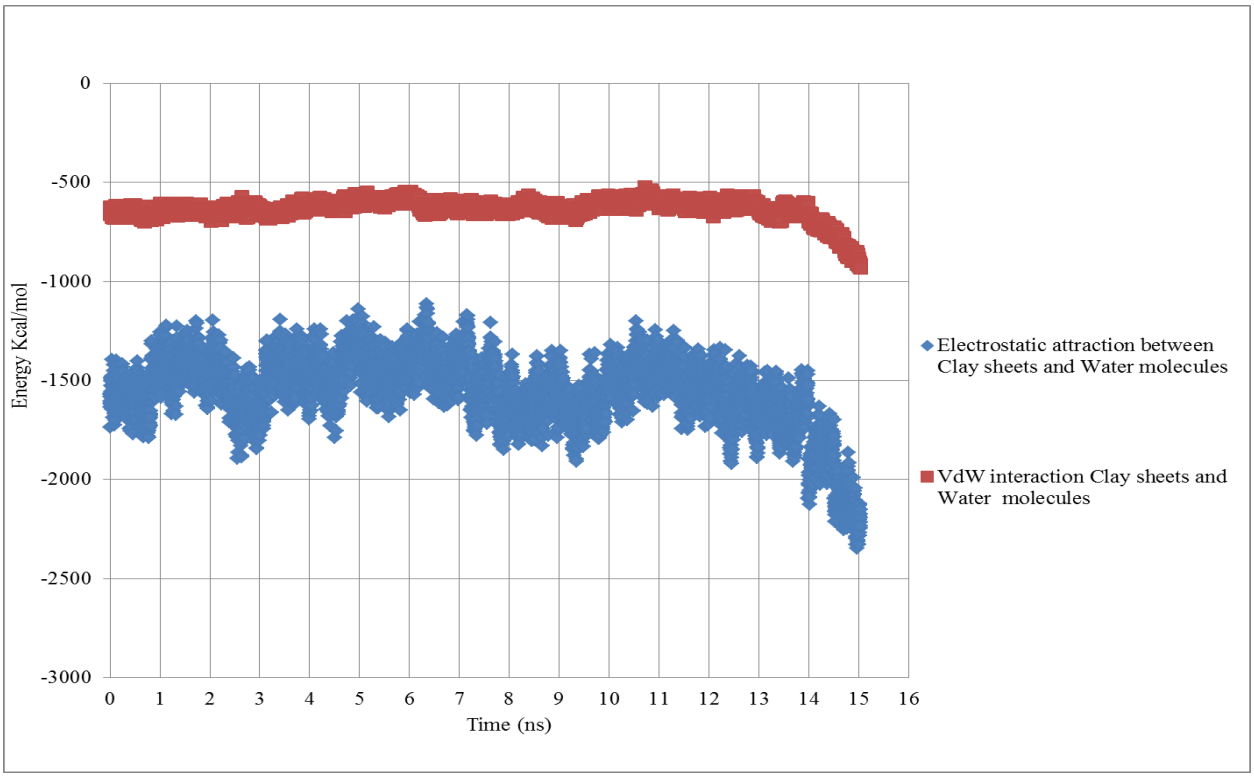

Figure A5. Interaction between clay sheets and water molecules clustered around clay sheets

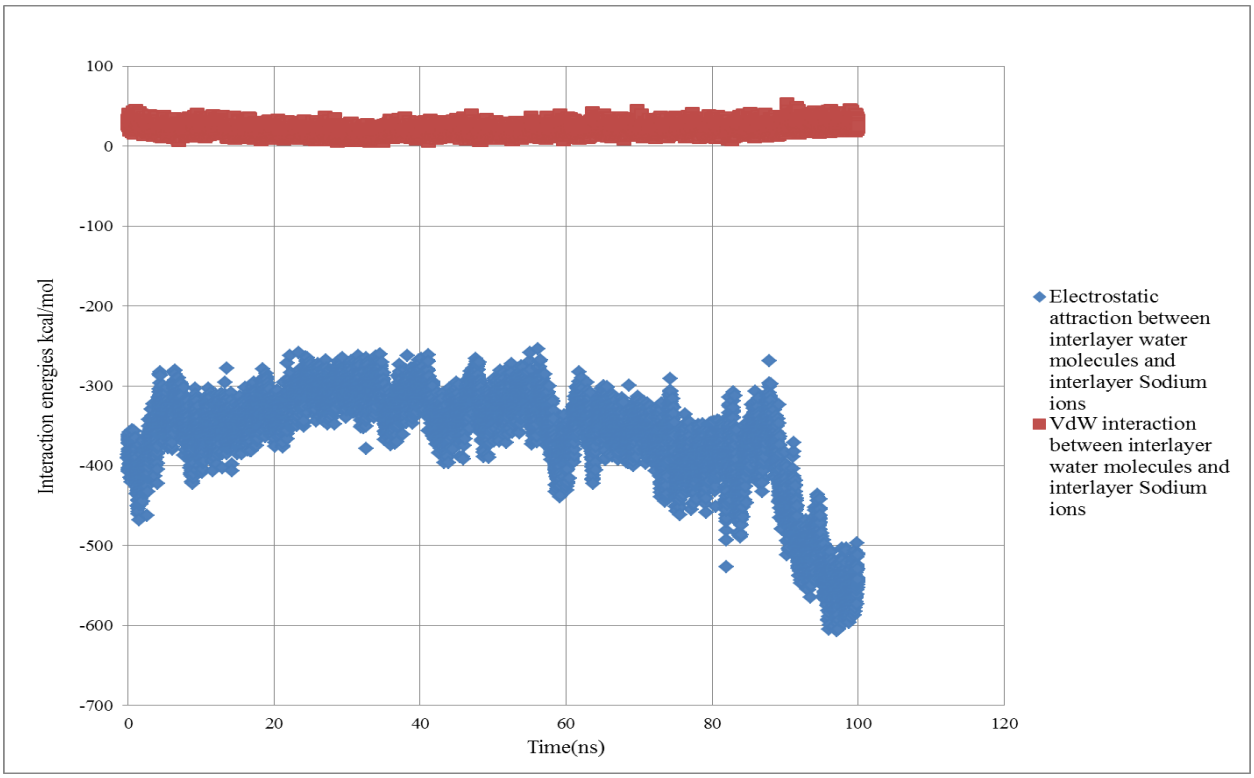

Figure A6. Interaction between interlayer water and interlayer sodium ions

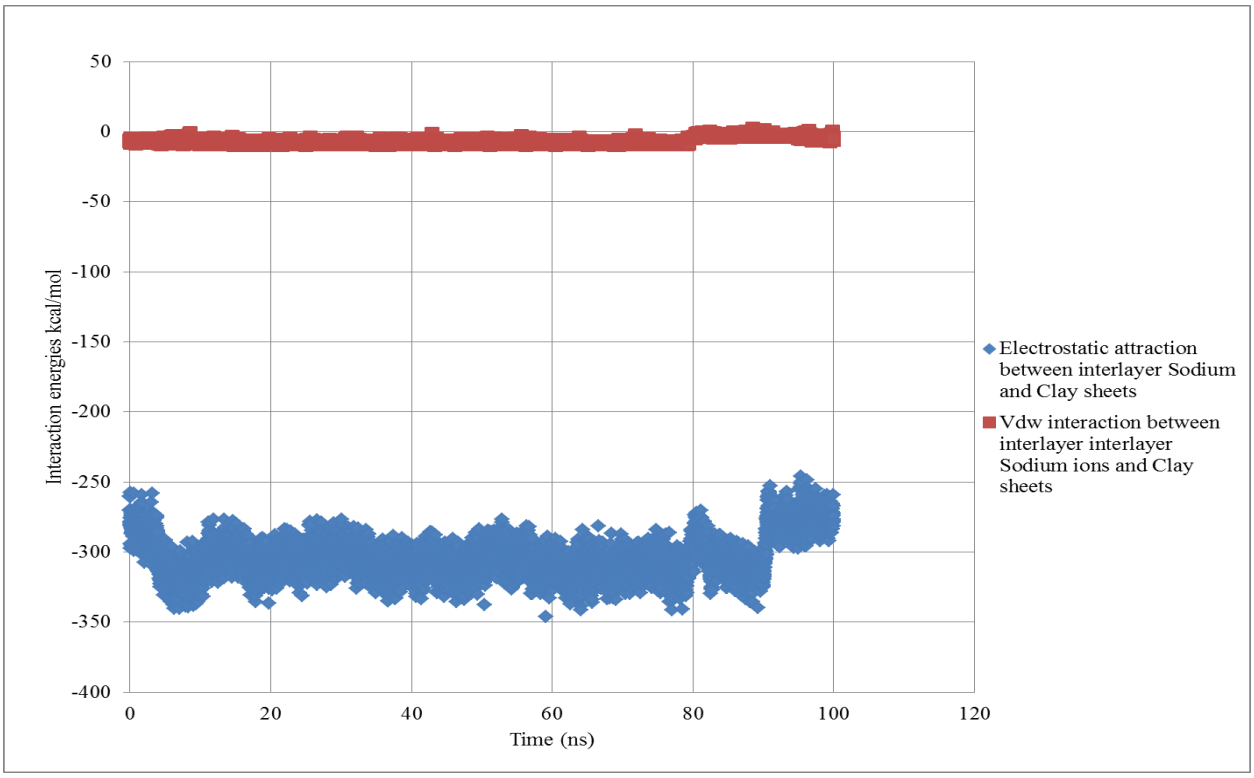

Figure A7. Interaction between interlayer sodium ions and clay sheets

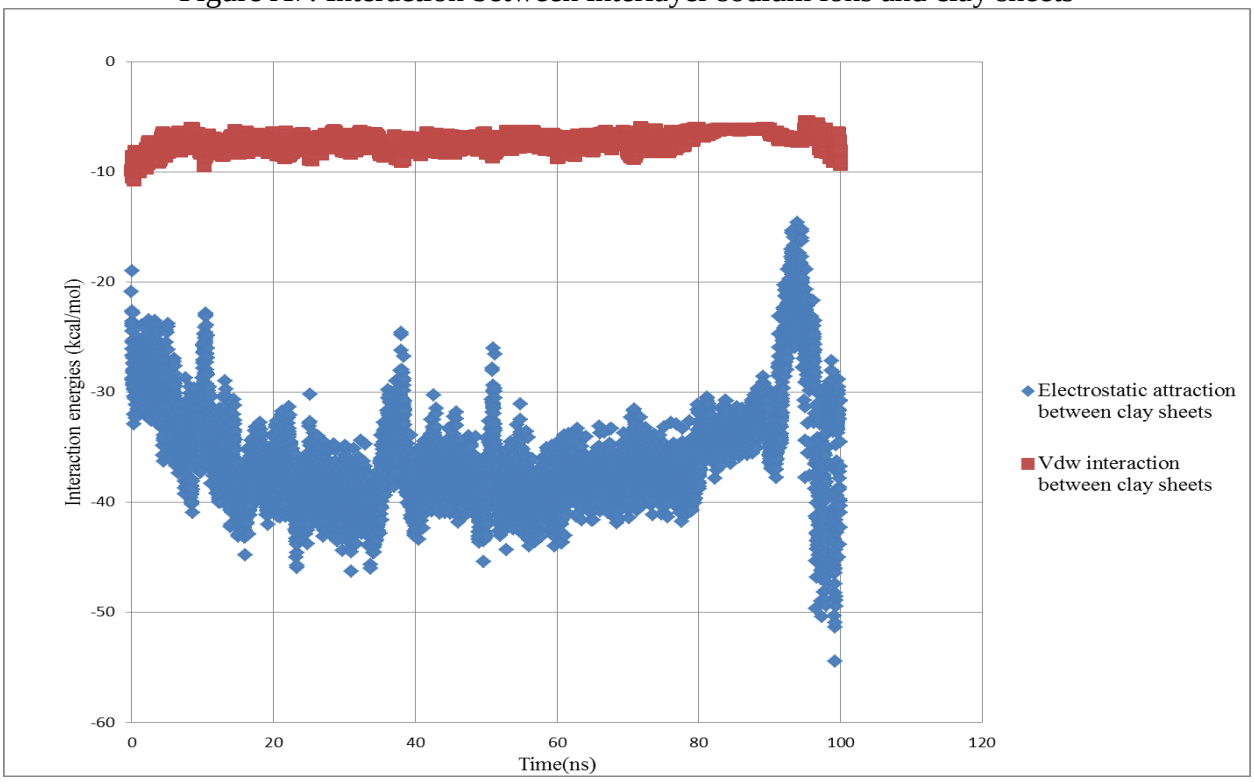

Figure A8. Interaction energies between clay sheets

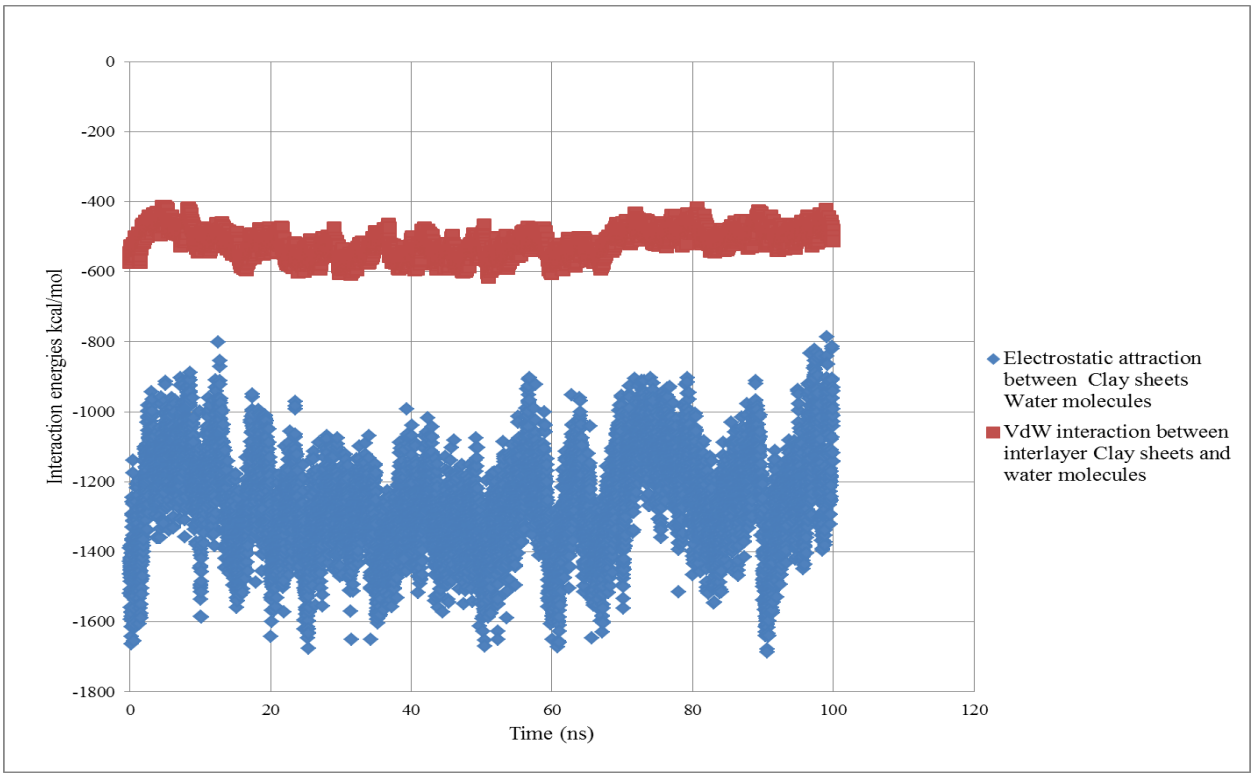

Figure A9. Interaction between clay sheets and water

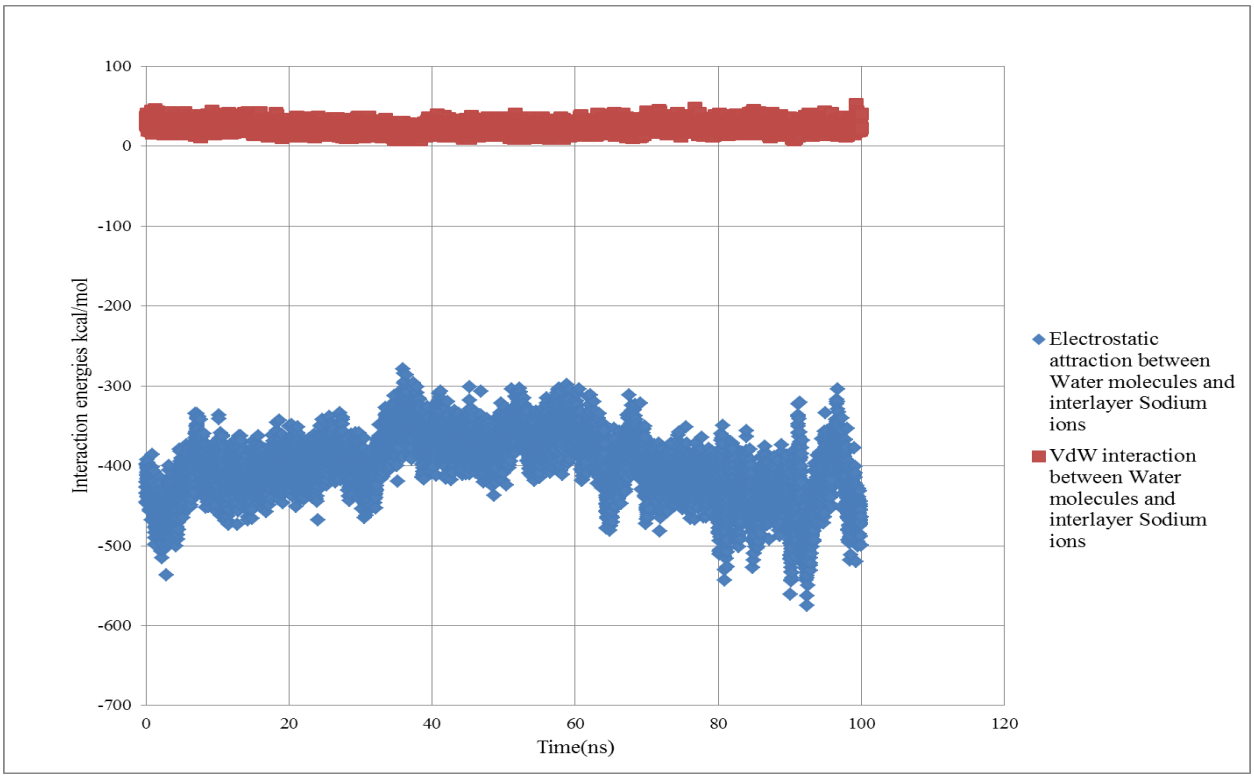

Figure A10. Interaction between clustered water molecules around clay sheets and interlayer ions